Stable Water Isotopologues in the Indian Summer Monsoon Rainfall

A thesis submitted in partial fulfillment of

the requirements for the degree of

Doctor of Philosophy

by

Midhun M

(Roll No. 11330015)

Under the guidance of

Prof. R. Ramesh

Geosciences Division

Physical Research Laboratory, Ahmedabad, India.

DISCIPLINE OF PHYSICS

INDIAN INSTITUTE OF TECHNOLOGY GANDHINAGAR

2015

Declaration

I declare that this written submission represents my ideas in my own words and where others' ideas or words have been included, I have adequately cited and referenced the original sources. I also declare that I have adhered to all principles of academic honesty and integrity and have not misrepresented or fabricated or falsified any idea/data/fact/source in my submission. I understand that any violation of the above can cause disciplinary action by the Institute and can also evoke penal action from the sources which have thus not been properly cited or from whom proper permission has not been taken when needed.

Midhun M

(Roll No: 11330015)

Date: November 27, 2015

CERTIFICATE

It is certified that the work contained in the thesis titled **"Stable Water Isotopologues in the Indian Summer Monsoon Rainfall"** by **Midhun M** (IITGn Roll No: 11330015), has been carried out under my supervision and that this work has not been submitted elsewhere for a degree.

Date:

Prof. R. Ramesh
(Supervisor)
Outstanding Scientist
Physical Research Laboratory
Ahmedabad, India.

Acknowledgements

First and foremost I express my gratitude to my thesis supervisor Prof. R.Ramesh for his invaluable guidance throughout the course of this work. I am thankful to Dr. M.G. Yadava, Dr. Sanjeev Kumar, Prof. J.S. Ray and Prof. Sunil Singh for their most supporting words and the scientific suggestions and discussions. I thank Dr. Amit Kesarker of NARL and Dr. Kei Yoshimura of Atmosphere and Ocean Research Institute (AORI), The University of Tokyo, for introducing me in to the field of numerical climate modeling. I thank R.A. Jani for discussions and introducing me to the mass spectrometer analyses in the stable isotope lab.

I thank Prof. G. Bala (CAOS, IISc), Prof. Terry Quinn (Jackson School of Geosciences, The University of Texas at Austin) and one anonymous reviewer for their valuable comments on this thesis.

I thank Prof. G S Bhat (IISc, Banglore), Dr. Debasis Sengupta (IISc Banglore) and Dr. M. Ravichandran (INCOIS, Hyderabad) for allowing me to participate in cruises and for providing the meteorological data. I thank Dr. Ramya, Masood, Samresh (ISER Bhopal), Dr. Ashutosh (Delhi University), Sandeep (IIT Delhi), Prof. Rajiv Sinha (IIT Kanpur), and Prof. S. Shalivahan (ISM Dhanbad) for their help in collecting rain samples. I also thank ISRO-GBP for the financial support.

I thank all my teachers in PRL, Prof. M.M Sarin, Dr. A.K. Singal, Dr. Dibyendu Chakrabarty, Prof.S. Ramachandran, Dr. Kuljeet Marhas, Dr. Vinay K Ray, Dr. Varun Sheel and Dr. Jitesh Bhatt for their nice lectures during the course work period. I am thankful to Dr. R.D. Deshpande for his encoraging comments on this work. The generous support from Dr. Bhushit, Dr. Shyam Lal, S. Venkataramani, T.A. Rajesh, D.K Rao, Virendra, Dr. Neeraj Rastogi and Dr. Navin Juyal is greatly appreciated. The help from computer center and library staff especially Samuel Johnson, Jigar, Tejas and Dr.Nistha is greatly acknowledged.

Together with Bhavya, Shraddha, Rupa, Niharika, Trina and Akash, I had a very nice time in the stable isotope lab. The discussion with Amzad, Naveen and Arvind were really supportive. I also thank N.B Vaghela Bhai for his all support and help in lab. I am tankful to Thermo engineer Manoj Tank for his timely help in the lab. I thank my friends Prajeesh A.G (IITM, Pune) and Rajeev S.K (IIT Delhi) for their help during this work.

I also acknowledge Pauline, Parulben, Sasi Kumar, Tejas, Sivadasan, Nandini, Priti, Richa, Sentil Babu, Manan Shah, Lakhan Bhai, Bankim Bhai, G.P Patel, Ranganathan, Jayashree, Prabha Ben, Nilesh Bhai, Ubale, Jayati Patel and Jaldhi for their help at various stages.

I also thank to all my dear batch mates, Gangi, Aathi, Girish, Gaurav, Monojith, Gulab, Yashpal, Dilip Nandi, Arko, Damodar, Naveen Negi, Avdesh, Tanmoy, Priyanka, Anjali, Upendra, Dinesh, Wageesh, Rajeev, Gorav Sharma and Nigam for creating a wonderful time in the hostel and at PRL. I sincerely thank Manu, Anirban, Ikshu, Abhaya, Arun, Girish, Tanmoy, Guruprasad, Ashim, Lalit, Deepak, Dipti, Ali, Jabir, Nijil, Vishnudath and many others for making a memorable atmosphere in the hostel and the PRL. I deeply express my thanks to all my dear seniors Chinmay, Susanta, Prasant,Vineeth, Srinivas, Sunil, Arun Awasthi Fazlul, Shashi, and friends Balaji, Ejaz, Sneha, Upasana, Subha Anand, Komal, Rajlaxmi, Nisha and many others.

I will gratefully remember the moments with Blesson, Ranjith, Bivin Geo George and Linto. I thank Chithrabhanu, Swapna for sharing a wonderful time in my life. The moments shared with Anju, Apurv, Neetha, Sreeja, Nita, Aswathi and little angels Gargi, Allen and Aaron were really sweet and memorable.

Last but not least, I thank my amma, achan, Smruthy, Lekshmy and her parents for their love and support.

Midhun M

Abstract

Stable oxygen isotope ratios ($\delta^{18}O$) of tree cellulose and speleothem carbonate are useful proxies for past monsoon rain in many tropical regions, as in such region a decrease in rain $\delta^{18}O$ accompanies an increase in rainfall on a monthly time scale. This amount effect varies spatially; therefore a local calibration, with actual measurements of rain amount and its $\delta^{18}O$ is required. Such observations, however, are quite limited in space and time. This thesis is aimed to improve the understanding of factors that control the $\delta^{18}O$ of Indian monsoon rainfall. For the present study water vapor samples were collected from the marine atmosphere over the Bay of Bengal (BoB) and rainfall sampled from Central and Northern India. The multiple simulations from isotope enabled General Circulation Models (GCM) are also used to understand the variability of the $\delta^{18}O$ of the Indian Summer Monsoon (ISM) rainfall on daily to interannual time scales.

Measurements of stable isotopic compositions ($\delta^{18}O$ and δD) of water vapor collected from the BoB helps characterize both ISM vapor and North East Monsoon (NEM) vapor. This study shows that vapor $\delta^{18}O$ is higher during ISM compared to NEM with higher d-excess during NEM. This seasonal difference is possibly due to the seasonality in sea surface conditions, change in circulation pattern and changes in the type of rain forming systems (monsoon depression during ISM vs. tropical cyclones during NEM). The stable isotopic composition of water vapor estimated using Craig and Gordon model with the closure assumption (i.e., evaporation from the BoB is the only source of vapor) matches well with the measured values during non rainy days of ISM, whereas, it shows a large deviation from the model estimate during NEM season. The deviation from model estimate is negatively correlated with the rainfall along parcel trajectory (upstream rainfall) during both the seasons. The convective downdraft associated with tropical cyclones during NEM also plays major role in the lowering of vapor $\delta^{18}O$.

During ISM 2013, rain water samples were collected on a daily basis from six different cities (Ahmedabad, Bhopal, New Delhi, Kanpur, Varanasi and Dhanbad) spread over central and northern India and stable isotopic analyses were carried out. A weak amount effect (negative correlation between local rain and its $\delta^{18}O$) is observed at five out of the six stations, which explains ∼7-22 % of intraseasonal variation of $\delta^{18}O$ of rain. The nudged simulations from an isotope-enabled General Circulation Model (IsoGSM) is compared with the observations. Though the model has some limitation in simulating the accurate spatio-temporal pattern of rainfall, the model simulated rain $\delta^{18}O$ is in good agreement with the observations. This study suggests strong control of moisture transport pathways on daily rain $\delta^{18}O$ at Ahmedabad, Bhopal and New Delhi. At New Delhi this effect is observed on intraseasonal to interannual timescales.

Many isotope enabled General Circulation Models (GCM) are used to aid the interpretation of rainfall-^{18}O based proxies; nevertheless, all such simulations taken together remained to be evaluated against observations over the Indian Summer Monsoon (ISM) region. This study also examine ten such GCM simulations archived by the Stable Water Isotope INtercomparison Group, phase 2 (SWING2). The spatial patterns of simulated ISM rainfall and its $\delta^{18}O$ are in good agreement with the limited observations available. Simulations nudged with observed wind fields show better skill in reproducing the observed spatio-temporal pattern of rainfall and its $\delta^{18}O$. A large discrepancy is observed in the magnitude of the simulated amount effect over the Indian subcontinent between the models and observations, probably because models simulate the spatial distribution of monsoon precipitation differently. Nudged simulations show that interannual variability of rainfall $\delta^{18}O$ at proxy sites are controlled by either regional (rather than local) rainfall or upstream rain out. Interannual variability of rainfall $\delta^{18}O$ over the East Asian region is well correlated with El Niño Southern Oscillation (ENSO), while it is only weakly correlated over the Indian sub-continent.

Key points:

- An important data set of stable isotopic composition of water vapor from Bay of Bengal during ISM and NEM were generated and studied for the first time.
- The role of moisture pathways on ISM rainfall $\delta^{18}O$ variability over central and northern India is addressed using observations and model simulation.
- The present day ISM simulations from ten isotope-enabled GCMs were validated and used to examine the factors that control interannual variability of ISM rainfall $\delta^{18}O$.

Keywords: *Indian Summer Monsoon, Stable water isotopologues, Amount effect, isotope enabled General Circulation Models, Paleomonsoon*

Abbreviations

δD	Stable hydrogen isotopic composition of water relative to VSMOW standard.
δD_p	Stable hydrogen isotopic composition of precipitation relative to VSMOW standard.
δD_v	Stable hydrogen isotopic composition of water vapor relative to VSMOW standard.
$\delta^{18}O$	Stable oxygen isotopic composition of water relative to VSMOW standard.
$\delta^{18}O_p$	Stable oxygen isotopic composition of precipitation relative to VSMOW standard.
$\delta^{18}O_v$	Stable oxygen isotopic composition of water vapor relative to VSMOW standard.
‰	per mil (parts per thousand).
AS	Arabian Sea.
BoB	Bay of Bengal.
CAM	Community Atmosphere Model.
CE	Common Era.
CMAP	CPC Merged Analysis of Precipitation.
ECMWF	The European Center for Medium-Range Weather Forecasts.

ENSO	El Niño Southern Oscillation.
GCM	General Circulation Model.
GISS	Goddard Institute for Space Studies.
GMWL	Global Meteoroic Water Line.
GNIP	Global Network for Isotopes in Precipitation.
GPCP	Global Precipitation Climatology Project.
HadAM	Hadley Center Atmospheric Model.
HYSPLIT	The Hybrid Single Particle Lagrangian Integrated Trajectory Model.
IAEA	International Atomic Energy Agency.
IRMS	Isotopic Ratio Mass Spectrometer.
ISM	Indian Summer Monsoon.
IsoGSM	Isotope-enabled General Spectral Model.
IST	Indian Standard Time.
ITCZ	Inter Tropical Convergence Zone.
JJAS	June, July, August, September.
LLJ	Low Level Jet.
LMDZ	Laboratoire de Meteorologie Dynamique GCM.
MERRA	Modern-Era Retrospective Analysis For Research And Applications.
MIROC	Model for Interdisciplinary Research on Climate.

NARM	Internal laboratory slandered: NARMada river water.
NCEP	National Center for Environmental Prediction.
NEM	North East Monsoon.
NOAA	National Oceanic and Atmospheric Administration.
PCE	Post Condensation Exchange.
SST	Sea Surface Temperature.
SWI	Stable Isotopologueous of Water.
SWING2	Stable Water Isotope INtercomparison Group, phase 2 (SWING2).
TRMM	Tropical Rainfall Measuring Mission.
VSMOW	Vienna Standard Mean Ocean Water.
WMO	World Meteorological Organization.

Contents

List of Figures

List of Tables

Chapter 1

Introduction

Global climate change has become a major concern for both the public and scientists. The climate modeling community is engaged in developing new, state-of-the art models to predict anticipated temperature rise in the future. As most of the processes in climate are coupled through different feedback mechanisms, it is quite a challenge to understand the consequences of global warming (e.g.: - changes in rainfall, intensity and frequency of storms, etc.). In this situation, deciphering the past climate changes is a novel approach to understand long term climate variability resulting from different natural and man made forcings. Since the availability of observed climate data is limited at the best to last two the centuries, scientists examine some "climate imprints" which are called climate proxies, to understand past climate variability. Stable isotopologues of water in precipitation ($H_2^{18}O$, HDO etc), which get recorded in climate proxies such as ice core, speleothem, tree ring, etc have been successfully used in the reconstruction of past climate. These reconstructions are done using the temperature effect (a positive linear correlation between the surface air temperature and the relative concentrations of $H_2^{18}O$ or HDO with respect to H_2O) in high latitudes and the amount effect (a negative correlation between the amount of rain and the relative concentrations of $H_2^{18}O$ or HDO with respect to H_2O) in the tropics. But, in India, located in the tropical monsoon region, the amount effect shows large spatial variations. So more observations and studies are required to understand the major climate controls on the variability of stable water isotopologues in the

Indian monsoon rainfall.

1.1 Indian summer monsoon

The seasonal reversal of wind associated with the migration of east-west oriented Inter Tropical Convergence Zone (ITCZ) gives enhanced rainfall over India and adjoining countries during the boreal summer [*Gadgil*, 2003]. This is called the Indian Summer Monsoon (ISM). ∼80% of the annual total rainfall over Indian plains occurs during the ISM season (June to September). Since ISM rainfall is the major source of water for agriculture over India, inter-annual variations of ISM have a major impact on food production and consequently on the economy of the country [*Gadgil and Gadgil*, 2006]. Moreover, the occurrence of drought (10 % deficit in the ISM seasonal total rain compared to its long-term mean $\sim 85cm$) and floods associated with excess monsoon (10 % excess in the ISM seasonal total rain compared to its long-term mean) causes serious damage to ecosystems, and injury and loss of human life. Thus understanding the causes of interannual variations of ISM is important to make an accurate forecast and projection of ISM under the global warming scenario.

During the boreal summer, due to increased solar radiation over northern hemisphere, a low pressure forms over northern India, called the heat low. This extends from north-Rajasthan to Kolkata and is called the monsoon trough. At the same time, the southern hemisphere experiences winter and forms a high pressure area over the subtropical Indian ocean, called the Mascarene High. This latitudinal pressure gradient causes a strong cross equatorial flow (at the western equatorial Indian ocean) which further become south westerly due to the Coriolis force and hits the Indian continent (Fig 1.2). This south westerly wind is called the Low Level Jet stream (LLJ). LLJ brings moist air from the Indian ocean to the Indian sub-continent and this air mass is uplifted by strong convection over the Indian subcontinent and the Bay of Bengal (BoB). The counterpart of LLJ, at 200 hPa, is the strong easterly jet which completes the Hardly-cell-like monsoon circulation.

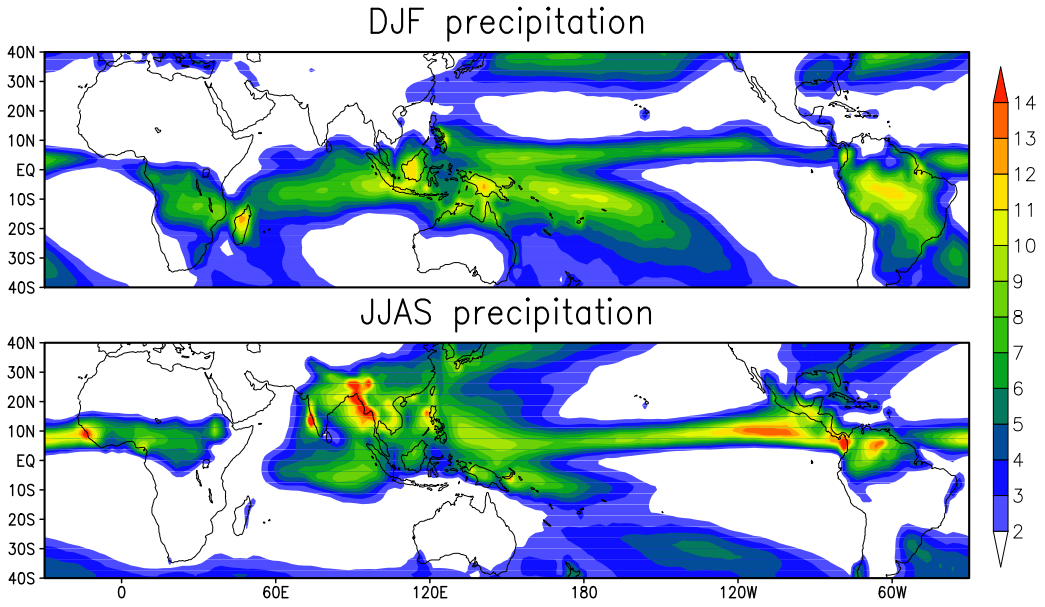

Figure 1.1: *Seasonality of ITCZ. Average rainfall (mm/day) during December to February (top panel) and June to September (bottom panel). The seasonal migration of east-west oriented rainfall belt (ITCZ) can be seen in the figure (source: GPCP data).*

ISM shows variability on different timescales due to both internal dynamics and external forcings. However the observational data is limited to mid 19^{th} century, which limits our understanding of monsoonal variability on longer timescales. Thus isotope based proxies could offer very important new data on monsoon variability. This thesis is focused on understanding the isotope-climate linkage, which will be helpful to interpret stable isotope (e.g., $\delta^{18}O$) based proxies over the ISM region.

1.2 Stable isotopologues of water

Isotopes are atoms with the same atomic number but different masses due to difference in the number of neutrons. Isotopes are classified into two; radioactive isotopes which undergo different types of nuclear decay and stable isotopes which do not undergo any decay. In the case of water, there are two stable isotopes for hydrogen (^{1}H and ^{2}H) and three for oxygen (^{16}O,^{17}O and ^{18}O). Water molecules

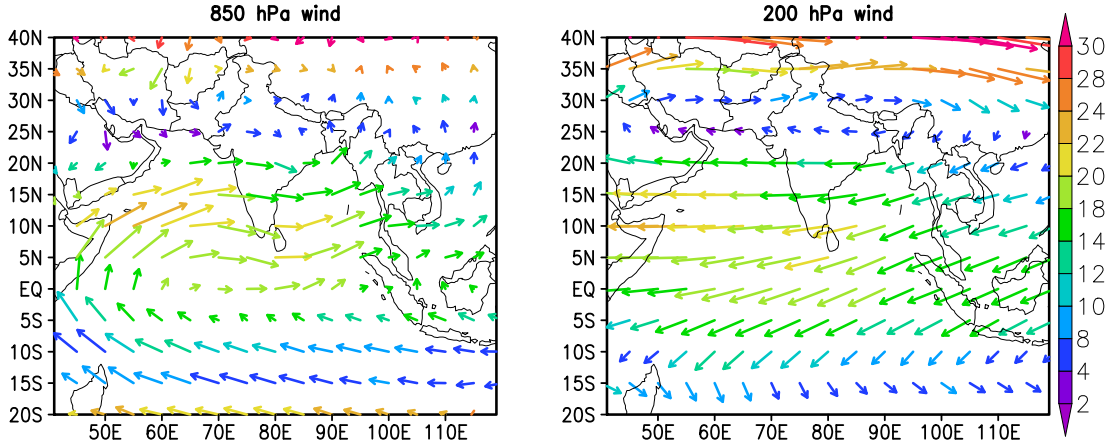

Figure 1.2: *Climatological (1981-2010 CE) mean lower tropospheric (850 hPa) and upper tropospheric (200 hPa) wind vectors during ISM (source: NCEP Climate Forecast System Reanalysis). Color of the arrow shows wind speed according to the scale on right.*

formed by different combinations of these isotopes are called stable isotopologues of water (Table. 1.1). In the literature they are also called *stable water isotopes* (SWI).

1.2.1 Notations

Isotopic ratio: Isotopic ratio is the ratio of the abundances of the heavier isotope and lighter (i.e., more abundant) isotope.

$$R = \frac{\text{Abundance of the heavier isotope}}{\text{Abundance of the lighter isotope}} \; (e.g., \frac{^{18}O}{^{16}O}, \frac{D}{H})$$

In mass spectrometry, the measurement of the the absolute abundances of isotopes are not made, but the relative variations of isotopic ratios are reported. For this, ratios are expressed in terms of deviations (δ) from the isotopic ratio of an international standard. Water isotopic compositions are mostly reported with respect to the standard provided by the International Atomic Energy Agency (IAEA): Vienna Standard Mean Ocean Water (VSMOW) [*Gonfiantini*, 1978]. For example, the heavy isotopic content (D or ^{18}O) in a water sample is reported

Table 1.1: *Stable isotopes of hydrogen and oxygen and their different combinations form water isotopologues, and their natural abundances [source: Clark and Fritz, 1997].*

Isotope	Abundance (%)	Water isotopologues	Abundance (%)
H	99.98	$H_2{}^{16}O$	99.73
D	0.015	$HD^{16}O$	0.015
^{16}O	99.76	$D_2{}^{16}O$	2.24×10^{-6}
^{17}O	0.035	$H_2{}^{17}O$	0.035
^{18}O	0.205	$HD^{17}O$	5.25×10^{-6}
		$D_2{}^{17}O$	7.88×10^{-10}
		$H_2{}^{18}O$	0.20
		$HD^{18}O$	3.07×10^{-5}
		$D_2{}^{18}O$	4.6×10^{-6}

as follows.

$$\delta D = \left(\frac{R_{Sample}}{R_{Standard}} - 1 \right) \times 10^{3}\text{‰}$$
$$\delta^{18}O = \left(\frac{R_{Sample}}{R_{Standard}} - 1 \right) \times 10^{3}\text{‰}$$

1.2.2 Isotopic fractionation

Relative mass difference and changes in the moment of inertia and symmetry of isotopically substituted water molecules ($H_2^{18}O$ or HDO) lead to changes in its thermodynamical properties (e.g., vapor pressure) as well as physical properties (e.g., rate of diffusion) relative to lighter water molecule (H_2O). This results in the redistribution of abundances of isotopologues during chemical or physical processes. This effect is called fractionation. The fractionation factor (α) is defined as the ratio of isotopic ratios in two co-existing phases (or the ratio of isotopic ratios of product to that of reactant). i.e., α between vapor and liquid is

$$\alpha_{vapor}^{liquid} = \frac{R_{liquid}}{R_{vapor}}$$

In ‰ (per mille) notation α is represented as,

$$\epsilon = (\alpha - 1).10^3$$

In hydrological cycle water isotopologues may undergo two kind of fractionation processes as described below.

Equilibrium fractionation

Equilibrium fractionation occurs at thermodynamic equilibrium conditions. e.g., condensation, equilibration of water vapor and water in a closed system. Equilibrium fractionation (hereafter α refers to equilibrium fractionation only) is more at low temperature and disappears at very high temperature. It can be written as a function of temperature (T in Kelvin) as follows.

$$\alpha = \exp\left(\frac{C_1}{T^2} + \frac{C_2}{T} + C_3\right)$$

When $T > 273.15$K, $C_1 = 1137$, $C_2 = -0.4156$ and $C_3 = -0.002066$ for ^{18}O and $C_1 = 24884, C_2 = -76.248$ and $C_3 = 0.052612$, for D. In the case of $T < 273.15$K, $C_1 = 0$, $C_2 = 11.839$ and $C_3 = -0.028224$ for ^{18}O and $C_1 = 16289, C_2 = 0$ and $C_3 = -0.0945$, for D. These constants were empirically determined by *Majoube* [1971a,b]

Kinetic fractionation

Kinetic (also called as non-equilibrium) fractionation is a type of isotopic fractionation associated with diffusion of water molecules. When water vapor moves across a humidity gradient in the atmosphere, it experiences fractionation due to the lower diffusivity of the heavier isotopologues. When water vapor undergoes diffusion, the associated kinetic isotopic fractionation (α_k) can be written as

$$\alpha_k = \frac{\rho}{\rho_i}$$

where ρ is the resistance to diffusive flow for the lighter isotopologoue (H_2O) and ρ_i is that for the heavier isotopologoue (i.e.,$H_2^{18}O$ or HDO). ρ can be split into

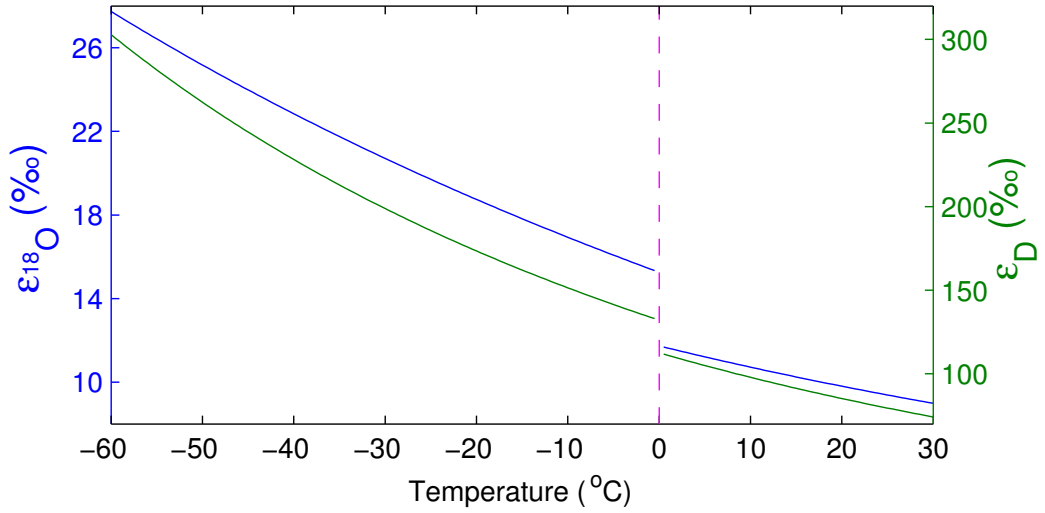

Figure 1.3: *Equilibrium fractionation factor (in ‰ units) as a function of temperature [Majoube, 1971a,b]. Below zero the equilibriam fractionation is between ice and vapor whereas, above zero vapor and water are in isotopic equilibrium. This causes the discontinuity at 0°C. (Blue-oxygen isotopes; green-hydrogen isotopes)*

two components, molecular (ρ_m) and turbulent (ρ_t). Since $\rho = \rho_m + \rho_t$, α_k can be written as

$$\alpha_k = \frac{\rho_m + \rho_t}{\rho_{m,i} + \rho_{t,i}} = \frac{1}{\rho_{m,i}/\rho + \rho_{t,i}/\rho}$$

Now we define $\theta = \rho_m/\rho$, where $\theta = 1$ represents pure molecular diffusion and $\theta = 0$ represents pure turbulent diffusion. Turbulent transport does not cause isotopic fractionation. i.e., $\rho_{t,i} = \rho_t$. Thus α_k can be written as

$$\alpha_k = \frac{1}{\theta(\rho_{m,i}/\rho_m) + 1 - \theta}$$

ρ_m is proportional to D^{-n} where D is the molecular diffusivity of water through air and the exponent n varies from 1 (for a stagnant diffusion layer) to 0.5 (for a moderately turbulent layer). Finally, the expression for kinetic fractionation factor is

$$\alpha_k = \frac{1}{1 - \theta + \theta\left(\frac{D_i}{D}\right)^n} \tag{1.1}$$

Molecular diffusivity of a gas A through gas B (e.g., water vapor through air) as given by the gas kinetic theory,

$$D_{A,B} \propto \frac{(\frac{1}{M_A} + \frac{1}{M_B})T^3}{P\sigma_{A,B}^2 \Omega_{A,B}}$$

Where M = molecular mass, T= absolute temperature, P= total pressure, σ = sum of atomic radii and Ω =interactive correction term [*Chapman and Cowling*, 1970]. The above equation predicts the value for $D_{HDO}/D_{H_2O} = 0.9852$ and $D_{H_2^{18}O}/D_{H_2O} = 0.9708$, but the actual measured values are 0.9756 and 0.9703 respectively [*Merlivat*, 1978].

1.3 Modeling of fractionation of water isotopologues

1.3.1 Rayleigh model

The Rayleigh model predicts the evolution of the stable isotopic composition of a reservoir from which the substance is continuously removed. [*Clark and Fritz*, 1997]. For example, in the atmosphere, when a moist air mass cools (either by adiabatic expansion or radiative cooling) its relative humidity becomes 100 % and it starts to condense. During condensation fractionation occurs in isotopic equilibrium and the remaining vapor (rain) gets depleted(enriched) in ^{18}O (and D). The Rayleigh model assumes that, i) the abundance of heavier isotopes (N^*) is much less than that of the lighter (N), ii) the process occurs under instantaneous isotopic equilibrium, iii) the process is isothermal and iv) no isotopic gradient exists across the reservoir. At any instant, the stable isotope ratio of the vapor (R) and rain is given by

$$R = \frac{N^*}{N}$$

$$\text{isotopic ratio of instantaneous rain} = \frac{dN^*}{dN}$$

on differentiating R

$$dR = \frac{dN^*}{N} - \frac{RdN}{N}$$

By definition $\alpha = \frac{dN*}{dN}/\frac{N^*}{N} = \frac{dN*}{dN}/R$. i.e.,$\frac{dN*}{N} = \alpha R\frac{dN}{N}$. Then the above equation becomes

$$\frac{dR}{R} = (\alpha - 1)\frac{dN}{N}$$

on integrating from initial isotopic ration R_0 to final R and from the initial abundance of lighter isotope from N_0 to N

$$R = R_0 f^{\alpha-1} \tag{1.2}$$

Where f is the fraction of substance remaining in the reservoir (i.e., $f = \frac{N+N*}{N_0+N*_0} \approx \frac{N}{N_0}$). Taking natural logarithm on both sides of equation 1.2 and assuming $\ln(1 + \delta \times 10^{-3}) = \delta \times 10^{-3}$, the Rayleigh equation becomes

$$\delta = \delta_0 + (\alpha - 1)10^3 \ln f \tag{1.3}$$

The variation of the oxygen and hydrogen isotopic composition of the water vapor, rain and the accumulated rain formed from the vapor at any instant according to Rayleigh fractionation model are shown in Fig 1.4 [*Clark and Fritz*, 1997].

1.3.2 Isotope enabled general circulation model

A general circulation model (GCM) is a numerical model of the global atmospheric circulation. GCM basically solves numerically a set of equations called the primitive equations. These consist of i) equation of continuity, ii) conservation of momentum, iii) thermodynamic energy equations, and iv) equation for hydrostatic equilibrium. A detailed description of these equations is beyond the scope of this thesis [please see *Washington and Parkinson*, 2005]. Stable isotopologues are incorporated into GCMs (called isotope enabled GCMs) hydrological cycle as tracers [i.e, $H_2^{18}O$ and HDO in addition to H_2O, *Joussaume et al.*, 1984]. In such GCMs these tracers ($H_2^{18}O$ and HDO) undergo transport and other physical process similar to that of normal water (H_2O) but with different rates (fractionation) during diffusion and phase change. Isotopic fractionation is parametrized

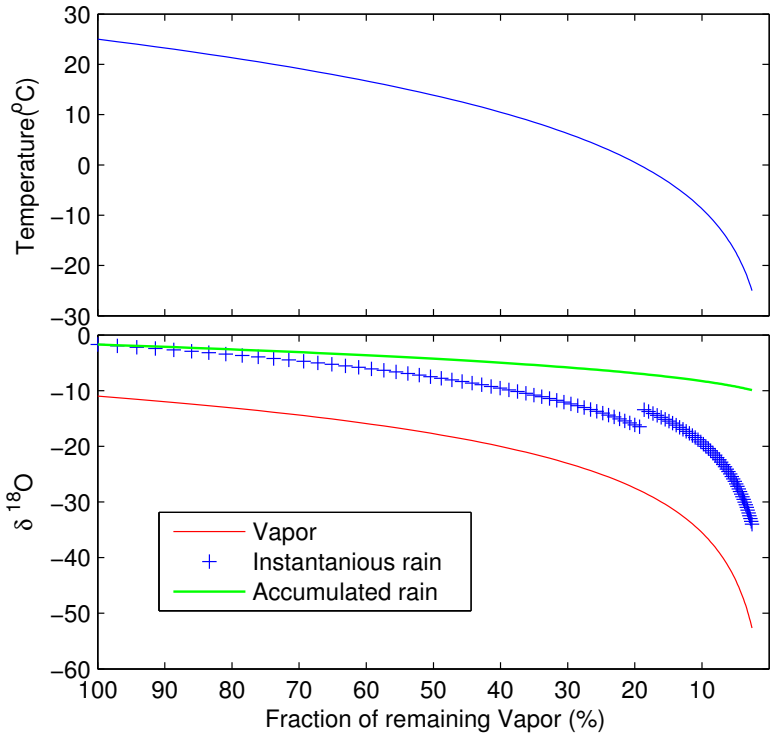

Figure 1.4: *Rayleigh model: An air mass cooled from* 25^oC *to* -25^oC *condenses. Its fraction of remaining vapor is calculated using the Clausius-Clapeyron equation (top panel). Isotopic compositions of remaining vapor, instantaneous rain and accumulated rain are calculated using the Rayleigh model. At any instant, the average temperature from the starting point is used for calculating the fractionation factor* (α)*. The* $\delta^{18}O$ *of instantaneous rain show a discontinuity at* 0^oC *due to the discontinuity in equilibrium fractionation factor. Initial* $\delta^{18}O$ *of the vapor is* $-11‰$

in terms of meteorological variables (temperature, humidity etc.). A general description about parameterization of isotopic fractionation used in isotope enabled GCMs is given below:-

The Craig-Gordon model for evaporation

Craig and Gordon [1965] developed a model to describe the isotopic fractionation associated with evaporation. In this approach evaporation occurs in two steps, i) at a saturated liquid-air interface where both condensation and escape from liquid surface occur, and isotopic equilibrium is maintained ii) above the saturated

layer, due to humidity gradient, water molecule diffuses. The diffusion above the equilibrium layer involves both turbulent and molecular diffusions. Molecular diffusion causes kinetic fractionation, while turbulent diffusion does not.

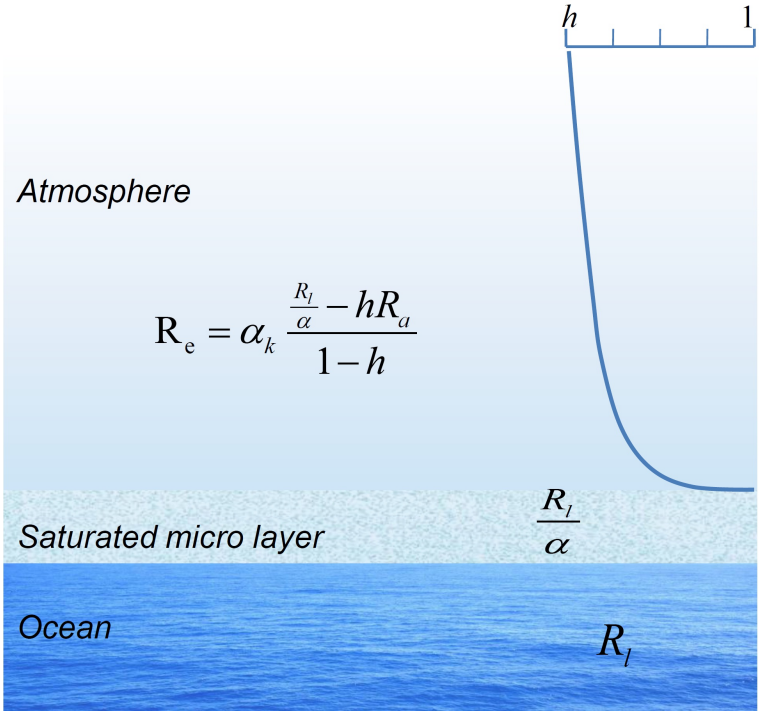

Figure 1.5: *A schematic representation of the Craig-Gordon model for the isotopic fractionation during evaporation.*

The evaporation flux E across the diffusion layer above the liquid-air interface is given by

$$E = \frac{q_s - q}{\rho} = \frac{q_s(1-h)}{\rho} \tag{1.4}$$

where q_s is the saturation mixing ratio of water vapor at the liquid-air interface, q is the water vapor mixing ratio at the turbulent atmosphere, ρ is the resistance coefficient and h is the atmospheric relative humidity normalized to the liquid surface temperature. h (hereafter called normalized humidity) is calculated as follows:-

$$h = \frac{q}{q_s(SST)} \tag{1.5}$$

where q is the mixing ratio of water vapor in the atmosphere and $q_s(SST)$ is the saturation water vapor mixing ratio at sea surface temperature. Equation 1.4 can

be modified for each isotopologoue (subscript i for HDO or $H_2^{18}O$) as follows

$$E_i = \frac{q_{si} - q_i}{\rho_i} = \frac{q_s(R_l/\alpha - hR_a)}{\rho_i} \tag{1.6}$$

where α is the equllibrium fractionation factor between liquid and vapor (> 1), R_l is the isotopic ratio of evaporating water body (e.g., lake water) and R_a is that of boundary layer water vapour. Dividing equation 1.6 with equation 1.4 gives

$$R_e = \frac{R_l/\alpha - hR_a}{(1-h)\rho_i/\rho} \tag{1.7}$$

Where R_e is the isotopic ratio of evaporation flux. Substituting $\alpha_k = \rho/\rho_i$ in equation 1.7 gives

$$R_e = \alpha_k \frac{R_l/\alpha - hR_a}{(1-h)} \tag{1.8}$$

α_k is the kinetic fractionation factor. This equation is widely used in the isotope enabled General Circulation Models [e.g., *Risi et al.*, 2010a; *Yoshimura et al.*, 2008] to calculate isotopic ratio of evaporation flux from open water bodies.

The values for α_k in the above equation is calculated using the equation (1.1 with suitable choice of θ and n. For evaporation from ocean, *Merlivat and Jouzel* [1979] parameterized α_k as a function of near surface wind speed as follows:

$$\alpha_k = \begin{cases} 1 - A, \text{ for } V < 7(m/s) \\ 1 - (B.V + C), \text{ for } V > 7(m/s) \end{cases} \tag{1.9}$$

Where V is the wind velocity at 10 m above ocean surface and constants A, B, and C are respectively 0.006, 0.000285, and 0.00082 for ^{18}O and 0.00528, 0.0002508, and 0.0007216 for ^{2}H. This method is widely used in isotope enabled GCMs.

Condensation

For condensation due to supersaturation, models assume equilibrium fractionation. But when temperature (T) goes below -20^oC, in a supersaturated condition, vapor to ice deposition takes place. In this process, diffusion occurs resulting in kinetic fractionation. So generally models parametrize effective fractionation (α_{eff}) during condensation as follows.

$$\alpha_{eff} = \alpha \left(\frac{S}{\alpha\ (D/D')(S-1)+1} \right) \tag{1.10}$$

$$S = \begin{cases} 1, \text{ for } T > -20^{o}C \\ 1 - \lambda T, \text{ for } T < -20^{o}C \end{cases} \tag{1.11}$$

where S is the super saturation index parameterized by T and λ is a tunable parameter which varies among isotope-GCMs and ranges from 0.003 to 0.005.

Post-condensation exchange

When a raindrop falls down through the atmosphere, it experiences evaporation depending upon the ambient humidity. Similar to the Craig and Gordon model, the raindrop will be in isotopic equilibrium with the vapor on the drop's surface (a saturated layer) and it diffuses into the ambient atmosphere according to the humidity gradient. *Kinzer and Gunn* [1951] developed the equation for calculating the rate of mas loss of rain drop (i.e., $\frac{dm}{dt}$, where m is the mass of rain drop)

$$\frac{dm}{dt} = 4\pi a(X_a - X_b)kD^{-n} \tag{1.12}$$

where $k = F(aV/2\pi)^{\frac{1}{2}}$. a, V, X_a, X_b and F are respectively the radius of the rain drop, fall velocity of rain drop, water vapor density at the surface of rain drop, water vapor density at the ambient atmosphere and ventilation factor. D, n are same as defined in the section 1.2.2 (in this case n =0.58). By dividing the isotopic analogue of equation 1.12 with equation 1.12 and re-arranging [*Stewart*, 1975], we get,

$$m\frac{dR_r}{dm} = \beta\left(R_r - \gamma R_v\right)$$

where R_r and R_v are isotopic ratio of rain drop and ambient vapor. Here $h = X_b/X_a$, $\beta = (1-\mu)/\mu$, $\gamma = \alpha h/(1-\mu)$, $\mu = \alpha\left(D/D_i\right)^n(1-h)$. On integrating above equation

$$R_r = (R_{r0} - \gamma R_{v0})(m/m_0)^{\beta} + \gamma R_{v0} \tag{1.13}$$

Subscript 0 refers to the initial values before the isotopic exchange. When h =1, equation 1.13 becomes $R_r \approx \alpha R_{v0}$, i.e., isotopic equilibrium between rain and vapor. When h is close zero, equation 1.13 becomes $R_r \approx R_{r0}(m/m_0)^{\left(\frac{1}{\alpha(D/Di)^n}-1\right)}$, which predict a Rayleigh-like enrichment in R_r. However, the final value of R_r will depends on the parameters such as rain type (convective or stratiform) rain drop distribution etc. Hence many models assume that ∼45 % of rain undergoes post condensation exchange (PCE) during convective rainfall, while ∼95 % of stratiform rainfall undergoes PCE. Thus the resultant isotopic ratio will be

$$R_r = A\left[(R_{r0} - \gamma R_{v0})(m/m_0)^{\beta} + \gamma R_{v0}\right] + (1 - A)R_{r0}$$

where A is the fraction of precipitation that undergoes PCE.

1.4 Observed isotopic effects in precipitation

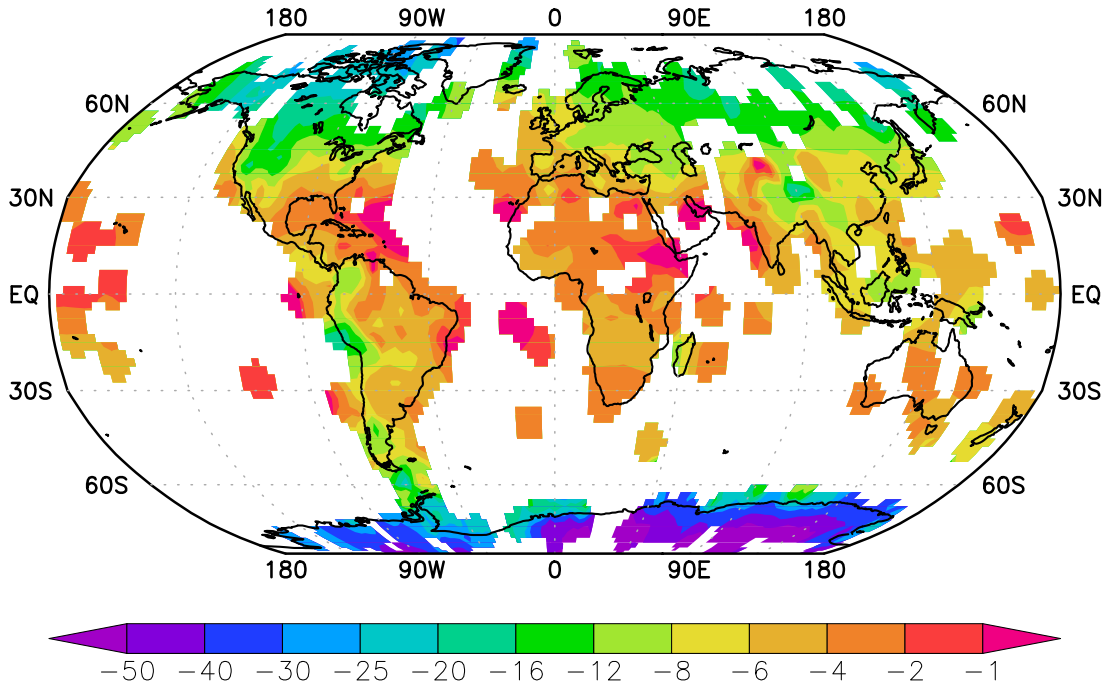

Figure 1.6: *Global annual mean $\delta^{18}O$ of precipitation. Data sources: GNIP data and Antarctica snow isotope data from Masson-Delmotte et al. [2008].*

Temperature effect

A strong positive relation is observed between the mean annual surface temperature and $\delta^{18}O_p$ (Fig. 1.7). The major source of vapor is the evaporation from tropical ocean. This vapor is transported towards the poles. In such a case, the temperature effect can be explained using the Rayleigh equation (Fig. 1.4 and Eq. 1.2). When vapor moves from the equator to the poles, due to the decreasing temperature, vapor starts condensing and this leads to further ^{18}O depletion in the vapor. According to equation 1.2, the magnitude of this depletion mainly depends on the fraction of remaining vapor (f), which is proportional to the temperature (Clausius-Clapeyron relation). This leads to the observed temperature-$\delta^{18}O_p$ relation. The temperature effect results in two other kinds of isotopic effects; the **latitude effect** (progressive reduction in $\delta^{18}O_p$ towards poles, Fig. 1.6) and the **altitude effect** (reduction in $\delta^{18}O_p$ with increase in altitude, Fig. 1.8)

Continental effect

A progressive depletion in $\delta^{18}O_p$ with increasing distance from the moisture source (usually distance from the ocean) is observed. This is due to the progressive rain out with preferential removal of ^{18}O during the rain which results in the ^{18}O depletion of the remaining vapor and causes further ^{18}O depletion in downstream rainfall. An example is shown in Fig. 1.9.

Amount effect

In tropics no temperature effect is observed, instead an anti-correlation between monthly precipitation and $\delta^{18}O_p$ (Fig.1.10) is observed. Many studies carried out using numerical models (ranging from a simple 1-D model to isotope enabled GCMs) to understand the physical mechanisam that leads to the amount effect [*Dansgaard*, 1964; *Lee and Fung*, 2008; *Risi et al.*, 2008, 2010b] show the major reasons to be: i) Heavier isotopologues preferentially condense during precipitation; higher the rainfall, larger is the depletion in ^{18}O of the remaining vapor, leading to a stronger ^{18}O depletion of rain, ii) ^{18}O enrichment in rain due to

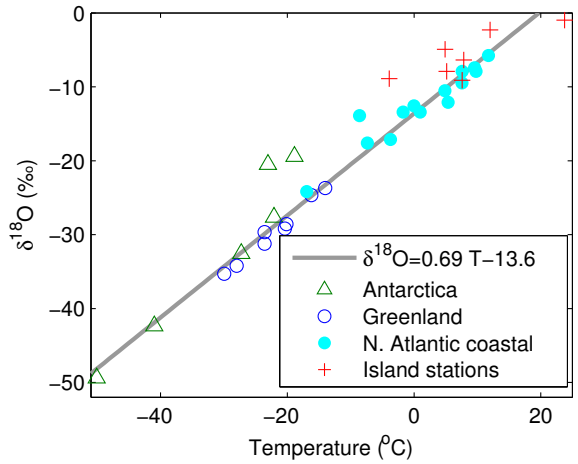

Figure 1.7: *Global T-$\delta^{18}O_p$ relation. Figure modified from Dansgaard [1964]*

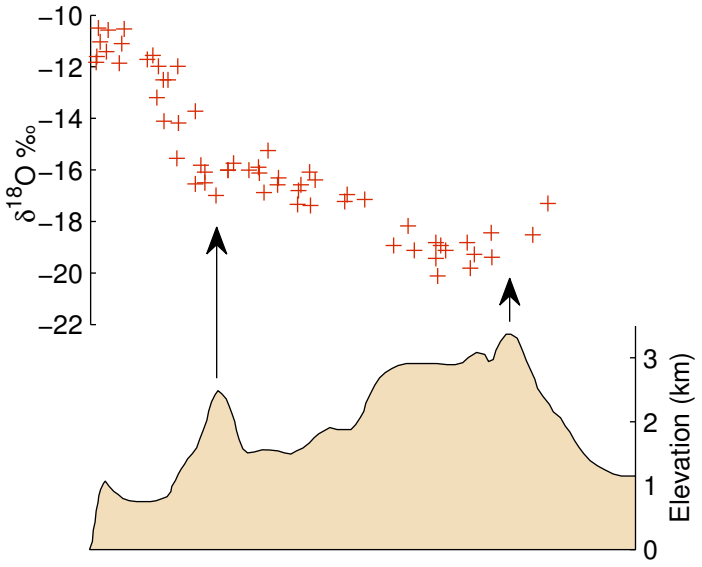

Figure 1.8: *Altitude effect: variations in $\delta^{18}O_p$ along a high altitude mountain region [source: Clark and Fritz, 1997]*

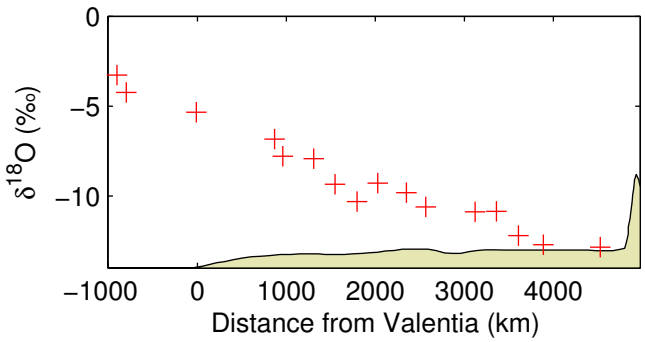

Figure 1.9: *Continental effect: variation in $\delta^{18}O_p$ as function of distance from the ocean [source: Clark and Fritz, 1997]*

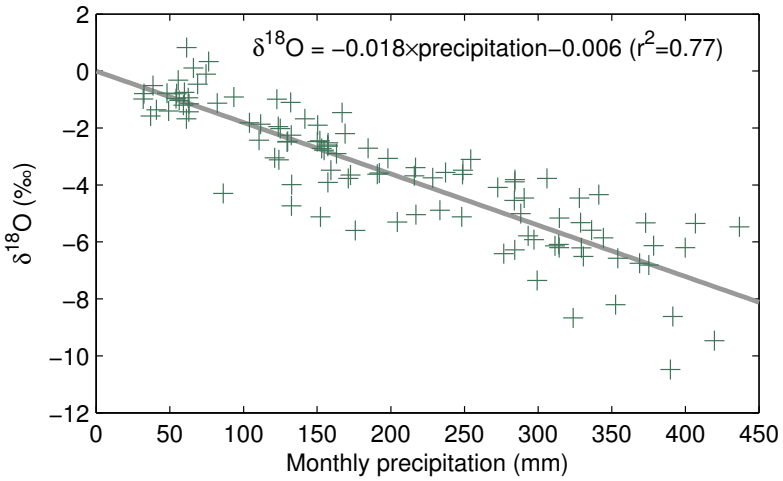

Figure 1.10: *Amount effect: relationship between mean monthly $\delta^{18}O_p$ and rainfall. Data were taken from nine selected tropical Island GNIP stations [Bony et al., 2008].*

re-evaporation of rain at sub-cloud level, which is likely to be higher when rain amounts are low, and iii) more intense the convection, the stronger are the convective downdrafts, bringing more of ^{18}O depleted vapor from higher altitudes to the sub-cloud layer and subsequently feeding the system through convective updraft. Recent studies suggest that the $\delta^{18}O_p$ variability in the tropics is also related to the extent of organized convection, the $\delta^{18}O$ of vapor that converges at low levels or the altitude of moisture convergence [*Kurita*, 2013; *Lawrence*, 2004; *Lekshmy et al.*, 2014; *Moore et al.*, 2014], in addition to the rain amount.

1.5 Global meteoric water line and *d*-excess

In the global data on precipitation $\delta^{18}O$ and δD collected by the Global Network of Isotopes in Precipitation (GNIP, a linear relation between δD and $\delta^{18}O$ is observed. *Craig* [1961] reported this as $\delta D = 8\times\delta^{18}O+10$. This is called Global Meteoric Water Line (GMWL). The slope 8 of GMWL can be explained using the Rayleigh model as demonstrated below:-

Instantaneous vapor δ (δ_v) according to the Rayleigh model can be written as

$$(\delta_v + 1000) = (\delta_{v0} + 1000) f^{\alpha-1}$$

Where δ_{v0} is the initial vapor isotopic composition. On differentiating the above equation,

$$d\delta_v = (\delta_{v0} + 1000)(\alpha - 1) f^{\alpha-2} df$$

Using the above two equations,

$$d\delta_v = (\delta_v + 1000)(\alpha - 1)\frac{df}{f}$$

Thus the slope of $\delta^{18}O$-δD relations can be written as

$$\frac{d\delta D_v}{d\delta^{18}O_v} = \underbrace{\left(\frac{\delta D_v + 1000}{\delta^{18}O_v + 1000}\right)}_{1}\underbrace{\left(\frac{\alpha_D - 1}{\alpha_{^{18}O} - 1}\right)}_{2} \tag{1.14}$$

In the above equation term 2 varies from 8.22 at 30^oC to 11.1 at -30^oC. Term 1 varies from ∼0.9 at tropics to ∼0.7 at poles. Hence the resultant slope during Rayleigh condensation process exhibits a slope close to 8. The intercept 10 is attributed to the kinetic effect during evaporation from the ocean. *i.e.,* when rainfall follows a slope of 8 on $\delta^{18}O$-δD diagram, the intercept depends on the initial $\delta^{18}O$ and δD of source vapor. Hence the intercept of 10 is corresponds to the global average d-excess (Deuterium excess), a parameter defined below.

d-excess is defined as

$$d\text{-excess} = \delta D - 8 \times \delta^{18}O \tag{1.15}$$

Condensation at isotopic equilibrium maintains a slope close to 8 which keep the d-excess of rain invariant. Hence d-excess of rain is more likely to preserve its source vapor d-excess values. During evaporation from the ocean, kinetic fractionation occurs. According to *Merlivat and Jouzel* [1979], the extent of kinetic

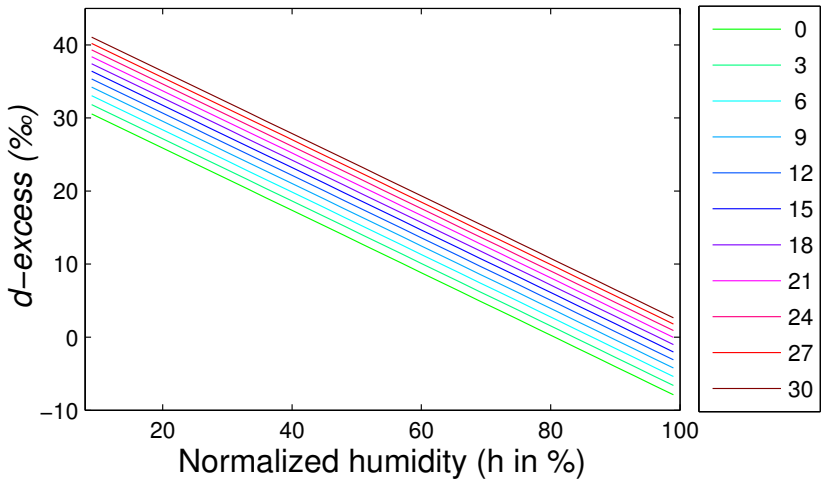

Figure 1.11: *The relationship between d-excess and normalized humidity for different values of SST (colored lines, SST in °C), predicted by Merlivat and Jouzel [1979] with the closure assumption.*

fractionation depends on the normalized humidity above the sea surface. The kinetic fractionation factors of D and ^{18}O are comparable whereas equilibrium fractionation factor of D is eight times higher than ^{18}O. Thus a negative relation between the normalized humidity and d-excess is expected. Figure 1.11 shows the relationship predicted by *Merlivat and Jouzel* [1979] using the closure assumption (i.e., R_e=R_a in equation 1.8).

1.6 Rationale behind the present study

Limited observational data on $\delta^{18}O_p$ (e.g., GNIP) over the ISM region indicate large spatial variations in the amount effect. South western coastal India and north-eastern India show no, or even an inverse (i.e., a positive correlation between $\delta^{18}O_p$ and rainfall) amount effect [*Breitenbach et al.*, 2010; *Warrier et al.*, 2010; *Yadava et al.*, 2007] whereas inland stations do show a significant amount effect [*Yadava and Ramesh*, 2005]. Hence a more quantitative understanding of isotope climate linkage in the ISM region may help improve the calibration of paleomonsoon proxies. Limited spatial and temporal coverage of $\delta^{18}O_p$ data complemented with data from an isotope enabled GCM could be useful in this

endeavor.

Over the ISM region, vapor from BoB is one of the major sources of moisture. The factors controlling the $\delta^{18}O$ and d-excess of marine boundary layer is essential to understand the $\delta^{18}O$ of precipitation at any land site. However, a systematic study on marine vapor isotopic composition is globally very rare [*Gat et al.*, 2003; *Uemura et al.*, 2008].

Over the Asian monsoon region, pioneering work using GCM was done by *Hoffmann and Heimann* [1997] using ECHAM3, demonstrating the control of amount of precipitation on seasonal and spatial distribution of $\delta^{18}O_p$ over the monsoon region. Later ECHAM4 [*Vuille et al.*, 2005] produced a strong temperature effect in the tropics, but unsupported by observations: the simulated amount effect too was stronger than in observations. A negative relation between the interannual variation of monsoon $\delta^{18}O_p$ and the JJAS wind shear index, which is a good indicator of large scale monsoon circulation intensity was also found. More recently, *Ishizaki et al.* [2012] showed that condensation along the trajectory before an air mass reaches a site drives interannual variation of $\delta^{18}O_p$ at the site, using an isotope enabled model (CCSR/NIES/FRCGC AGCM5.7b).

Although the parameterization of isotopic fractionation relies on simple equations, $\delta^{18}O_p$ simulated by GCMs is highly sensitive to other physical parameterizations, such as the ones for convection and boundary layer. [*Field et al.*, 2014; *Lee et al.*, 2009; *Noone and Sturm*, 2010]. As the parameterization of convection in the tropics differs significantly among models, inference based on a single model output could perhaps be biased. Consequently, an inter-comparison of multi-model simulations could be quite useful to improve our understanding of isotope-climate linkages.

1.7 Objectives of the present study

- To understand the stable isotopic characteristics of monsoon vapor over the Bay of Bengal, a source of monsoon rain for central and northern India.
- To understand the role marine surface conditions and other atmospheric processes on the $\delta^{18}O$ and d-excess of marine vapor.
- To understand the factors that control the $\delta^{18}O$ variability of ISM rainfall over central and northern India.
- To validate the simulations from an isotope enabled GCM using a new high resolution $\delta^{18}O_p$ and δD_p data set, generated by author.
- To check the performance of different isotope enabled GCMs in predicting the spatio-temporal distribution of ISM $\delta^{18}O_p$.
- To understand the controls on interannual variability of ISM $\delta^{18}O_p$ using both observations and isotope enabled GCM simulations.

1.8 Outline of the thesis

This thesis contains six chapters. A short description of the contents of each chapter are given below :-

- **Chapter 1:** This chapter briefly describes the importance and mechanism of ISM, stable isotope systematics and the relevance of the present study.
- **Chapter 2:** This chapter describes the study area, sample collection and mass spectrometric measurement techniques. The details of models and other data sets used in the study are also presented.
- **Chapter 3:** This chapter discusses the studies carried out by the author on marine water vapor over Bay of Bengal during ISM 2012 and NEM 2013.
- **Chapter 4:** This chapter discusses the factors that control ISM $\delta^{18}O_p$ during 2013. Simulations from IsoGSM for the same period are also discussed.

- **Chapter 5:** In this chapter a set of ten isotope enabled GCM simulation is compared with observations. The cause of interannual variation of ISM $\delta^{18}O_p$ is also discussed in this chapter.

- **Chapter 6:** This chapter lists the major conclusions from the present study followed by the scope for future studies.

Chapter 2

Data and Methods

2.1 Study area

Rain water samples were collected during ISM 2013 (June to September), from six stations across India; Ahmedabad, Bhopal, New Delhi, Kanpur, Varanasi and Dhanbad (see Fig.2.1). Water vapor samples were collected during two cruises; i) Sagar Kanya (SK-296) during 12 July to 6 August, 2012 (south west monsoon 2012) ii) Sagar Nidhi (SN-082) during 15 November to 2 December, 2013 (north east monsoon) over the (BoB).

2.2 Sample collection

2.2.1 Rain sampling

Rain water was sampled as per the protocol proposed by IAEA [http://www-naweb.iaea.org/napc/ih/documents/other/gnip_manual_v2.02_en_hq.pdf]. A plastic carbouy connected with funnel is placed in an open space to collect unobstructed rainfall. Measures were taken to prevent evaporation of collected rain from the carbouy. Samples accumulate for 24 hours were transferred to leak proof polypropylene bottles everyday at 9 AM Indian Standard Time (IST), whenever it rained. These samples were taken to the laboratory for further stable isotopic analysis.

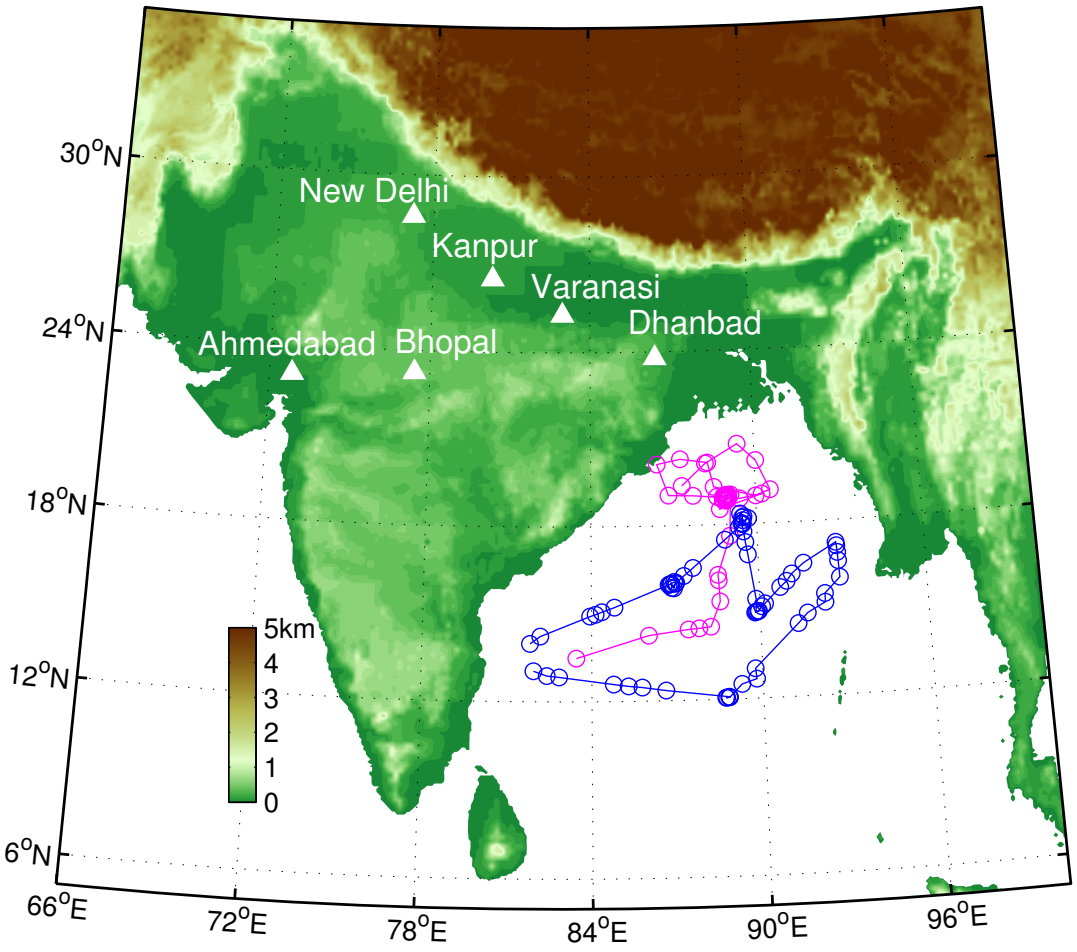

Figure 2.1: *Study area: white filled triangles show the rainwater collection stations, blue and magenta circles and lines represent the locations of water vapor sampling and cruise track respectively during the cruise SK-296 and SN-082.*

2.2.2 Water vapor sampling

Water vapor samples were collected cryogenically using a glass trap (Fig. 2.2) maintained below -80^oC with an ethanol-liquid nitrogen bath [IAEA Protocol; http://www-naweb.iaea.org/napc/ih/documents/miba/water_vapor_protocol.pdf]. To ensure efficient trapping, the flow speed of air through the trap was maintained at ∼500 mL/min. Sampling duration was ∼3 hours to trap water vapor >2 ml in liquid form. Sample were transferred from the glass trap to 5.9 ml glass vials using a pipette connected with rubber suction ball. The efficiency of the trap was checked by connecting an extra cold trap to the outlet of original trap,

and no significant condensate was found in second trap.

2.3 Stable isotopic analysis

Stable isotopic analyses of rain and water vapor samples were done using a Isotopic Ratio Mass Spectrometer (IRMS). Mass spectrometry is the technique of separating molecules according to their mass to charge ratio. The present study uses a continuous flow IRMS, Thermo Delta-V-Plus IRMS, in which helium gas is used as carrier gas to carry gas samples in to the mass spectrometer.

2.3.1 Isotope ratio mass spectrometer

IRMS consists of three parts; i) source for ionizing the gaseous samples, ii) analyzer for separating the sample ion beams and iii) collector for detecting the ion currents.

Source: In the source, a thorium coated tungsten filament is made to emit electrons (with ∼100 eV energy) by applying ∼3.5A direct current. These electrons ionize the sample gas (efficiency ∼0.1%). A low magnetic field is applied to keep the electrons in a spiral path and thereby increase the ionization efficiency. Further the positively ionized gas molecules are accelerated by a high voltage (∼2.5 kV) and focused into the analyzer.

An ion (charge q and mass m) in an accelerating voltage (V) obtains a kinetic energy.

$$qV = \frac{1}{2}mv^2$$

Analyzer: A magnetic field B (∼0.38 Tesla for CO_2 analyses and ∼0.1 Tesla for H_2 analyses) is applied perpendicular to the ion beam around the flight tube. This separates the ionized beam which travels in a curved path according to the mass/charge ratio. The Lorentz force experienced by the ion while entering perpendicular to the magnetic field results in a centripetal force (with radius of

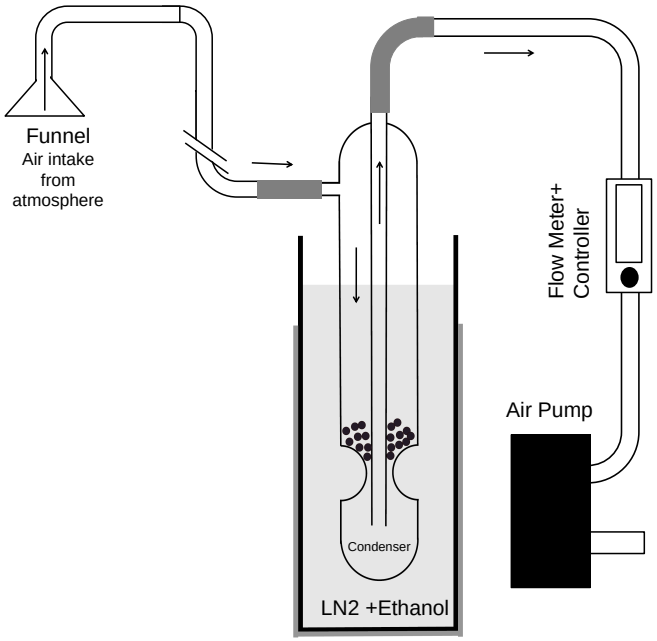

Figure 2.2: *Schematic diagram of water vapor collection.*

Figure 2.3: *Photograph of the vapor collection device installed in the ship*

curvature r).

$$q(v \times B) = \frac{mv^2}{r}$$

Thus the radius of curvature of the ion is,

$$r = \sqrt{\frac{2Vm}{B^2 q}}$$

For a constant V, B and q, the radius of curvature of the singly charged ion is directly proportional to the square root of its mass.

Collector: The currents of different ion beams are measured using detectors (Faraday cups), which are attached to very high resistances $\sim 10^9 \Omega$. Ions produce a voltage across the resistance, which is measured. This is proportional to the flux of ionized isotopologues entering into the cup.

2.3.2 $\delta^{18}O$ and δD measurements

For isotopic analysis using IRMS, the water sample has to be converted into suitable gas. But the gaseous form of water (water vapor) cannot be sent into the IRMS. Hence water is isotopically equilibrated with CO_2 and $\delta^{18}O$ of equillibrated CO_2 is then measured. For this equilibration, we used Thermo Finnigan Gas bench II device. 0.3 mL of the water sample is loaded in a $12mL$ glass vial and kept in the sample tray of the Gas bench II, whose temperature is kept constant at 23^oC (i.e., slightly above room temperature). Then head space of the vial is flushed using a mixture of helium ($\sim$ 99%) and CO_2 ($\sim$ 1%) with a flow speed of 100 mL/min for 10 minutes. Flushed vials are kept for isotopic equilibration for 18-20 hours. After equilibration, 100 μL of the equillibrated gas mixture is injected into IRMS through a gas chromatography column. Sample injunction cycle is repeated six times to improve the precision.

For δD measurements, 0.3 mL of the sample separately is loaded in a $12mL$ glass vial along with a platinum catalyst. Closed vials are then kept in the sample tray of Gas bench II, whose temperature is maintained at 23^oC. Then the vial

is flushed with mixture of helium ($\sim 99\%$) and H_2 ($\sim 1\%$) and kept for 2 hours for isotopic equilibration. Platinum catalyst helps the water-hydrogen isotopic equilibration. The equilibrated helium-hydrogen mixture is then taken into the IRMS through a gas chromatography column as mentioned earlier.

For $\delta^{18}O$ analysis, ions currents corresponding to the masses 44, 45 and 46 of CO_2 are measured [*Epstein and Mayeda*, 1953] and for the δD, those corresponding to masses 2 and 3 of H_2 are measured. While calculating the isotopic compositions of samples, isobaric interferences are corrected for as explained below. These corrections are done using a software, ISODAT, which controls the IRMS.

1. **Craig correction:** The ion currents corresponding to mass of 45 is contributed both by $^{13}C^{16}O_2$ and $^{12}C^{17}O^{16}O$. Similarly mass 46 is contributed by both $^{12}C^{18}O^{16}O$, $^{13}C^{17}O^{16}O$ and $^{12}C^{17}O^{17}O$. To avoid the effect of these interferences on final atomic ratios ($\delta^{18}O$ or ^{13}C), a set of equations called Craig corrections are applied. [*Craig*, 1957].

$$\delta^{13}C = 1.0676\delta_{45} - 0.0338\delta^{18}O$$

$$\delta^{18}O = 1.0010\delta_{46} - 0.0021\delta^{13}C$$

2. H_3 **correction:** During the ionization of hydrogen gas in the source, H_3^+ ions are also formed and this creates isobaric interference with HD^+ ions in the collector. The formation of H_3^+ ions is directly proportional to the concentration of H_2^+ ions. $(HD^+ + H_3^+)/H_2^+$ ratio for different H_2^+ ion currents are calculated and the effect of H_3^+ ion is removed.

$\delta^{18}O$ and δD are reported with respect to the international standard VSMOW. Due to the limited availability of the VSMOW standard, we prepared a large quantity ($20L$) of an internal laboratory standard (NARM, Narmada river water in this study) which is calibrated using VSMOW. All $\delta^{18}O$ (δD) measurements were made with respect to reference CO_2 (H_2) gas along with NARM

standard ($\sim$ 13 NARM standard per a batch of 88 samples). $\delta^{18}O$ of the reference ($\delta^{18}O^{ref}_{VSMOW}$) is calculated using the following equations.

$$\delta^{18}O^{ref}_{NARM} = \frac{-\delta^{18}O^{NARM}_{ref}}{1+\delta^{18}O^{NARM}_{ref}10^{-3}}$$

$$\delta^{18}O^{ref}_{VSMOW} = \delta^{18}O^{ref}_{NARM} + \delta^{18}O^{NARM}_{VMOW} + \delta^{18}O^{ref}_{NARM}\delta^{18}O^{NARM}_{VMOW}10^{-3}$$

Finally $\delta^{18}O$ of sample with respect VSMOW is calculated as,

$$\delta^{18}O^{sample}_{VSMOW} = \delta^{18}O^{ref}_{VSMOW} + \delta^{18}O^{sample}_{ref} + \delta^{18}O^{ref}_{VSMOW}\delta^{18}O^{sample}_{ref}10^{-3}$$

A similar procedure is used to calculate the δD of samples with respect to VSMOW. In the above set of equations, the effect of equilibrium fractionation during $CO_2 - H_2O$ and $H_2 - H_2O$ equilibration are not considered. Since all the samples and standards are kept in identical conditions, this effect does not the alter the final δ values.

2.3.3 Calibration of laboratory standard

The internal laboratory standard (NARM) is calibrated using international standard provided by IAEA. We participated in the Fourth inter laboratory comparison exercise for δD and $\delta^{18}O$ analysis of water samples (WICO-2011). The δD and $\delta^{18}O$ values measured by us are in good agreement with the IAEA consensus values. In September 2014 we re-calibrated the NARM using three international standards (Table 2.1) and the calibrated values are shown in table 2.2. We used two sets of NARM; running standard NARM for daily measurements and an NARM reservoir (NARM new), both were calibrated.

2.3.4 SWING2 models

In chapter 5 of this thesis, ten model simulations from Stable Water Isotope INtercomparison Group, phase 2 SWING2, archived at `ftp://swi.geo.su.se/SWING2` are compared. Details of SWING2 model simulations are presented in Table 2.3. All the models are forced with observed monthly sea surface temperatures (SST)

Table 2.1: *Measured and reported/consensus $\delta^{18}O$ and δD values of international standards and WICO-2011 samples. The errors are 1σ, and refer to external precision*

Sample Code	Measured $\delta^{18}O$	Reported values $\delta^{18}O$	Measured δD	Reported values δD
VSMOW	0.06 ± 0.07	0.0	0.1 ± 0.2	0.0
SLAP	-55.5 ± 0.1	-55.5	-427.7 ± 1.4	-428.0
GISP	-24.8 ± 0.07	-24.8	-190.5 ± 0.4	-189.5
OH-13	-1.0 ± 0.1	-0.96	-2.5 ± 0.4	-2.8
OH-14	-5.6 ± 0.1	-5.6	-38.4 ± 0.1	-38.3
OH-15	-9.5 ± 0.1	-9.4	-78.0 ± 0.3	-78.2
OH-16	-15.5 ± 0.1	-15.4	-114.9 ± 0.2	-114.6

Table 2.2: *Calibrated values of laboratory standards; calculated with respect to the international standards.*

Laboratory standard	$\delta^{18}O$ ‰	δD ‰
NARM (n=8)	-4.55 ± 0.07	-33.5 ± 0.3
NARM new (n=5)	-4.6 ± 0.1	-33.8 ± 0.4

[*Conroy et al.*, 2013; *Risi et al.*, 2012]. Three of the ten simulations were nudged with the reanalysis wind field (NCEP or ECMWF). The nudging technique basically involves the averaging of model outputs and reanalysis data during each time step of model integration and it is used as the input for model integration during the next time step. Nudging techniques help improve the modeled dynamical fields, which in turn helps to obtain a more realistic representation of the atmospheric circulation in the model.

For plotting Taylor diagrams [*Taylor*, 2001], we interpolated the model outputs and the observed gridded rainfall data sets to a T63 Gaussian grid using the bilinear interpolation technique (Climate Data Operator, https://code.zmaw.de/projects/cdo).

Table 2.3: *Details of SWING2 model used in the present study. Further details can be found at* http://www.giss.nasa.gov/projects/SWING2

Model	Resolution (degrees) (Latitude X Longitude)	Simulation type	References
GSM	1.914 x 1.875	Free and nudged with NCEP R2	*Yoshimura et al.* [2008]
LMDZ4	2.5 x 3.75	Free and nudged with ECMWF	*Risi et al.* [2010a]
GISS ModelE	2 x 2.5	Free and nudged with NCEP	*Schmidt et al.* [2007]
CAM2	2.812 x 2.812	Free	*Lee et al.* [2007]
HadAM3	2.43 x 3.75	Free	*Sime et al.* [2009]
GENESIS3	1.875 x 1.875	Free	*Mathieu et al.* [2002]
MIROC32	2.812 x 2.812	Free	*Kurita et al.* [2011]

2.4 Other data and online resources used in the present study

2.4.1 Global network of isotopes in precipitation

IAEA and World Meteorological Organization (WMO) established a global network for monitoring $\delta^{18}O$, δD and tritium concentrations in world wide precipitation since 1961 CE (GNIP data archived at www.iaea.org/water). Present study utilizes $\delta^{18}O$, δD and rainfall data from different GNIP station over the ISM region.

2.4.2 Reanalysis/satellite data

Wind field and specific humidity data were taken from the National Center for Environmental Prediction reanalysis-1 [NCEP, *Kalnay et al.*, 1996] and Modern-Era Retrospective Analysis For Research And Applications [MERRA, *Rienecker*

et al., 2011]. We used Tropical Rainfall Measuring Mission (TRMM) Multi-satellite Precipitation Analysis [*Huffman et al.*, 2007] daily rainfall data (3B42), monthly rainfall data from Global Precipitation Climatology Project [GPCP, *Adler et al.*, 2003], and CPC Merged Analysis of Precipitation [CMAP, *Xie and Arkin*, 1997].

Calculation of vertically integrated moisture flux

Vertically integrated moisture flux (Q) is calculated from reanalysis data using the following equations,

$$Q_u = \frac{1}{g}\int_{P_t}^{P_s} q.udP \tag{2.1}$$

$$Q_v = \frac{1}{g}\int_{P_t}^{P_s} q.vdP \tag{2.2}$$

Where Q_u and Q_v are the zonal and meridional component of Q, g is the acceleration due to gravity, q is the specific humidity, u and v are the zonal and meridional components of wind, and P_t and P_s represent the 300 hPa and surface pressure levels respectively.

2.4.3 Air parcel trajectory models

To understand the history of the air parcel that reaches the sampling station, back trajectories (up to the previous 120 hours) were generated using the Hybrid Single Particle Lagrangian Integrated Trajectory Model [HYSPLIT, http://ready.arl.noaa.gov/HYSPLIT.php; *Draxler and Rolph*, 2003]. HYSPLIT is forced with the data from Global Data Assimilation System. The advection of a air parcel is computed from the mean 3D wind field (V). Consider an air parcel moving from the initial-position P_t to the $P_{t+\Delta t}$. The first guess position estimated as

$$P'_{t+\Delta t} = P_t + V_{P,t}\Delta t$$

and the final position is,

$$P_{t+\Delta t} = P_t + 0.5(V_{P,t} + V_{P',t+\Delta t})\Delta t$$

The integration time Δt varies between 1 minute to 1 hour according to the prevailing wind speed. Hence the final trajectory is interpolated at every one hour interval. Hysplit also interpolates meteorological variables such as rainfall, pressure, potential temperature, temperature, and relative humidity along the trajectory from the model input data.

In order to account the sensitivity of HYSPLIT on the initial condition, an ensemble of 27 trajectories were calculated by making small perturbations in the starting point [i.e., latitude and longitude are changed by a factor of 1 grid point and the height is varied by 250 m; *Draxler*, 2003]. In such cases, the trajectory density at each grid point (at a resolution of $0.5^o \times 0.5^o$) was estimated as the normalized counts of trajectories that crossed each grid.

Chapter 3

Stable Water Vapor Isotopologues Over Bay of Bengal

Spatio-temporal variations of stable water isotopes (SWI), $\delta^{18}O_p$ and δD_p, have been studied globally for the last ∼50 years, but the variations in the vapor isotopic compositions ($\delta^{18}O_v$ and δD_v) are rarely recorded due to the difficult sampling procedure of atmospheric vapor for stable isotopic analysis. In recent years, with the aid of satellite based (for δD_v) and laser based instruments (for $\delta^{18}O_v$ and δD_v), the potential of stable isotopes of water vapor for probing atmospheric processes have been demonstrated [e.g., *Berkelhammer et al.*, 2012; *Good et al.*, 2015; *Gorski et al.*, 2015; *Noone*, 2012; *Worden et al.*, 2007]. Knowledge about the factors that control the stable isotopic compositions of atmospheric vapor helps improve the application of SWI to both paleoclimatology and hydrological cycle studies.

BoB is the one of the major sources of water vapor for monsoon rain over the Indian subcontinent during both ISM and NEM seasons. To characterize the isotopic compositions of vapor over BoB, boundary layer water vapor was collected during two cruises; i) during ISM (SK-296, cruise period July 12 to August 6, 2012) and ii) during NEM (SN-082, November 15 to December 1, 2013). Results from these expeditions are discussed in the following sections.

3.1 Isotopic characteristics of vapor during ISM

Forty-two samples of water vapor were collected from the top mast (25m above sea level) of R/V Sagar Kanya (SK-296). We carried out another simultaneous collection at 6m height, but the number of samples collected at this height is less (n = 28) due to the limited availability of liquid nitrogen for trapping on board the vessel. Rain water samples (n = 15, this number is limited by the occurrence of rain) and sea surface water samples (n = 42) were also collected, and all samples were analyzed for $\delta^{18}O$ and δD.

3.1.1 Air parcel back trajectory analysis

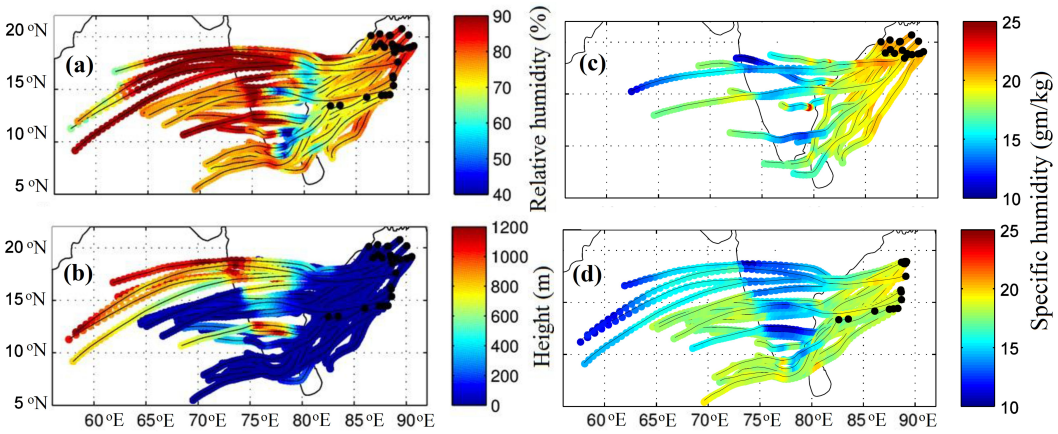

Figure 3.1: *Seventy-two hour air mass back trajectories from the sampling locations with (a) relative humidity, (b) air parcel height along the trajectory, and (c) specific humidity (in grams/kilograms) along the trajectories for the 14 samples collected prior to 19 July. (d) Same as Figure 3.1c but for the rest of the 28 samples. Black dots in the diagrams represent sampling locations.*

To understand the history of the air parcel, a 72 hour HYSPLIT back trajectory calculation is initiated from the time of sample collection for each sample (Fig 3.1). Due to the strong westerly monsoon winds, air parcels traveled from the Arabian Sea (AS) to the BoB during the sampling period. While crossing the southern peninsular India, air parcels dehydrated due to condensation over the Western Ghats. Model-derived heights of air parcels show a descending motion

of air to the east of the Western Ghats (narrow mountain range at the western peninsular India, Fig. 2.1) and mixing with hotter, drier air in the lower troposphere (the so-called "rain shadow effect"). This caused the low relative humidity (< 60 %) over peninsular India, and the parcel gained moisture after entering the BoB (see Fig 3.1 a&b). A major amount of the moisture collected by us thus seems to have originated from the BoB. There is no descending motion seen in the back trajectory over the BoB during this season, implying that there is little chance of mixing of air above the atmospheric boundary layer with the advected air parcel coming through peninsular India.

3.1.2 δD, $\delta^{18}O$ and meteorological parameters during the cruise SK-296

Table 3.1: *A summery of isotopic composition of samples collected during the cruise SK-296.*

	Range (‰)	Mean ± standard deviation (‰)
$\delta^{18}O_v$ at 25 m	−14.1 to −9.8	−11.4 ± 0.9
δD_v at 25 m	−97.2 to −69.1	−78.2 ± 5.7
Vapor d-excess at 25 m	6.9 to 19.4	12.6 ± 3.0
$\delta^{18}O_v$ at 6 m	−13.6 to −10.0	−10.9 ± 0.8
δD_v at 6 m	−94.0 to −68.3	−74.6 ± 5.4
Vapor d-excess at 6 m	5.7 to 16.4	12.7 ± 2.4
$\delta^{18}O_p$	−5.0 to 0.0	−2.7 ± 1.4
δD_p	−28.5 to 4.3	−11.6 ± 10.3
Rain d-excess	4.6 to 12.6	9.5 ± 2.2
Surface water $\delta^{18}O$	−2.5 to 0	−0.4 ± 0.4
Surface water δD	−8.9 to 5.2	−3.1 ± 2.1
Surface water d-excess	3.7 to 11.1	6.3 ± 1.2

Fig. 3.2 shows the time series of stable isotopic composition of water vapor and the associated meteorological parameters. The isotopic compositions and d-

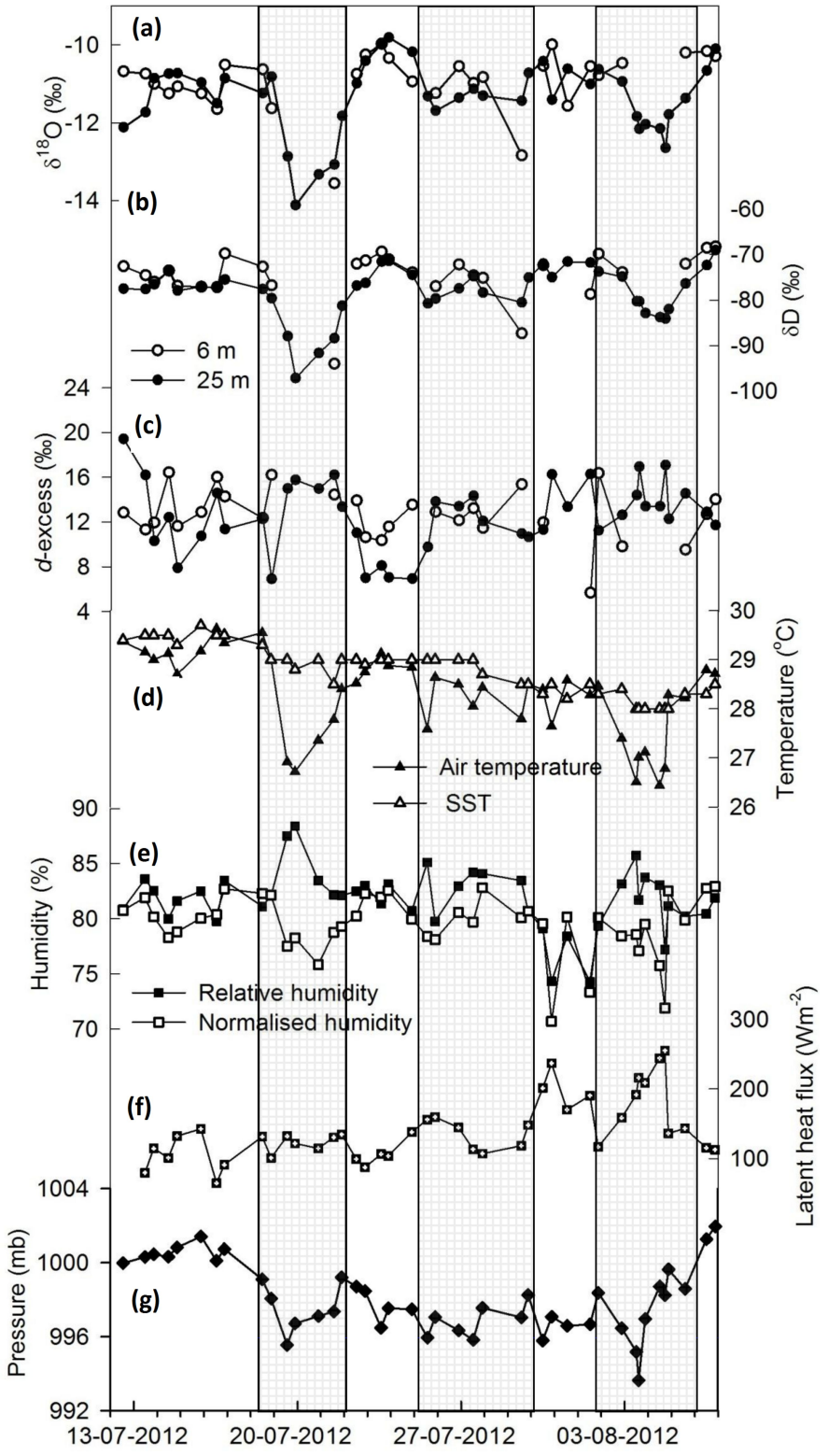

Figure 3.2: *Time series of (a) $\delta^{18}O_v$, (b) δD_v, and (c) d-excess values of marine vapor at 6m (open symbols) and 25m height (filled symbols) above sea level. (d) Air temperature and sea surface temperature. (e) Relative humidity and normalized humidity h. (f) Latent heat flux. (g) Atmospheric pressure at 25m above sea level. Shaded regions represent the three rain spells during the cruise.*

excess of vapor at 6 and 25m did not show any statistically significant difference (Table 3.1). The linear correlation coefficient (r) between δD_v at 6 and 25m ($r = 0.78$) and that between $\delta^{18}O_v$ values ($r = 0.63$) at these two heights are significant. The d-excess of vapor values between these heights, however, are uncorrelated ($r = -0.13$). The reason is that the isotopic ratios show much larger range of variation relative to their respective experimental errors (a factor of 36−43 for $\delta^{18}O_v$ and 26−28 in δD_v while only 8−10 in d-excess) than d-excess of vapor.

The 3 hourly averaged wind (i.e., averaged over the duration of sample collection) was less than 10m/s up to 21 July, and it increased up to 20m/s later (22 July to 6 August 2012). The measured latent heat flux also shows a similar trend with a linear correlation coefficient r of 0.78 (P<0.01) with the wind speed. However, such a trend is observed in neither δD_v nor $\delta^{18}O_v$; rather, they show a correlation (r=−0.66 [P $<$ 0.01] for $\delta^{18}O_v$ and $r = 0.68$ [P $<$ 0.01] for vapor d-excess) with the latent heat flux and with the wind speed [$r = -0.53$ (P $<$ 0.01) for $\delta^{18}O_v$ and $r = 0.47$ (P $<$ 0.05) for vapor d-excess] during the latter sampling period. Two marked dips are observed in δD_v and $\delta^{18}O_v$, associated with the presence of monsoon depressions at the collection site, marked by a fall in atmospheric pressure and an increased rainfall (on 20 July and 4 August 2012).

3.1.3 Influence of local ocean surface conditions

Figure 3.2 is useful to infer the relations between isotopic compositions of atmospheric vapor and sea surface meteorological conditions. The expected relation between relative humidity and d-excess [due to diffusive transport, *Uemura et al.*, 2008] was not observed. This is due the smaller variations in SST compared to those in air temperature; thus, it appears that relative humidity may not be a good indicator here of kinetic fractionation during evaporation. As predicted by *Merlivat and Jouzel* [1979], vapor d-excess , however, is inversely correlated with normalized humidity h. Twenty-five percent of the variance in vapor d-excess is explained by the normalized relative humidity [d-excess $=(-0.55 \pm 0.14) \times h + (56 \pm 12), r = 0.5, P < 0.01$ at 25 m height]. Interest-

ingly, the regression slope of − 0.55‰/% and intercept 56‰ agree within the cited uncertainties, respectively, with the slope of − 0.61‰/% and intercept 55‰ obtained by *Uemura et al.* [2008] for marine vapor over the Indian sector of the Southern Ocean (35-65^{o}S and 20-115^{o}E) during the austral summer of 2006 (however, h correlated with relative humidity, i.e., $r = 0.9$ in their study). These results perhaps point toward the possible existence of a global relation between h and vapor d-excess as predicted by equation 1.8, although the coefficient of determination here is less than that in the Southern Ocean (r $\sim$ 0.8) [*Uemura et al.*, 2008]. This may be a result of less temporal variability of h over the BoB during the sampling monsoon period or may be due to the weakening of the h-d-excess relation above $h = 80\%$, as seen in isotope-enabled global models [*Uemura et al.*, 2008]. Atmospheric air temperature also shows a significant positive linear correlation with δD_v and $\delta^{18}O_v$ [r = 0.61 (P $<$ 0.01) for δD_v and r = 0.62 (P $<$ 0.01) for $\delta^{18}O_v$], while they are uncorrelated with SST observations. This is likely due to the cooling of surface air during rainfall and associated isotopic equilibration of vapor with falling raindrops.

Table 3.2: *Linear correlation coefficients (r) between different parameters for all the collected samples (second column) and only samples collected after 21 July 2012 (third column).Double star indicates significant r values with P<0.01, single star indicates P<0.05, and no star indicates insignificance. As $\delta^{18}O_v$ and δD_v are significantly correlated, only correlation with $\delta^{18}O_v$ is presented.*

Parameters	**All Samples (n = 42)**	**Post 21 July 2012 (n = 27)**
Normalized humidity with d-excess	− 0.50**	− 0.66**
d-excess with latent heat flux [1]	0.19	0.68**
$\delta^{18}O_v$ with air temperature	0.63**	0.80**
$\delta^{18}O_v$ with latent heat flux	− 0.17	− 0.66**
d-excess with wind speed	0.24	0.47*
$\delta^{18}O_v$ with wind speed	− 0.07	− 0.53**

The factors determining the variations in $\delta^{18}O_v$ and vapor d-excess sampled up to 21 July 2012 and later appear to be quite different. The later samples exhibit better correlations with meteorological parameters such as air temperature, normalized humidity, latent heat flux, and wind speed than the earlier ones. Figures 3.1 c & d show that less moisture is advected to the sampling location in the later than the earlier period. As local evaporation contributed more vapor than advection during the later period, this resulted in better correlation coefficients as observed (Table 3.2). Another reason could be that the spatial variability in the position of the vessel was more restricted for about 10 days (21 to 31 July) in this period.

3.1.4 Comparison with the Craig and Gordon model and influence of advected moisture

Figure 3.3 shows the comparison of data with predicted values from the C-G model using global closure assumption ($R_e = R_a$ in equation 1.8). The equilibrium fractionation factor (α) is taken from *Majoube* [1971a,b], and the kinetic fractionation factor α_k is calculated using wind-dependent parameterization proposed by *Merlivat and Jouzel* [1979] (Equation 1.9). The model estimates that $\delta^{18}O_v$ is closer to observation during non-rainy days and not on rainy days. This is due to exchange and re-evaporation from the falling raindrops. In addition, downdrafts during convective rain events can bring vapor with more depleted δ values and higher vapor d-excess values from the boundary layer above to the surface [*Knupp and Cotton*, 1985; *Kurita*, 2013]. We infer that it is imperative to account for (a) isotopic exchange between vapor and raindrops [*Stewart*, 1975], (b) the mixing with the boundary layer vapor laterally advected to the collection site, and (c) vertical mixing during convective downdraft to significantly improve the model prediction.

The strong southwesterly winds provide a continuous supply of the moisture to the sampling location, so the isotopic exchange occurring along its trajectory needs to be considered to explain the observed variations in $\delta^{18}O_v$. Evaporation

[1]Latent heat flux is measured during the cruise using eddy covariance technique

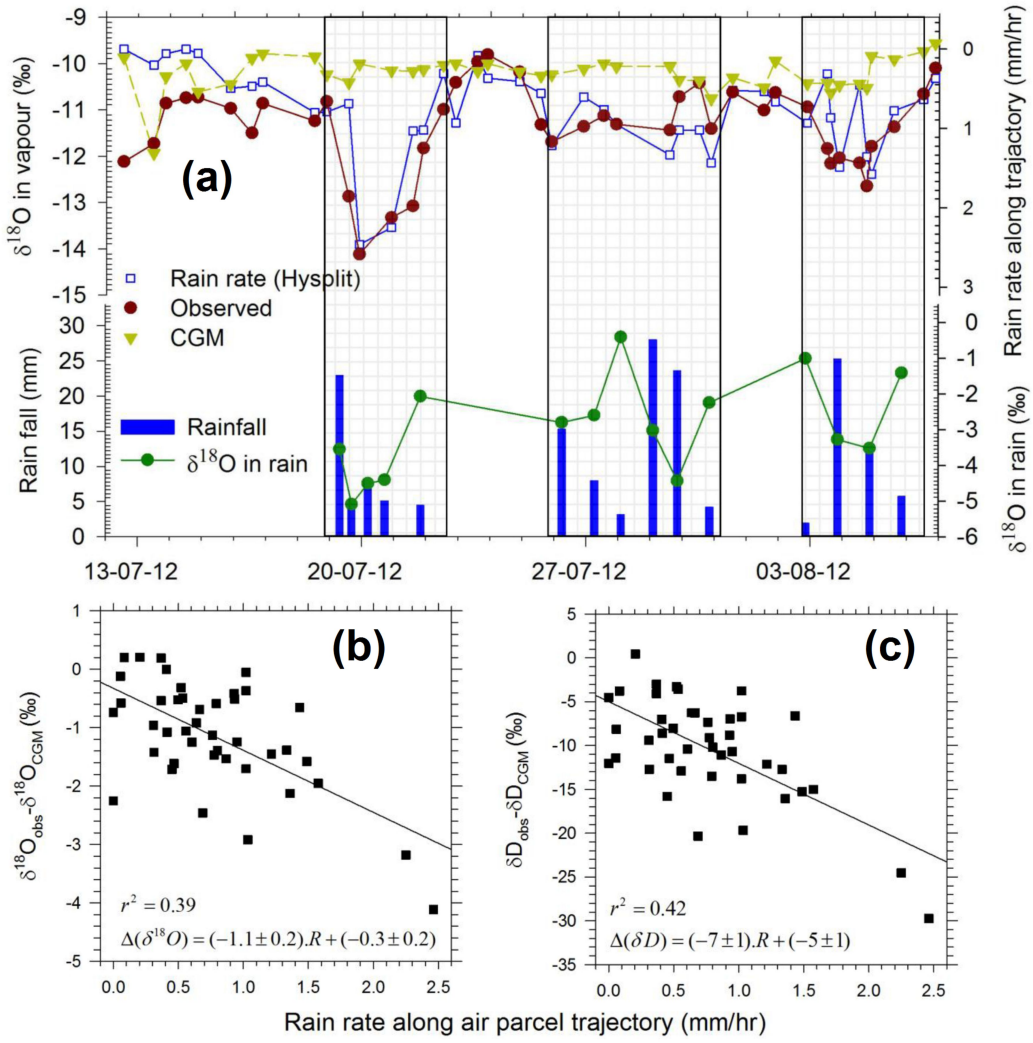

Figure 3.3: *(a) Comparison of observed variations in $\delta^{18}O_v$ (filled circles) with C-G model results (inverted triangles). The shaded area shows three rain spells that occurred during sampling. The rain rate (open square) plotted in the upper panel is the average rain rate along the 24h air parcel trajectory. The accumulated rain amount collected during the cruise (vertical bars) and its $\delta^{18}O_r$ (filled circle) are also shown in bottom panel. (b) The relation between the deviation between the observed $\delta^{18}O_v$ (represented as $\delta^{18}O_{obs}$) from the C-G model result (represented as Δ ($\delta^{18}O$) in the regression line) and the average rain rate along the 24h back. The R in the regression equation represents the rain rate. (c) Same as in b, but for δD_v.*

of and isotopic exchange with falling raindrops along the air parcel trajectory may cause advection of depleted vapor to the collection site. The observed negative correlation of $r = -0.62$ between the observed deviations in $\delta^{18}O_v$ (-0.65 for δD_v) from the C-G model prediction on the other hand and the average rain rate along the trajectory for the previous 24h (HYSPLIT-derived rain rate) prior to sampling (see Figure3.3) is consistent with the above hypothesis. Recently, *Kurita* [2013] have also shown that the rain activity along the air parcel back trajectory significantly depletes the isotopic composition of surface vapor over the tropical oceans. When raindrops evaporate into unsaturated air, vapor relatively depleted in ^{18}O (and D), with higher vapor d-excess values results, as observed by us during the three spells of rain (shaded region in Fig. 3.2).

3.2 Isotopic characteristics of water vapor during NEM

During November 15 to December 1, 2013, water vapor was collected from R/V Sagar Nidhi (cruise SN-082) over BoB (total $\sim$ 140 samples from 8 and 25 meters above the sea level). Surface water samples (n = 69) and rain water (n = 15) were also collected during the expedition and all samples were analyzed for $\delta^{18}O$ and δD. Figure 3.5 shows the time series of the stable isotopic compositions of water vapor samples collected and the 3 hour running mean of meteorological parameters during NEM season (cruise SN-082). A summery of stable isotopic composition of vapor, surface water and rain is given in table 3.3.

3.2.1 Air parcel back trajectory analysis

During NEM, two distinct types of back trajectories are observed (Fig. 3.4); one originating from land (north-eastern India) and the other, from (sea) BoB alone. The parcels that moved through continents had very low relative humidity and subsequently gained moisture from BoB before they reached the sampling location. The parcels that had the end points of trajectories over BoB had higher relative humidity. Along the back trajectory, over BoB, the height of the parcel

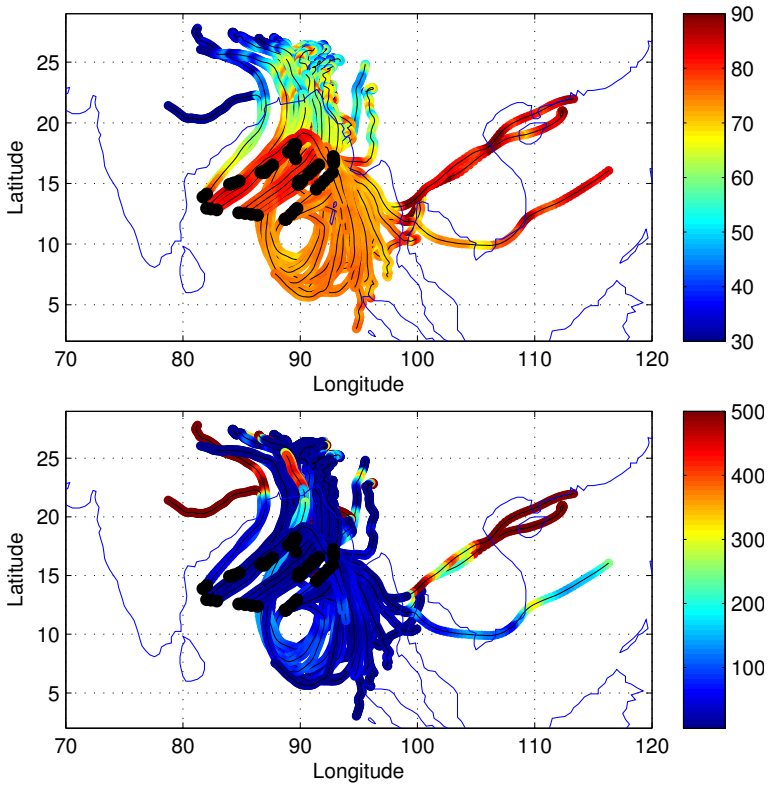

Figure 3.4: *Seventy-two hour air mass back trajectories from the sampling locations with relative humidity (top panel) and air parcel height along the trajectory (bottom panel). Black dots in the diagrams represent sampling locations*

remained near the ground level (below 100m a.s.l).

3.2.2 Influence of local ocean surface conditions

Similar to the results from ISM cruise, the vapor d-excess is correlated with normalized humidity (r = −0.64 at 8m a.s.l, r = −0.55 at 25m a.s.l). The slope of this relation is slightly lower than (-0.33 ± 0.06 at 8m height and -0.47 ± 0.07 at 25m height) that during ISM, while the intercepts (45 ± 4.5 at 8m height and 56 ± 5 at 25m height) are close to that of ISM. d-excess -normalized humidity relation is further described in section 3.3. As observed in the previous cruise, $\delta^{18}O_v$ is well correlated with surface air temperature (r = 0.57 for 8m height and r = 0.65 for 25 m height). The cooling of surface air due to rain along with rain-vapor isotopic interactions are the reasons for such a relation. This is discussed in detail in the next section.

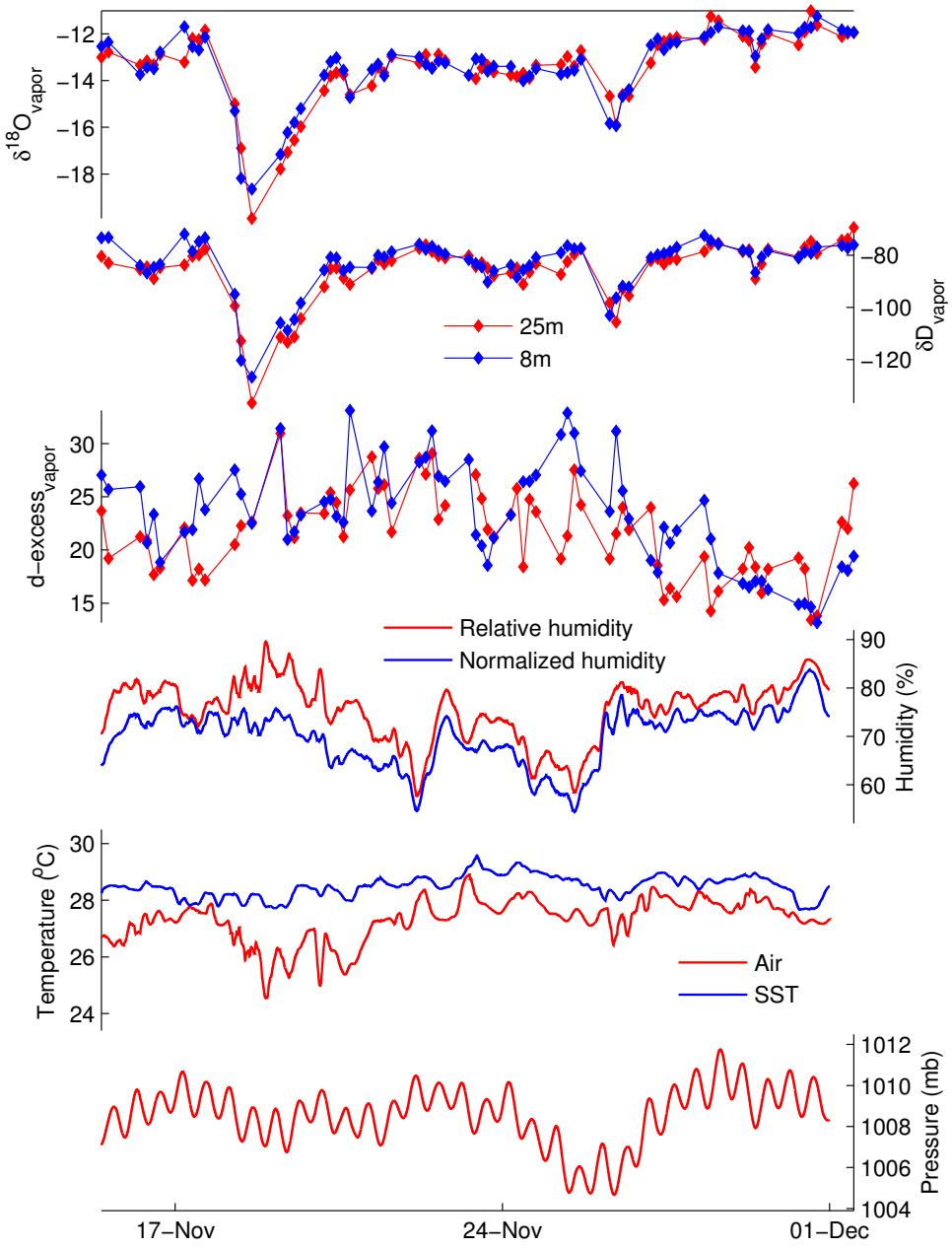

Figure 3.5: *Time series of $\delta^{18}O_v$, δD_v, and d-excess values of marine vapor at 8m (blue line and scatter) and 25m height (red line and scatter) above sea level. 3-hr running means of air temperature, sea surface temperature, relative humidity, normalized humidity (h) and atmospheric pressure at 25m above sea level are also shown.*

Table 3.3: *A summery of $\delta^{18}O$, δD and d-excess of the samples collected during SN-082*

	Range (‰)	Mean ± standard deviation (‰)
$\delta^{18}O_v$ at 25m	−19.9 to −11.0	−13.5 ± 1.6
δD_v at 25m	−136.6 to −69.4	−86.0 ± 11.3
d-excess at 25m	13.4 to 30.9	21.6 ± 3.9
$\delta^{18}O_v$ at 8m	−18.6 to −11.2	−13.4 ± 1.5
δD_v at 8m	−126.7 to −71.9	−83.8 ± 10.6
d-excess at 8m	13.2 to 33.1	23.3 ± 4.8
$\delta^{18}O_p$	−13.0 to −1.8	−5.0 ± 2.9
δD_p	−88.3 to −3.3	−28.1 ± 23.4
Rain d-excess	7.2 to 17.3	12.5 ± 2.8
Surface water $\delta^{18}O$	−2.0 to 0.4	2.1±4.0
Surface water δD	−12.8 to 9.6	−0.4±0.5
Surface water d-excess	0.3 to 8.9	5±1.8

3.2.3 Comparison with the Craig and Gordon model and influence rain-vapor interaction

The back trajectory analysis shows that the major source of vapor during NEM is BoB (Fig 3.4). But the $\delta^{18}O_v$ values predicted by Craig and Gordon model during non-rainy days (during NEM) are higher by 2−3‰ compared to the observations. The more depletion in the $\delta^{18}O_v$ during NEM could be due to the seasonality $\delta^{18}O_v$ over BoB. This is discussed further in section 3.4.

Similar to the ISM cruise, the lower values of $\delta^{18}O_v$ are associated with higher rain along the parcel trajectory. The highest depletion in $\delta^{18}O_v$ is observed on 19 November 2013, but no rain was recorded at the station; but very high rain along the HYSPLIT trajectory is observed. This depletion in $\delta^{18}O_v$ may the result of advected vapor which is depleted in $\delta^{18}O_v$ due to i) the rain-vapor isotopic exchange en-route and ii) unsaturated downdraft from the convective system.

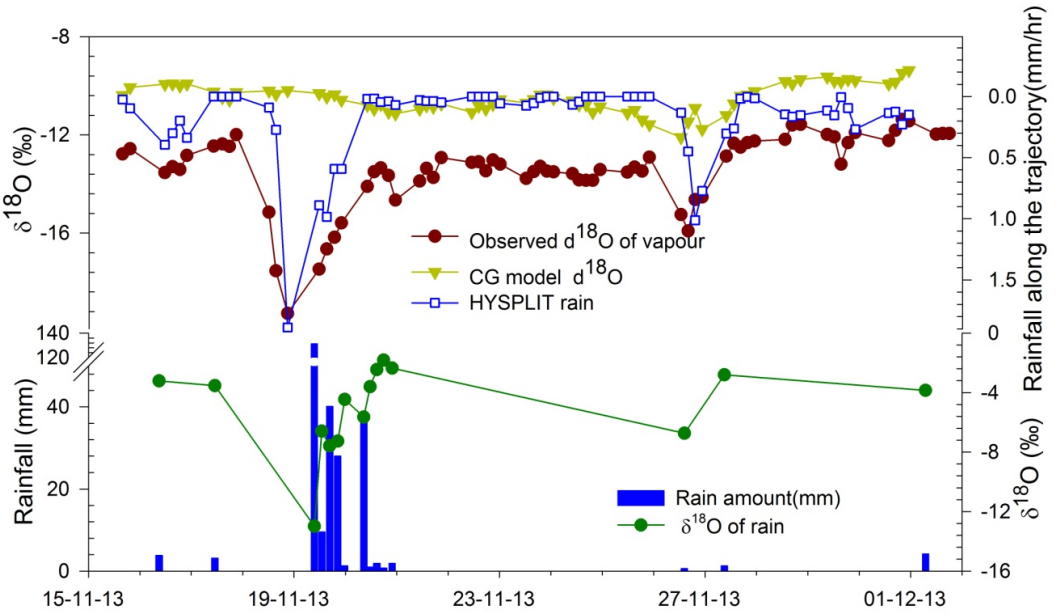

Figure 3.6: *Comparison of observed variations in $\delta^{18}O_v$ (filled circles) with C-G model results (inverted triangles). The rain rate (open square) plotted in the upper panel is the average rain rate along the 24h air parcel back trajectory. The rainfall collected during the cruise (blue vertical bars) and its $\delta^{18}O_r$ (filled circle) are also shown in bottom panel.*

3.3 Relationship between *d*-excess and normalized humidity

After the emergence of laser based instruments for $\delta^{18}O$ and δD measurements, much work has been carried out to verify the d-excess -normalized humidity relation over the marine atmosphere [e.g., *Benetti et al.*, 2014; *Steen-Larsen et al.*, 2014]. During condensation under isotopic equilibrium condition, the rain preserves the d-excess values of its source vapor. Hence the d-excess in ice cores is more likely bear the influence of the source vapor. *Merlivat and Jouzel* [1979] predict a negative correlation between d-excess and normalized humidity at the sea surface during oceanic evaporation. This relation is observed over the Southern Ocean and the Atlantic ocean. Over BoB the relation is appears to be weaker.

The d-excess -h relation is much stronger during NEM compared to that

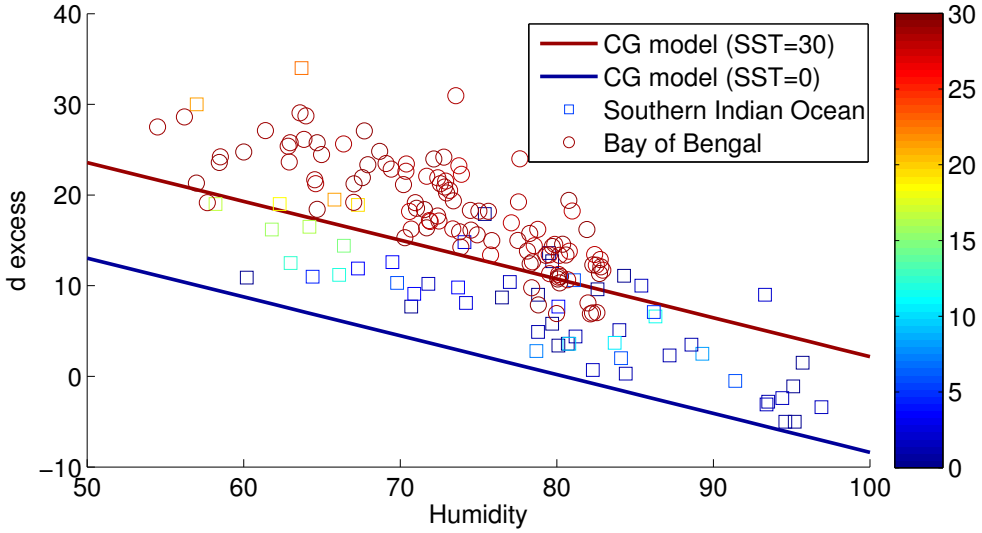

Figure 3.7: *Relation between water vapor d-excess and normalized humidity. Open circles represent the samples collected from BoB during July-August 2012 and November 2013. Open square represents data reported by Uemura et al. [2008]. Solid lines shows the d-excess -normalized humidity relation as simulated by Craig and Gordon model with closure assumption with U_{10m} = 5 m/s and SST = 30°C (red line) and SST = 0°C (blue line). Color of the marker shows the SST during sample collection.*

reported for the ISM. We combined the 25m data sets of d-excess and normalized humidity from both the ISM and NEM season, the regression equation becomes d-excess = $(0.64 \pm 0.05)\times$h+(65 ± 4), r = 0.78, n = 107. This relation suggests that over BoB the relation between d-excess and the normalized humidity is prominent on seasonal time scales. Figure 3.7 shows the comparison of d-excess h relation obtained over the BoB to a previous work over the Southern Ocean. Compared to the Southern Indian Ocean, the intercept of linear regression is higher in the BoB owing to its higher sea surface temperature.

3.4 Seasonality

Figure 3.8 shows the distribution of observed $\delta^{18}O$ and d-excess for both the cruises. The observations suggest that during ISM, $\delta^{18}O_v$ is relatively less de-

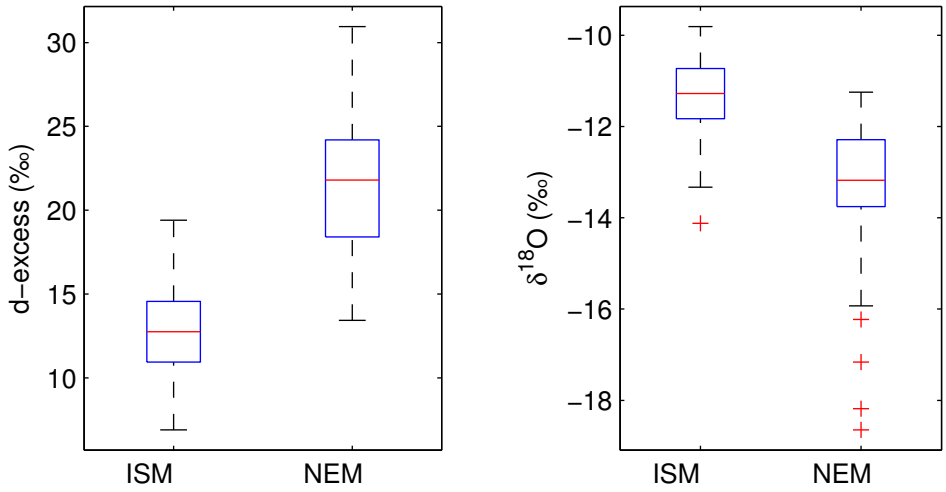

Figure 3.8: *Box and whisker plots showing the distribution of observed $\delta^{18}O_v$ and vapor d-excess during two cruises (SK-296 during ISM and SN-082 during NEM). Only the sample collected at height of ∼25m above sea level is considered. On each box, the central mark is the median, the edges of the box are the 25^{th} and 75^{th} percentiles, the whiskers extend to the most extreme data points that are not considered as outliers, and outliers are marked individually by the "+" symbol. At each station, correlation coefficients for each of the ten simulations are represented by box and whisker plots.*

pleted and has lower variability, while during NEM it is more depleted and with a large variability. Though the excess ^{18}O depletion during rain spells are observed in both the seasons, the magnitude of the depletion due to the storm activity during NEM is much higher compared that of rain spells associated with depressions during ISM. Vapor d-excess during ISM and NEM also show a similar difference with low d-excess during ISM. It should be noted that the $\delta^{18}O_v$ during non-rainy days (considering the rain along the back trajectory) of NEM is more depleted in ^{18}O compared to that of ISM.

Seasonality in the sea surface conditions can influence the isotopic composition of surface vapor. Figure 3.9 shows the seasonality in the ocean surface conditions such as SST, near surface atmospheric temperature and relative humidity for both the BoB (averaged over the region 85^o-91^{o}E and 10^o-19^{o}N) and the Arabian Sea (AS) (averaged over the region 65^o-72^{o}E and 10^o-19^{o}N). Climatological values of

air temperature and relative humidity climatology were from NCEP reanalysis and SST climatology taken from NOAA Optimum Interpolated SST. To check the influence of seasonality in these parameters on the $\delta^{18}O_v$ and d-excess , we calculated $\delta^{18}O_v$ and d-excess of surface vapor using the Craig and Gordon model by applying the closure assumption. Craig and Gordon model simulates a weak seasonality in vapor $\delta^{18}O$ values ($\sim$0.6 ‰) with a significant seasonality in the d-excess ($\sim$3-4 ‰). The amplitude of simulated seasonality in $\delta^{18}O$ is weaker due to less seasonal change in SST of the AS and the BoB, whereas the d-excess responds to normalized humidity which has a seasonal fluctuation of $\sim$15 % both in the BoB and the AS. So the observed difference in surface vapor $\delta^{18}O$ and d-excess cannot be completely explained by the C-G model.

Figure 3.10 shows the vertical averaged atmospheric meridional circulation simulated by IsoGSM [*Yoshimura et al.*, 2008] . During July the BoB is characterized by south-westerly with strong upward motion (convection), while during November the winds are northerly and have a descending motion before they enter the BoB. Thus winds during NEM may bring water vapor which is depleted in ^{18}O and has higher d-excess from higher altitudes to the ground during November. This effect of circulation on d-excess is simulated by IsoGSM. In July the lower d-excess (below 15 ‰) is observed up to 600 hPa in the areas of strong convection over the BoB, while this level comes down to below 800 hPa during November. Hence this prevailing circulation during November may also play a significant role in seasonality of $\delta^{18}O_v$ and d-excess .

3.5 Conclusion

In this chapter, a new data set of $\delta^{18}O$ and δD surface water vapor from BoB is presented. We observe a seasonal difference in the stable isotopic compositions, with higher (lower) values of $\delta^{18}O_v$ and lower (higher) values of vapor d-excess during ISM (NEM). The observed seasonal differences in $\delta^{18}O_v$ and vapor d-excess are possibly due to i) change ocean surface conditions (humidity and SST), ii) $\delta^{18}O$ depletion in the surface sea water due to the increased river runoff by the

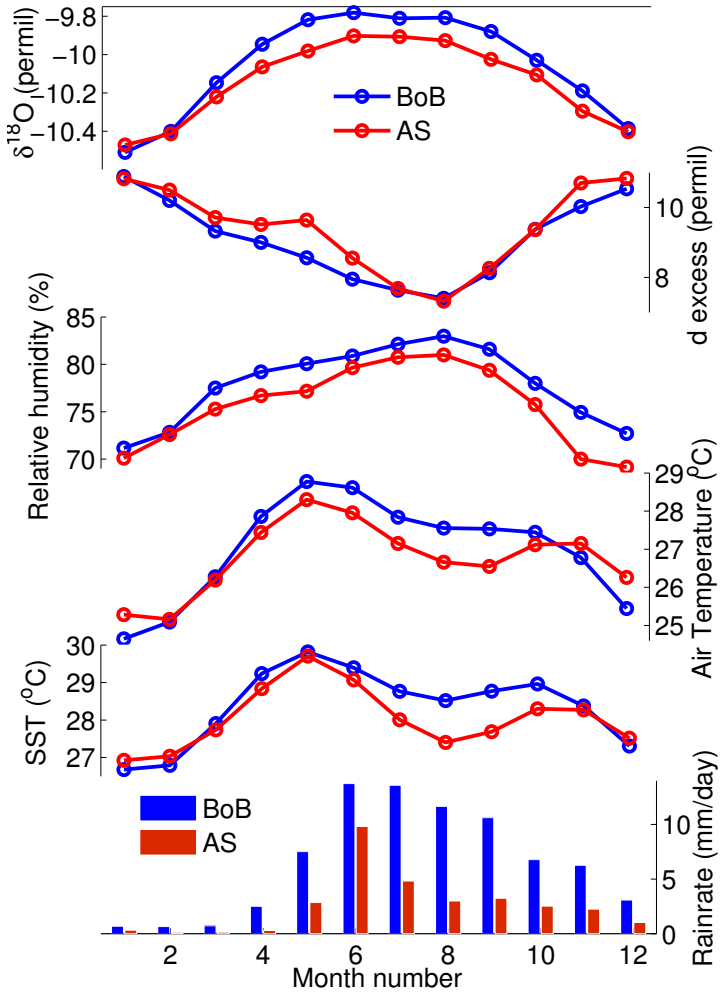

Figure 3.9: *Seasonality in $\delta^{18}O_v$ and d-excess predicted by C-G model owing to the change in relative humidity, air temperature and SST over BoB and the Arabian Sea. Seasonality in the rainfall is shown in the bottom panel [Source: NCEP and GPCP]*

end of ISM season iii) shift in circulation pattern and iv) change in the weather systems (i.e., monsoon storm/depressions vs. tropical cyclones). The estimation of $\delta^{18}O$ near surface vapor using the Craig -Gordon model with the closure assumption is close to the observed $\delta^{18}O_v$ values during non rainy days of ISM, but the observed $\delta^{18}O_v$ values are more negative during rainy days. These deviations are associated with rain-vapor isotopic exchange over the upstream region, as well as the mixing of surface vapor with the more ^{18}O depleted vapor from higher altitudes by convective downdrafts. The *d*-excess -normalized humidity relation appears to be weaker during both ISM and NEM over BoB compared

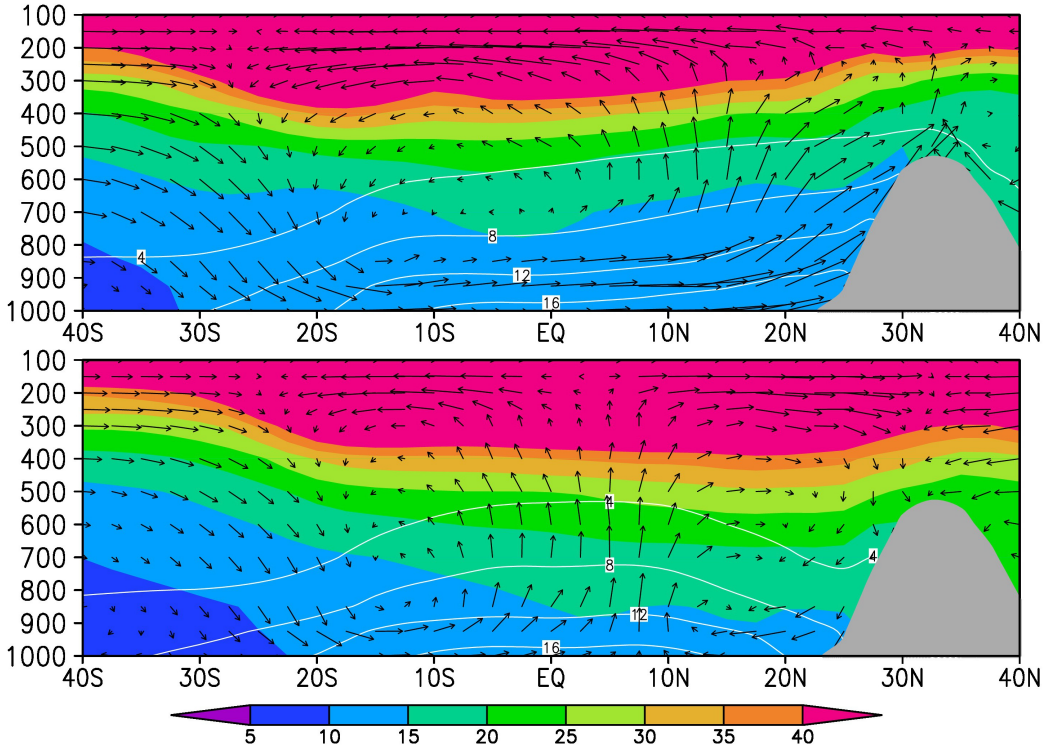

Figure 3.10: *Latitude-height diagram of longitudinally averaged (80°-100° E) atmospheric circulation, d-excess and specific humidity for July (top) and November (bottom). Vectors show winds, but the vertical component is exaggerated by a factor 50. Shaded colors show the d-excess and white contours represent specific humidity (gm/kg). The gray shading shows the topography. The diagram is produced using IsoGSM output.*

to that over southern Ocean and Atlantic. Over BoB, humidity during ISM is higher compared to NEM and a corresponding inverse seasonal difference is observed vapor d-excess , suggesting that d-excess - normalized humidity relation over BoB could be stronger on the seasonal time scale.

Chapter 4

Stable Water Isotopologues of Summer Monsoon Rainfall over Central and Northern India

This chapter presents the spatio-temporal variations of daily $\delta^{18}O_p$ and δD_p (stable isotopic composition of precipitation) during ISM 2013 over the northern Indian region. The main objectives are i) to check the potential of $\delta^{18}O_p$ in estimating the water vapor budget in the Indo-Gangetic plain ii) identify the local and remote meteorological parameters that control $\delta^{18}O_p$ and iii) to validate the monsoon simulations by the isotope enabled version of Experimental Climate Prediction Centers Global Spectral Model [IsoGSM; *Yoshimura et al.*, 2008].

4.1 Sampling strategy

Stations for rainwater collection are selected according to the wind pattern during ISM. The northern Indian region is characterized by two moisture transport pathways; the Arabian Sea (AS) branch and the Bay of Bengal (BoB) branch. Over the Indo-Gangetic plain, most of the precipitation originates from rainfall associated with the north-westward movement of monsoon depressions that form over the head bay (BoB). Four rain sampling stations where established along this transect (Station: Dhanbad, Varanasi, Kanpur and Delhi). North western

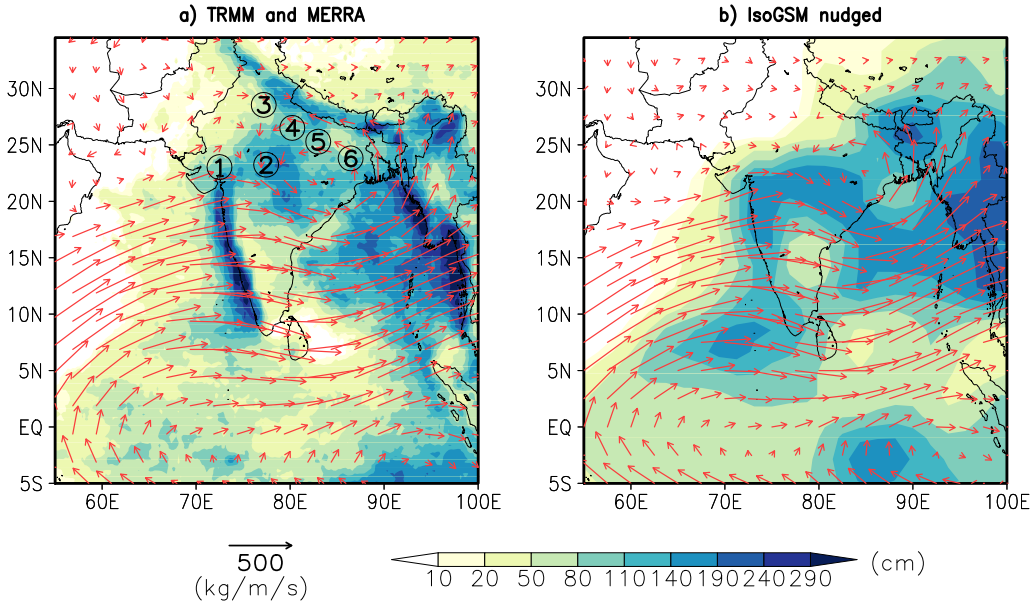

Figure 4.1: a) *The patial pattern of total rainfall (shaded, source: TRMM 3B42) and the mean vertically integrated moisture flux (vector, source: MERRA) during the months June-September, 2013. Sampling stations represented by circles are 1) Ahmedabad, 2) Bhopal, 3) New Delhi, 4) Kanpur, 5) Varanasi and 6) Dhanbad.* **b)** *Same as figure 4.1a, but from IsoGSM nudged simulations.*

and central India get a major portion of their rain from the AS branch. Rainwater samples were collected from two stations which are mainly influenced by the AS branch of moisture transport, (Ahmedabad and Bhopal) to characterize their isotopic composition. All samples were collected on a daily basis during June to September, 2013. Since we conducted sampling during only one ISM season, this data would not be an accurate representation of true climatology and insufficient to address the interannual variability. This is a major caveat of the present study. To overcome this, we compiled all the previously reported data from this region along with model simulations.

4.2 Rainfall, $\delta^{18}O_p$ and *d*-excess during ISM 2013

During 2013, ISM rainfall over India was ~6% higher compared to the long term climatology (http://www.imd.gov.in/section/nhac/dynamic/monsoon_

Table 4.1: *Rainfall and its isotopic characteristics at each station in 2013*

Station	Number of samples	Rainfall (mm)	JJAS rain weighted mean $\delta^{18}O_p$(‰)	LMWL[1]				Local Amount Effect[2]	
				d-excess (‰)	Slope	Intercept	r^2	Slope (‰/mm)	r^2
Ahmedabad	49	1249	−5.0±4.4	13.5±3.6	7.8±0.2	11.5±0.7	0.98	−0.05±0.01	0.23
Bhopal	58	960	−6.0±4.4	10.8±2.0	7.7±0.1	8.2±0.6	0.99	−0.05±0.02	0.07
New Delhi	26	530	−8.7±4.4	12.2±2.1	7.6±0.1	7.8±1.2	0.99	−0.08±0.03	0.19
Kanpur	28	989	−8.2±2.9	13.0±4.0	8±0.2	11.7±1.6	0.98	−0.02±0.02	0.05
Varanasi	38	726	−9.7±3.2	11.8±2.4	7.6±0.1	7.4±1.2	0.99	−0.09±0.03	0.15
Dhanbad	61	656	−8.9±3.2	11.3±2.1	7.6±0.1	7.2±0.9	0.99	−0.07±0.03	0.07

[1] Local Meteoric Water Line: δD_p=(slope) × $\delta^{18}O_p$ +(intercept)

[2] Amount effect: $\delta^{18}O_p$=(slope) × rainfall + constant

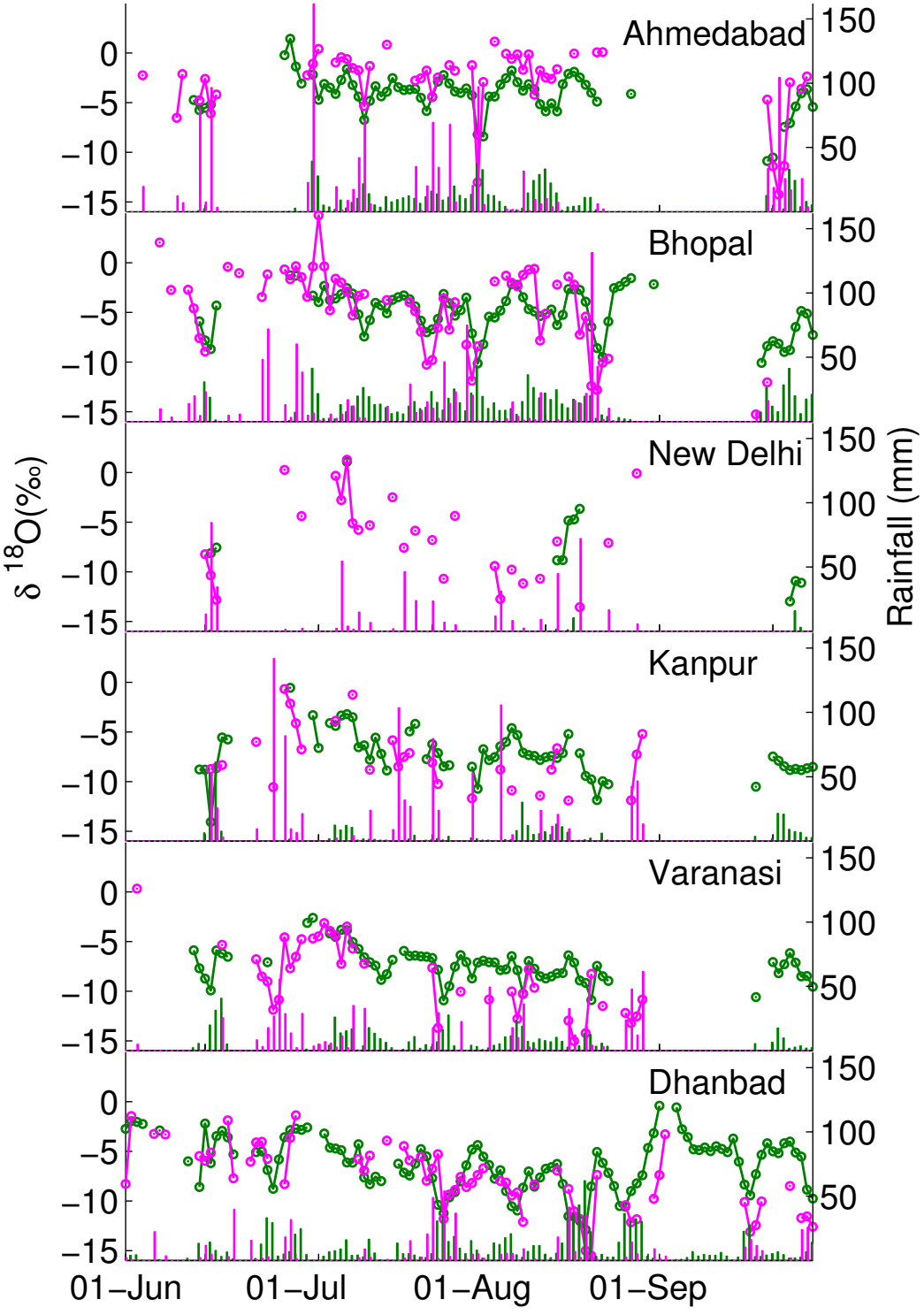

Figure 4.2: *Time series of rainfall (vertical bars) and $\delta^{18}O_p$ (line and scatter); magenta color represents observation and green color represents nudged IsoGSM simulations.*

Table 4.2: *A summary of ISM $\delta^{18}O_p$ and d-excess (source: GNIP)*

Stations	Month	Rainfall (mm) Average	Number of samples	JJAS Total	$\delta^{18}O_p$ (‰) Average	Number of samples	JJAS average	d-excess (‰) Average	Number of samples	JJAS average
Kolkata	Jun	196.97	3	1102.94	−7	1	−7.35	9.9	1	6.61
Latitude: 22°47'52"N	Jul	366.9	3		−8.10 ±0.67	3		6.10 ±3.63	3	
Longitude: 88°22'18"E	Aug	265.7	3		−6.43 ±0.12	3		9.67 ±2.85	3	
(270 km from Dhanbad)	Sep	273.37	3		−7.47 ±1.18	3		1.93 ±4.94	3	
Allahabad	Jun	168	1	1513	−6.3	1	−9.6	8.4	1	8.18
Latitude: 25°27'0"N	Jul	513	1		−7.39	1		5.62	1	
Longitude: 81°43'60"E	Aug	608	1		−12.21	1		9.28	1	
(120 km from Varanasi)	Sep	224	1		−10.05	1		10.9	1	
Lucknow	Jun	165.15	2	708.4	−8.91	1	−8.48	13.68	1	8.65
Latitude: 26°52'29"N	Jul	124.25	2		−8.53 ±2.13	2		8.24 ±2.04	2	
Longitude: 80°56'20"E	Aug	145	2		−8.88 ±1.38	2		6.94 ±3.44	2	
(90 km from Kanpur)	Sep	274	2		−7.99 ±1.69	2		6.71 ±1.71	2	
New Delhi	Jun	79.13	49	665.48	−0.77 ±3.75	43	−5.62	1.98 ±8.27	39	7.55
Latitude: 28°34'48"N	Jul	214.75	47		−4.95 ±2.68	40		8.02 ±5.97	36	
Longitude: 77°11'60"E	Aug	247.27	47		−6.52 ±2.65	41		8.17 ±3.49	37	
	Sep	124.33	48		−8.08 ±3.76	37		9.05 ±8.47	33	
Sagar	Jun	211.67	3	1865.27	−9.75 ±0.25	2	−6.82	9.00 ±4.00	2	9.31
Latitude: 23°49'34"N	Jul	541.93	3		−4.50 ±0.54	3		8.04 ±1.08	3	
Longitude: 78°45'45"E	Aug	320.37	3		−5.42 ±4.22	3		9.29 ±1.77	3	
(170 km from Bhopal)	Sep	791.3	2		−8.19 ±0.59	2		10.28 ±1.48	2	
Ahmedabad (events)	Jun	15.87	6	791.61	−3.90 ±3.33	6	−3.5	7.83 ±2.12	6	7.4
Latitude: 23°1'48"N	Jul	41.91	7		−2.91 ±3.25	7		6.51 ±7.38	7	
Longitude: 72°33'0"E	Aug	25.3	12		−3.58 ±2.71	12		8.97 ±2.58	12	
	Sep	16.57	6		−3.30 ±3.34	6		5.13 ±4.23	6	

Table 4.3: *Correlation coefficient between modeled (IsoGSM) and observed rainfall and $\delta^{18}O_p$. Bold numbers represent the significance level P<0.05.*

Station	Correlation Coefficient (r)	
	Rainfall	$\delta^{18}O_p$
Ahmedabad	**0.39**	**0.68**
Bhopal	0.09	**0.68**
Delhi	0.01	0.63
Kanpur	0.09	**0.53**
Varanasi	0.06	**0.64**
Dhanbad	**0.31**	**0.58**

report_2013.pdf). The measured rainfall and its $\delta^{18}O_p$ at each station during ISM 2013 are depicted in figure 4.2 and seasonal total rainfall and its $\delta^{18}O_p$ at each station are shown in table 4.1. Rainfall at individual stations owe higher or lower relative to their climatological means. Generally, JJAS rain-weighted $\delta^{18}O_p$ of the year 2013 at each station is relatively more negative compared to the previous reported values at the nearest GNIP station (table 4.2). This can be attributed to the interannual variability of ISM $\delta^{18}O_p$. The slope of the Local Meteoric Water Line (LMWL) during 2013 at each site varied from 7.6 to 8.0 and the intercept varied from 7.2 to 11.7 ‰, which are comparable to the previously reported values over this region [*Deshpande et al.*, 2010; *Kumar et al.*, 2010; *Sengupta and Sarkar*, 2006]. Significant amount effect is observed at five stations, but it explains only ∼7-23 % of the observed variance of daily $\delta^{18}O_p$. Four out of six stations (all except Ahmedabad and New Delhi) show a significant temporal decreasing trend in $\delta^{18}O_p$ during the season. This trend is not statically significant at New Delhi due to a continuous 3-day ^{18}O-depleted rainfall event during the initial part of the season. However, long-term observations at New Delhi show statically significant trend in $\delta^{18}O$ during the ISM (Fig 4.11).

4.3 Comparison with IsoGSM simulations

IsoGSM simulation of SWI in ISM rainfall is evaluated using our observations. IsoGSM is forced with observed SST, and the wind field is constrained using spectral nudging technique with reanalysis data [i.e., NCEP reanalysis-2, *Kanamitsu et al.*, 2002]. Figure 4.1 shows the comparison of the spatial pattern of rainfall and moisture transport vectors between the nudged simulation of IsoGSM and observations. Linear correlation coefficient of the simulated spatial rainfall pattern with observation is 0.75 over the area shown in figure 4.1 (TRMM rainfall data are interpolated into the model grid for calculating the correlation coefficient). The model captures the anomalous rainfall over central Indian region, which is one of the major features of ISM 2013. IsoGSM underestimates the north western limit of ISM rainfall, especially in the region beyond Kanpur, the model is not able to simulate the observed rainfall. This is a major problem associated with most of the GCMs (for example, see Fig. 5.3 in the next chapter). However, as a result of nudging, the model simulated moisture flux is similar to the observations.

The model simulated temporal variation of daily rainfall is weakly correlated with TRMM observed rainfall (Fig. 4.3, TRMM observations are interpolated into model grids to perform the temporal correlation analysis at each model grid). Over northern India, these correlations are mostly insignificant. Over our sampling stations, simulated daily rainfall shows an insignificant correlation with measured rain amount (except at Ahmedabad and Dhanbad, table 4.3; Observed $\delta^{18}O_p$ and rainfall is correlated with those simulated at the nearest grid point of the model). This is an inherent problem with most of GCMs over ISM region. Interestingly, the simulation of $\delta^{18}O_p$ is more consistent with observations than rainfall (Table 4.3), except in New Delhi, where the model has a huge dry bias. The model predicted intraseasonal $\delta^{18}O_p$ is closer to the observations than that of rainfall. This may due to the dominant control of moisture transport pathways on $\delta^{18}O_p$ variability, an aspect further discussed in section 4.5.

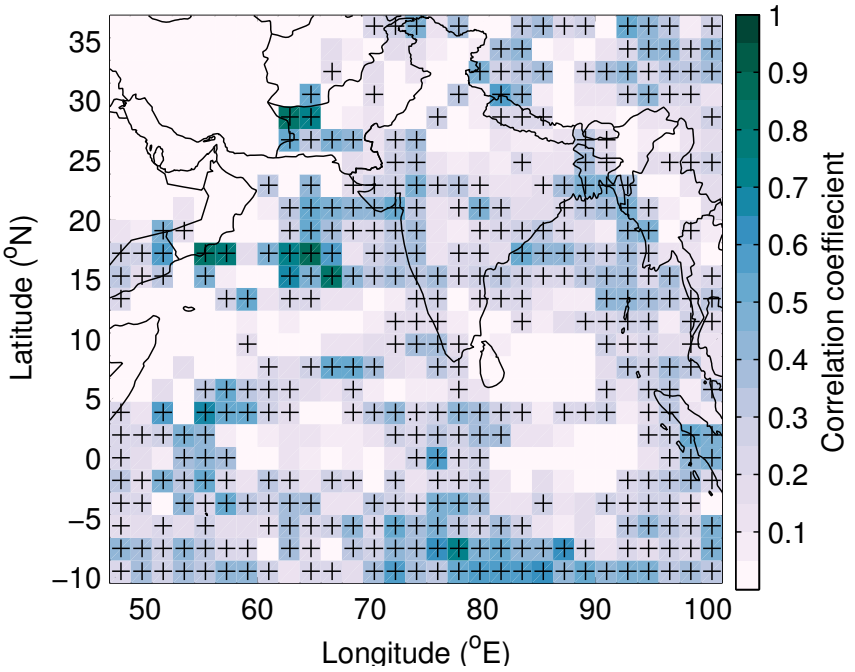

Figure 4.3: *Correlation coefficients between temporal variation of modeled (IsoGSM) and observed (TRMM) rainfall at each model grid point. Statistically significant correlations (P<0.05) are represented using "+" symbol*

4.4 Back trajectory analysis

To check the role of moisture sources and processes along parcel trajectory, HYSPLIT ensemble back trajectory analysis were carried out. For this, rainfall events are classified into three categories; i) enriched events (events with $\delta^{18}O_p > \mu + 0.5\sigma$, where μ and σ are the mean and standard deviation of $\delta^{18}O_p$ at each station) ii) median events (events with, $\mu - 0.5\sigma < \delta^{18}O_p < \mu + 0.5\sigma$) and iii) depleted events (events with, $\delta^{18}O_p < \mu - 0.5\sigma$). Composite of trajectory density for each category is calculated and depicted in figures 4.4 & 4.5. Rain during enriched events at Ahmedabad, Bhopal and New Delhi is solely contributed by the AS branch (Fig. 4.4). Respectively 16.6, 28.0 and 14.6 % of total rain at these stations are enriched events. At Ahmedabad and Bhopal, depleted events (contributes 43.2, 43.8 % of total rain, respectively) are associated with the trajectories from both the AS and the BoB branches, but the BoB branch slightly dominates. 49.2 % of the total rain at New Delhi occurred during depleted

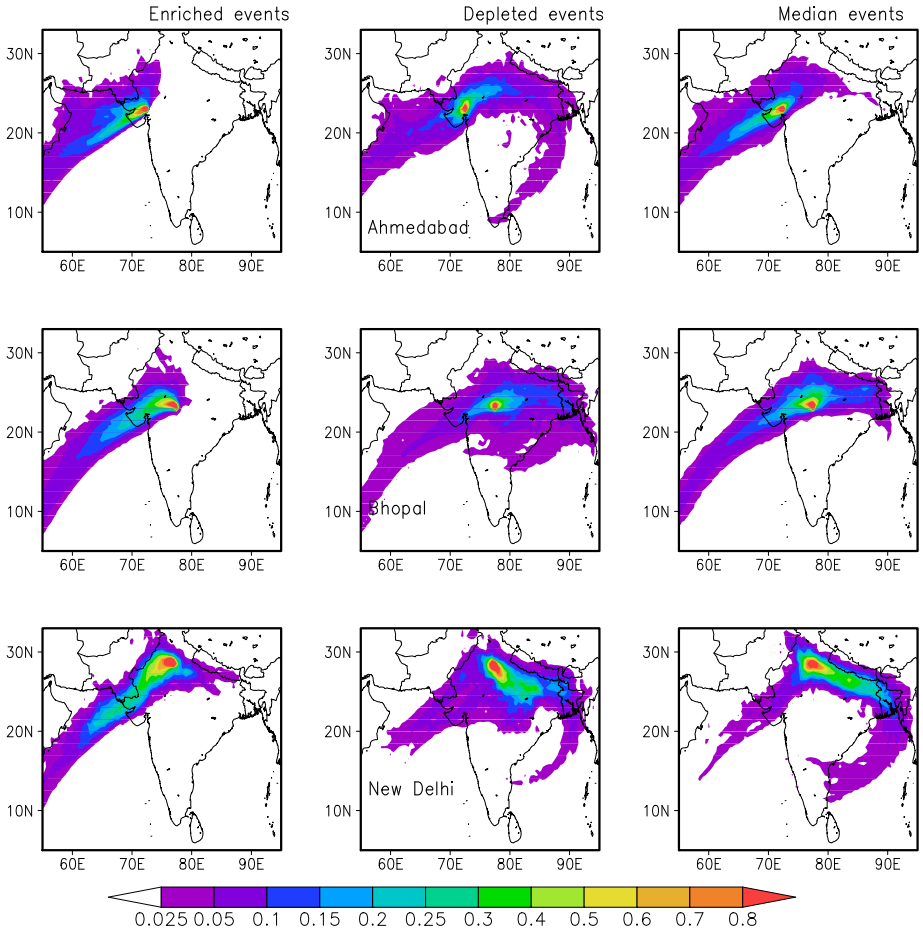

Figure 4.4: *Trajectory density during enriched, median and depleted events for the stations Ahmedabad (first row), Bhopal (second row) and New Delhi (third row). All the rain events are classified into 3 categories; enriched, median and depleted events as defined in the text.*

events with clearly dominated trajectories through BoB branch. Median events at Ahmedabad (40.2 % of the total rain) are mainly characterized by moisture transport through the AS branch, while both the branches equally contribute to the median events at Bhopal (28.2 % of the total rain). BoB branch is dominated during median events (36.2% of the total rain) at New Delhi. Generally at these stations, anomalous trajectory densities over the AS branch is observed during enriched events whereas, the most depleted events are characterized by more trajectories through the BoB branch (Fig. 4.6).

At Kanpur, Varanasi and Dhanbad 13.8, 20.9 and 20.2 % of the total rain is respectively contributed during the enriched events. During these events, at

Dhanbad, trajectories originate from the AS, and advance to the station via the head BoB, while the trajectories reaching Kanpur and Varanasi do not pass through the BoB (Fig. 4.5). During depleted events at these stations (30.3, 52.9 and 38.3 % of the total rain at Kanpur, Varanasi and Dhanbad), both the branches are present in the trajectories, but the BoB branch clearly dominates at Kanpur and Varanasi. At Kanpur, during median events (55.9 % of the total rain) trajectories belong mainly to the BoB branch with a little contribution from the AS branch. Both the AS and BoB branches contribute to median events at Varanasi (26.2 % of the total rain). Median events at Dhanbad (41.5 % of the total rain) are contributed by the BoB branch, which has an extension towards the AS through the peninsular India as observed during enriched events. Generally at these three stations enriched and depleted events show two distinct air parcel trajectories as seen in figure 4.6.

For stations Ahmedabad, Bhopal and New Delhi, $\delta^{18}O_p$ is well correlated with total rainfall along the five day back trajectory (Fig, 4.7). This correlation is stronger than the local amount effect, suggesting that condensation along the trajectory has a major role on $\delta^{18}O_p$ variability. A similar correlation between rain along the trajectory and $\delta^{18}O$ of boundary layer vapor over the tropical oceans were previously reported [*Kurita*, 2013; *Midhun et al.*, 2013]. This correlation is weaker at Dhanbad, Varanasi and Kanpur (Fig, 4.7).

4.5 Role of moisture source on $\delta^{18}O_p$

To check the role of moisture sources on $\delta^{18}O_p$, we performed correlation analysis between $\delta^{18}O_p$ and Q_v. As seen in the trajectory analysis (Fig. 4.9 & 4.8), $\delta^{18}O_p$ at New Delhi, Bhopal and Ahmedabad are strongly modulated by the variations in the moisture transport pathways. $\delta^{18}O_p$ shows a strong positive correlation with Q_v over the AS branch, while it shows significant negative correlation over the BoB branch. This relationship between $\delta^{18}O_p$ and Q_v is well captured in the IsoGSM simulations for Ahmedabad and Bhopal (Fig. 4.8), while it fails to reproduce it over New Delhi (Fig. 4.10). The model's failure may be

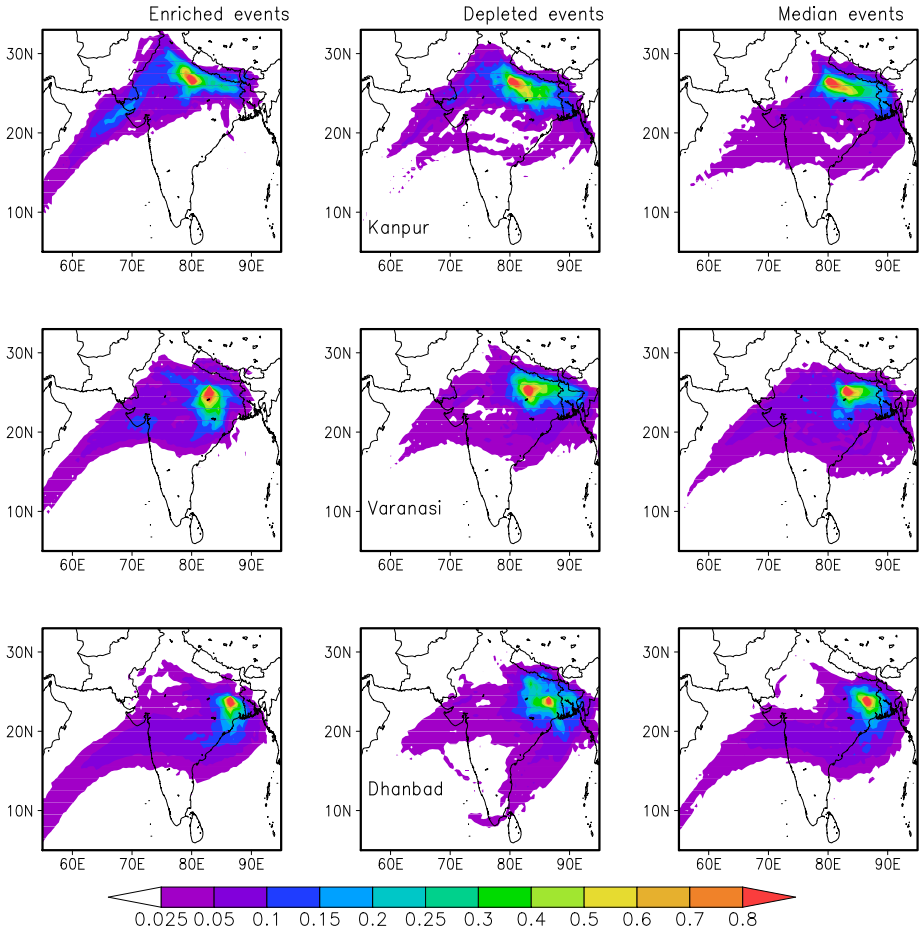

Figure 4.5: *Same as in Figure 4.4 but for stations Kanpur (first row), Varanasi (second row) and Dhanbad (third row).*

due to the dry bias in the modeled ISM rainfall over New Delhi (only 11 rainy days are simulated during ISM 2013 at New Delhi).

To check the role of switching the moisture source on $\delta^{18}O_p$ during the ISM on longer time scales, we also checked the $\delta^{18}O_p$ and Q_v relation over New Delhi using long term GNIP data set. Since New Delhi has $\delta^{18}O_p$ observations prior to 1979, we use NCEP reanalysis-1 to calculate Q_v. The observed ISM $\delta^{18}O_p$ - Q_v relation is strong and significant on monthly and interannual timescales. Again, it should be noted that IsoGSM fails to capture this relation over New Delhi on monthly and interannual timescales (Fig 4.10). Our analysis suggests that the dual moisture source has a significant role in modulating monsoon $\delta^{18}O_p$ on daily to interannual timescales over this region. These effects must be taken into

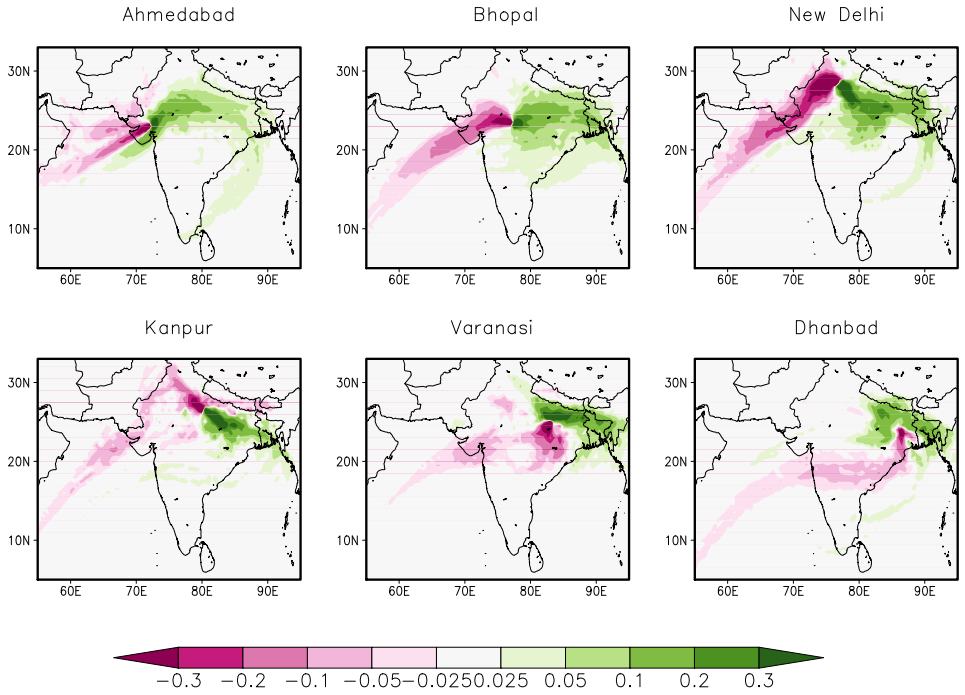

Figure 4.6: *Difference in the trajectory density between enriched and depleted events. Positive (negative) values represent higher trajectory-density during depleted (enriched) events.*

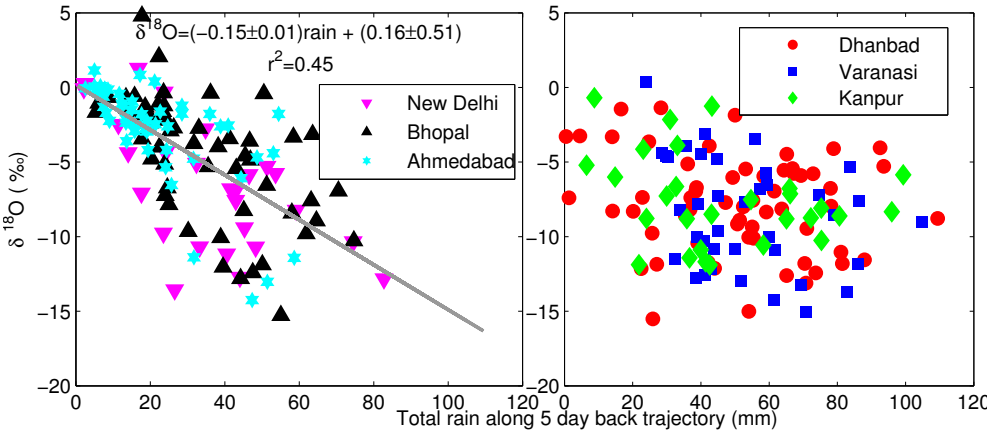

Figure 4.7: *Relation between the rainfall $\delta^{18}O$ and the total rain along 5-day back trajectory.*

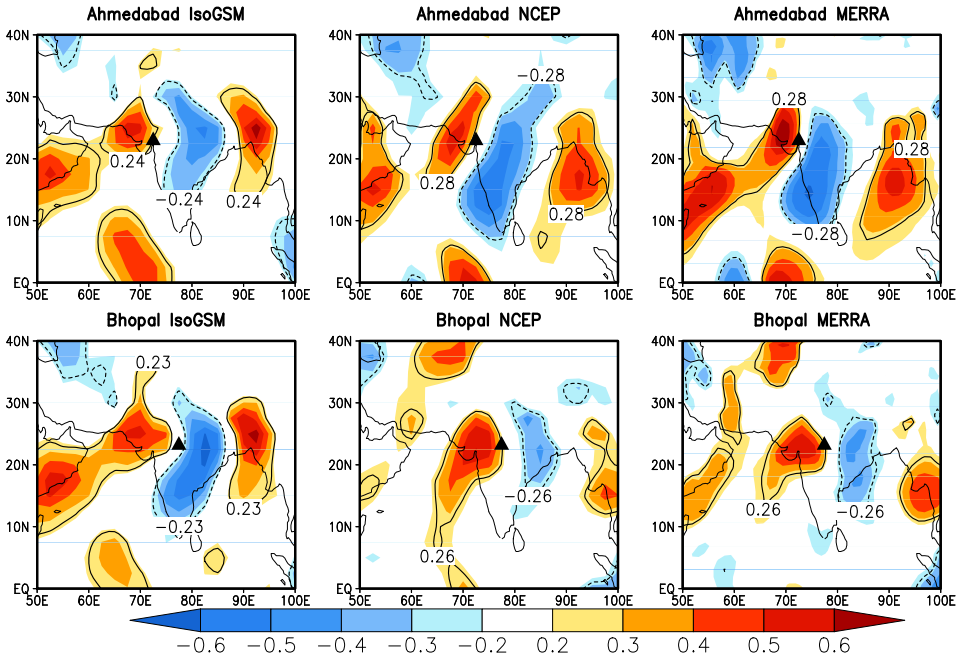

Figure 4.8: *Modeled (IsoGSM) and observed correlation (NCEP and MERRA) between $\delta^{18}O_p$ and meridional moisture transport vectors (Q_v) during ISM 2013 for station Ahmedabad and Bhopal. Black (continuous and dashed) contour lines represent the significant correlations at P=0.05 level. Filled triangle represents the location of $\delta^{18}O_p$ observation. Q_v, calculated using equation 2.1*

account while interpreting rainfall-^{18}O based proxies from this region.

4.6 Depleting trend in $\delta^{18}O_p$ during ISM

In the newly presented data as well as in the previously reported $\delta^{18}O_p$ from the northern Indian region, a significant depleting trend in $\delta^{18}O_p$ is observed during the ISM. *Sengupta and Sarkar* [2006] proposed that this trend could be due to the shift in the origin of monsoon depression from northern to southern (below 15^{o}N) BoB, resulting in a longer condensation history of the air parcel and gives more ^{18}O depleted rain over Kolkata. Later *Breitenbach et al.* [2010] attributed this depletion to the formation of fresh water plume in head BoB by discharge from Ganga-Brahmaputra river system. They estimated that, the corresponding depletion in $\delta^{18}O$ of surface water at head BoB can be up to $-4.5‰$, however

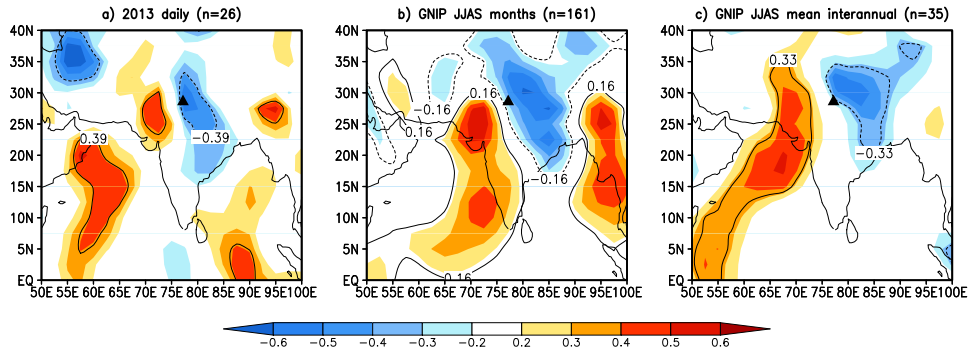

Figure 4.9: *Correlation between $\delta^{18}O_p$ and Q_v over New Delhi on different timescales; a) daily (2013 observations) b) monthly (GNIP data) and c) interannual (GNIP data).*

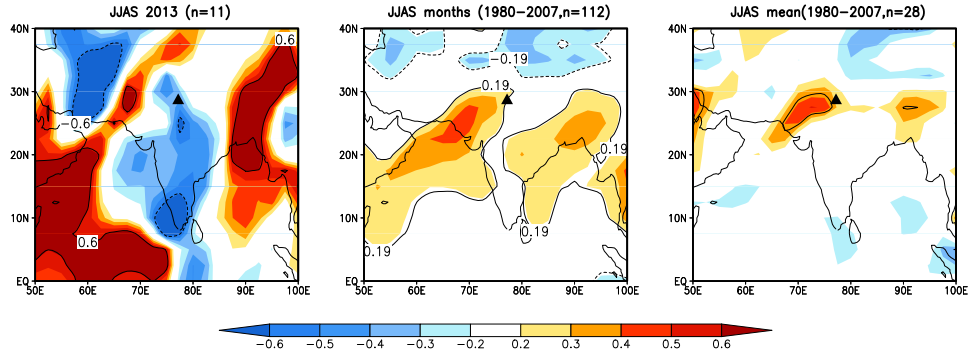

Figure 4.10: *Same as in figure 4.9, but from IsoGSM simulations*

the average of observed $\delta^{18}O$ of surface water over BoB is $\sim -0.4‰$ [*Achyuthan et al.*, 2013; *Sengupta et al.*, 2013; *Singh et al.*, 2010]. We also estimated the possible value of $\delta^{18}O$ of surface water at head BoB from climatological salinity (S) data using the reported $\delta^{18}O$-S relations [*Sengupta et al.*, 2013; *Singh et al.*, 2014], and is expected to have a range of -0.2 to -0.8 . Thus the evaporation from this freshwater plume can not contribute to the observed trend in $\delta^{18}O_p$. We observe that over the inland station New Delhi (Fig. 4.11), this trend is arising from the switching of moisture transport pathway from the AS branch to the BoB branch as the ISM season advances (Fig. 4.12). But the cause of similar trends observed over the stations closer to head BoB is not fully understood.

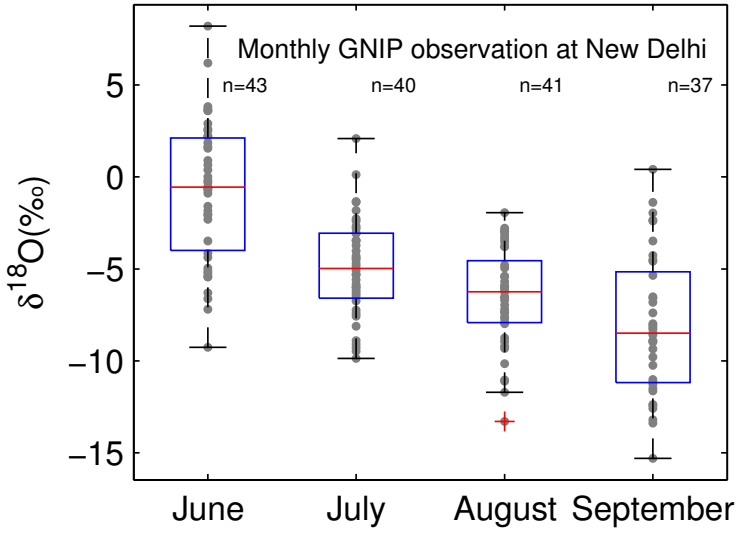

Figure 4.11: *Box and whisker plot showing the distribution of monthly $\delta^{18}O_p$ observations at GNIP station New Delhi. Gray circles show the individual observations.*

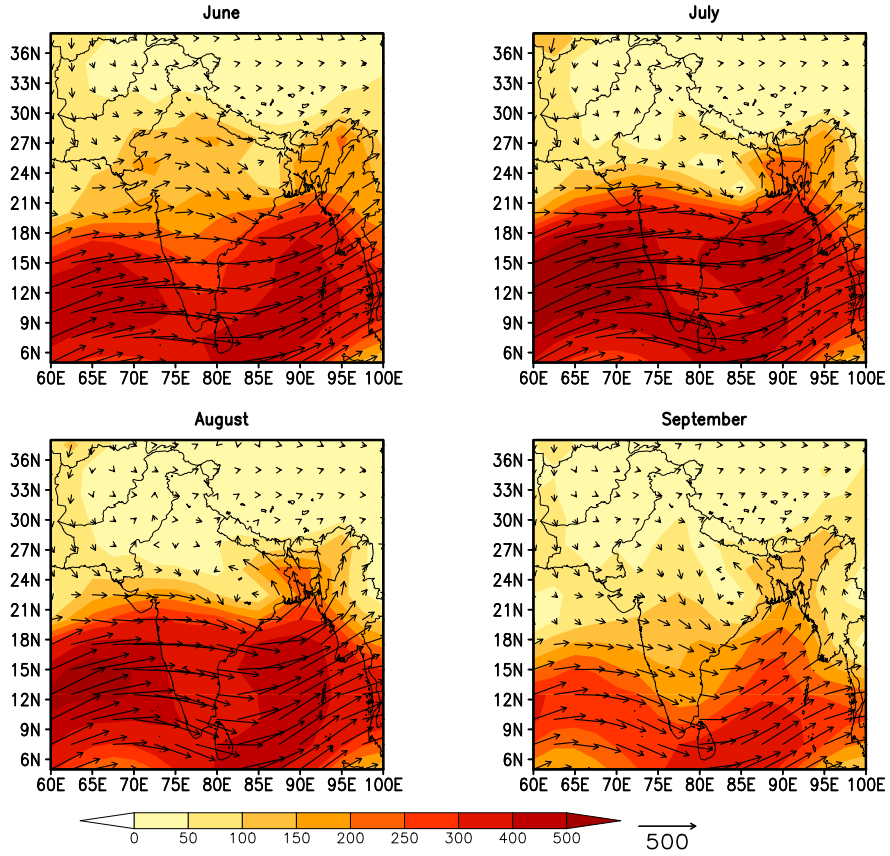

Figure 4.12: *Vertically integrated moisture transport flux (unit: kg/m/s, climatology) during June, July, August and September. Data source: NCEP Renalysis-1*

4.7 Continental effect

The gradual depletion in $\delta^{18}O$ of ground water observed along Kolkata-Delhi sector was explained as the continental effect of $\delta^{18}O_p$ [*Krishnamurthy and Bhattacharya*, 1991]. But this is neither observed in GNIP $\delta^{18}O_p$ (Table 4.2) nor in our observations along this sector. GNIP observations show a depletion in $\delta^{18}O_p$ at Allahabad (∼120 km from Varanasi) by ∼2‰ compared to that at Kolkata. A similar $\delta^{18}O_p$ depletion of ∼0.8 ‰ is observed at Varanasi compared to Dhanbad in our observations. But no further $\delta^{18}O_p$ depletion towards New Delhi is observed (both in GNIP and in our observations). *Sengupta and Sarkar* [2006] suggested that the $\delta^{18}O_p$ enrichment along Allahabad-Delhi sector is due to the possible contribution from the $\delta^{18}O$ enriched vapor by evapo-transpiration as well as from AS branch of moisture transport. Our study confirms the role of the AS branch of moisture flux at New Delhi and Kanpur as suggested by *Sengupta and Sarkar* [2006] and there by modulating the spatial variation of $\delta^{18}O_p$ along Kolkata-Delhi sector.

4.8 Conclusions

A new data set for ISM $\delta^{18}O_p$ and δD_p with high spatial and temporal resolution is presented.Local amount effect is observed at five out of six stations, but rainfall explains only ∼7-22 % of $\delta^{18}O_p$ variability. IsoGSM simulates the large scale feature of spatial rainfall pattern during 2013, but it fails to simulate the north-western limit of ISM rainfall. Though IsoGSM fails to simulate temporal variation of daily rainfall, the simulated $\delta^{18}O_p$ is in good agreement with observations. Both back-trajectory analysis and correlation analysis (between $\delta^{18}O_p$ and Q_v) suggest that $\delta^{18}O_p$ at Ahmedabad, Bhopal and Delhi are strongly influenced by the variations in moisture transport pathways. i.e., the contribution from AS enriches the $\delta^{18}O_p$ while it get depleted during the rain which cuased by the BoB component of moisture flux. The observed correlation between $\delta^{18}O_p$ and meridional moisture flux is well simulated by IsoGSM at Ahmedabad and Bhopal, but not at New Delhi. Moisture transport pathways play a major role on the

$\delta^{18}O_p$ variability on daily to interannual time scales over New Delhi. This must be taken into account while interpreting the ^{18}O based climate proxies from this region

Chapter 5

Multi-model Simulations of Stable Water Isotopologues in the Indian Summer Monsoon Rainfall

In this chapter the isotope enabled GCM simulations from Stable Water Isotope Intercomparison Group, Phase 2 (SWING2) were anlyzed to assess their ability to simulate the present day $\delta^{18}O_p$ of ISM. First, we check their ability to re produce the annual cycle of rainfall over India, and spatial distribution of rainfall over the ISM region (10^oS to 40^oN and 50^oE to 110^oE, Fig 5.1). This region, besides India, includes the Equatorial Indian Ocean in addition to some stations from southern China and South East Asia, which are all under the influence of ISM [*Wang*, 2005]. Next, we assess the skill of SWING2 models in reproducing the spatio-temporal variations of $\delta^{18}O_p$ over the ISM region. Finally, the possible role of local precipitation, regional precipitation and ENSO on the interannual variability of summer monsoon $\delta^{18}O_p$ is discussed.

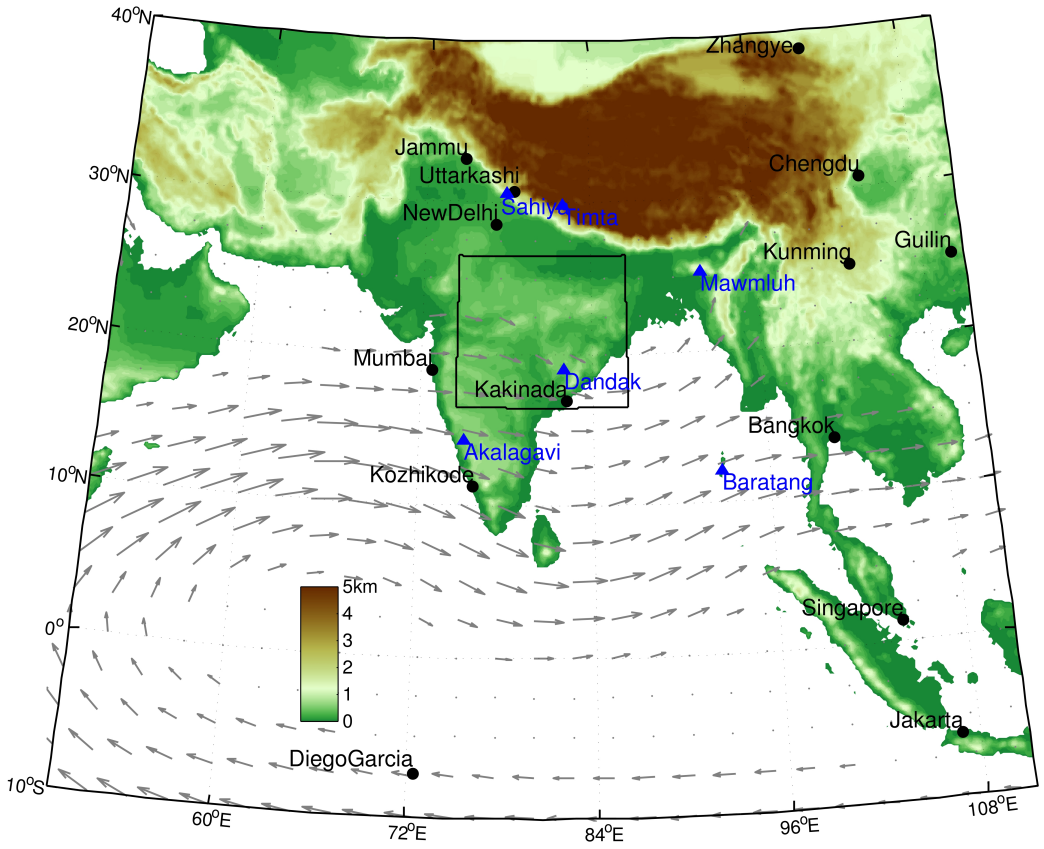

Figure 5.1: *Geographical map of South Asia showing topography (shaded, altitude above mean sea level), location of GNIP stations (black circles) and locations of major cave sites (blue triangles) over India. The area highlighted by the rectangle over central India indicates the core monsoon region (CMR). Winds at 850 hPa during ISM (called the Low Level Jet) is shown using gray arrows.*

5.1 Indian Monsoon Rainfall

5.1.1 Annual cycle of precipitation over the core monsoon region (CMR)

The annual cycle of rainfall over India is characterized by peak ISM rainfall during June-September (JJAS). To check the skill of SWING2 models in simulating this cycle, we analyze rainfall simulations over the CMR ($74.5 - 86.5^oE, 16.5 - 26.5^oN$), where the mean and standard deviation of JJAS rainfall are homogeneous [*Goswami et al.*, 2006]. 5.2a depicts the annual cycle of rainfall over CMR. Though most of the models produce high rainfall during JJAS, the amounts of

rainfall simulated by different models show a large spread. Model simulations exhibit good correlations with observation (GPCP), ranging from ∼0.85 to ∼0.99 (significant at P < 0.01 level) (Fig. 5.2b). Rainfall simulated by MIROC32, nudged GSM and free GISS are the closest to observations, whereas LMDZ (free and nudged) and nudged GISS exhibit significant dry bias while CAM2 and HadAM3 show wet bias. CAM2 simulates intense rainfall during pre-monsoon months as well, in contrast to observations [*Nanjundiah et al.*, 2005]. Nudged simulations of rainfall from GSM and LMDZ show improvement compared to their free runs, whereas no significant improvement was observed in nudged GISS relative to its free run.

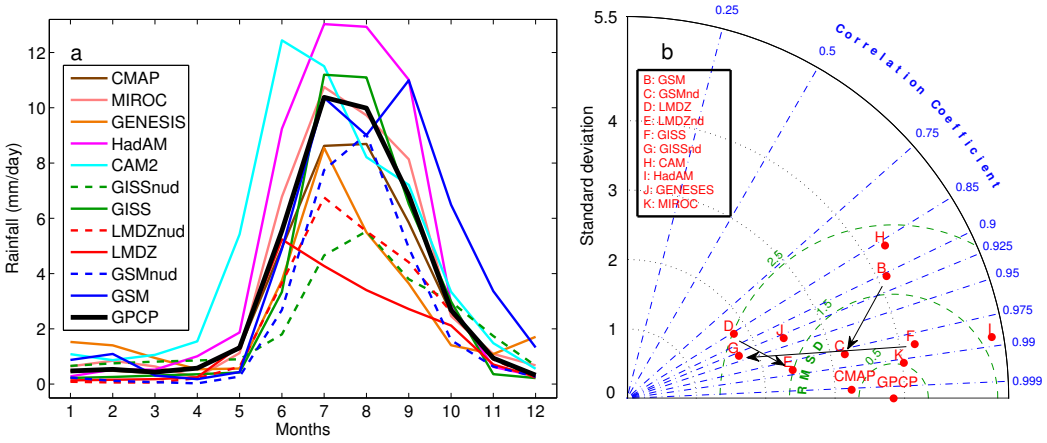

Figure 5.2: *a) Observed (GPCP and CMAP) annual cycle of monthly mean (1981-1999) rainfall over CMR, and those simulated by SWING2 models. b) Taylor diagram of annual cycle of rainfall over CMR simulated by different models and observations (GPCP, CMAP). GPCP rainfall is used as reference. Black arrows indicate the change from free" model simulation to model nudged with reanalysis winds. Green semi circles represent the bias removed root mean square deviation from the observations*

5.1.2 Spatial pattern of JJAS precipitation

The observed ISM rainfall shows a large spatial variability over the Indian subcontinent, with two rainfall maxima over the mountain ranges of Western Ghats

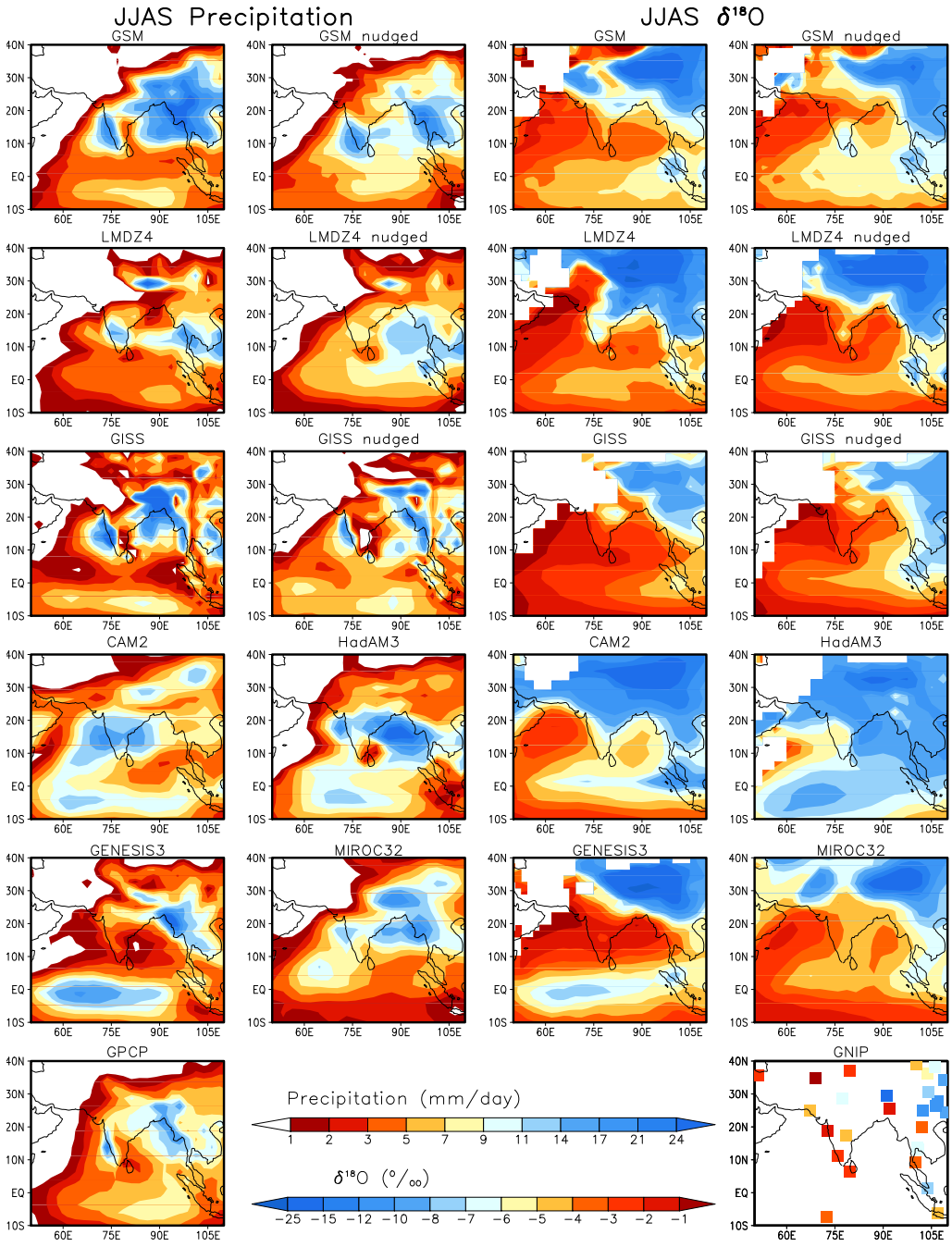

Figure 5.3: *Comparison of spatial patterns of precipitation simulated by SWING2 models with the observed (GPCP) rainfall (left two columns) and their $\delta^{18}O_p$ with GNIP $\delta^{18}O_p$ (right two columns) for the months June to September. A bias correction of +6 ‰ was applied to GENESIS simulated $\delta^{18}O_p$ [Mathieu et al., 2002].*

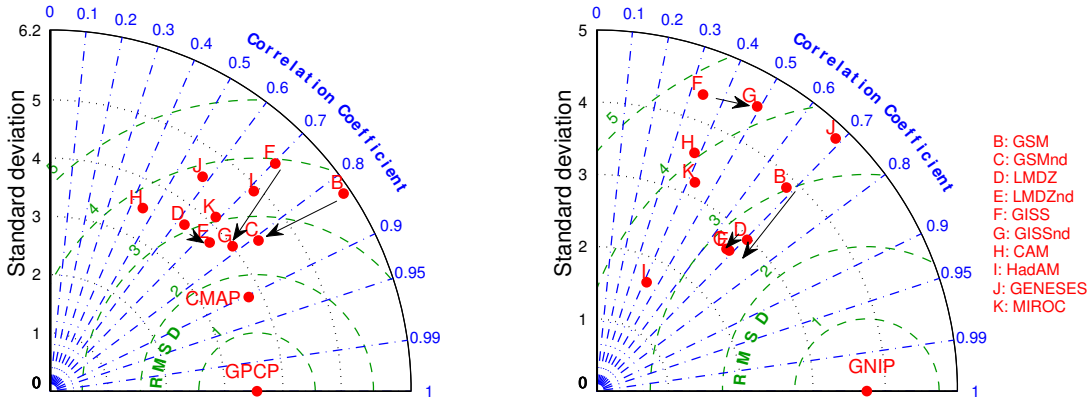

Figure 5.4: *a) Taylor diagram showing multi model comparison of spatial pattern of precipitation and b) its $\delta^{18}O_p$. GPCP rainfall data and GNIP $\delta^{18}O_p$ data are taken as references. Black arrows indicate the change from free" model simulation to model nudged with reanalysis winds.*

(western coast of peninsular India) and Myanmar (extending up to the northern Bay of Bengal). Its northwestern limit lies in the arid regions of Rajasthan, Punjab and parts of Pakistan. Model simulations of climatological mean JJAS precipitation over the ISM region are plotted in 5.3 and their coherence with observations are illustrated using a Taylor diagram in figure 5.4a. Though all the models simulate the annual cycle of rainfall with higher amounts during JJAS over CMR, the spatial patterns of rainfall vary significantly. Major features, e.g., rainfall peaks along the south western coast of India and the northern Bay of Bengal, are captured by most models. They fail to simulate the observed north western limit of JJAS rainfall (except for CAM2 and HadAM3). Recently, a very high resolution simulation of ISM using LMDZ (zoomed LMDZ with ∼35 km resolution over the ISM region) drastically improved the spatial pattern of ISM rain over India [*Sabin et al.*, 2013]. Hence the model resolution appears to significantly influence its output. Pattern correlation of gridded rainfall (for the area $50 - 110^oE$ & $10^oS - 40^oN$) between GPCP data and SWING2 models varied from ∼0.45 to ∼0.82 (significant at $P < 0.01$ level). The GPCP dataset is used as a reference in the Taylor diagram (CMAP shows a standard deviation similar to GPCP, but with a correlation of 0.90 with GPCP). Spatial patterns of rainfall are

considerably improved by the nudging technique in GSM, LMDZ and GISS (Fig. 5.3 & 5.4a); these are the best SWING2 models in this respect. The problem of over-prediction of rainfall peaks in the free runs of GSM and GISS vanished in their respective nudged simulations, whereas rainfall was underestimated in both (nudged and free runs) simulations for LMDZ.

5.1.3 Interannual Variability of ISM in CMR

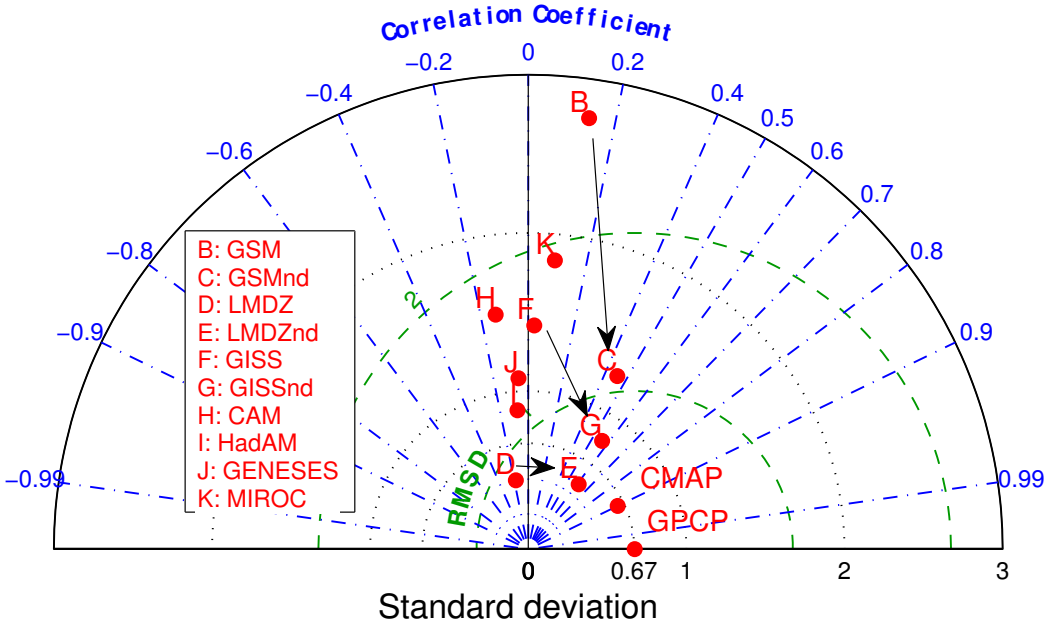

Figure 5.5: *Taylor diagram showing the performance of SWING2 models in reproducing interannual variations of ISM rainfall (JJAS-average rainfall) over CMR. GPCP data are used as reference. Black arrows indicate the change from free" model simulation to model nudged with reanalysis winds.*

A comparison of the interannual variability of JJAS rainfall simulated by SWING2 models with observations over CMR is presented in Fig. 5.5. Nudged simulations of GSM, LMDZ and GISS display significant positive correlations ($P < 0.05$) with the observations, while all the other models (forced by SST only) fail. Though the nudged simulation of LMDZ underestimates the JJAS rainfall, its interannual variability is the closest to observations among all the SWING2 models. Though SST fluctuations do lead to rainfall variability and circulation changes in the tropics, modeling ISM using SST forcing alone is inadequate; a

realistic representation of the atmospheric circulation plays a major role in the correct simulation of interannual variability of ISM.

5.2 $\delta^{18}O$ of precipitation

5.2.1 Comparison of observed $\delta^{18}O_p$ time series with that simulated by SWING2 models

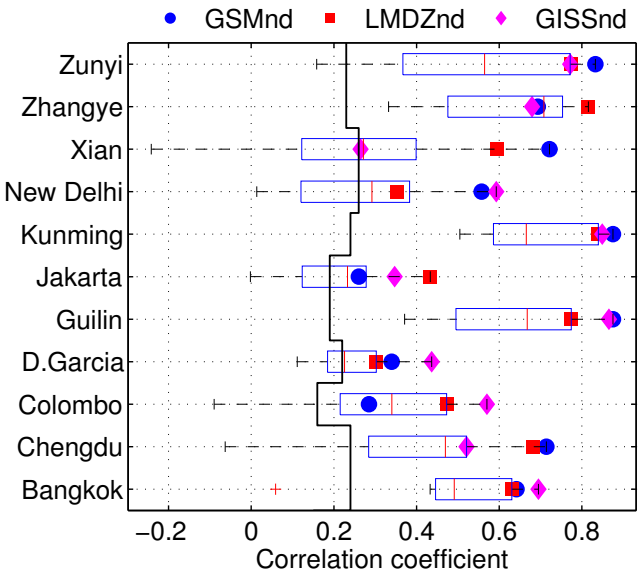

Figure 5.6: *The linear correlation coefficients between observations (GNIP) and simulations (SWING2) of monthly $\delta^{18}O_p$. All available monthly observations during 1981-1999 are used for this calculation (see Fig. 3.8 for the symbol description). Nudged simulations by GSM, LMDZ and GISS are also plotted using filled symbols (suffix "nd" refers to nudged). Values significant at $P = 0.05$ lie to the right of the zig-zag vertical black line.*

To validate the SWING2 models, we compared the time series of monthly $\delta^{18}O_p$ simulations and observations (Fig. 5.6). For this, we selected 11 GNIP stations which have at least 60 monthly $\delta^{18}O_p$ observations in common with the SWING2 simulation period (i.e., 1981-1999). Linear correlation coefficients (r) between each of the ten SWING2 simulated $\delta^{18}O_p$ and the observed GNIP $\delta^{18}O_p$ at these stations were calculated. The median correlation coefficients of the 10

simulations ranged from ~ 0.2 to ~ 0.7. For 3 GNIP stations over the East Asian region (Zhangye, Guilin and Kunming), all SWING2 models show significantly (at $P < 0.05$) strong positive correlations. Generally, the nudged simulations from GSM, LMDZ and GISS are closer to observations compared to (i) their respective free runs; and (ii) the rest of the SWING2 models as well. Improvements in correlation coefficients, relative to their free runs are statistically significant ($P < 0.05$) for 7 stations for GSM and LMDZ and 8 stations for GISS. This highlights the influence of the circulation pattern, better represented in the three nudged simulations, on rainfall $\delta^{18}O_p$.

5.2.2 Spatial pattern of JJAS $\delta^{18}O_p$

Spatial variations of $\delta^{18}O_p$ are mainly governed by isotopic effects such as latitudinal effect, continental effect, altitude effect, amount effect etc [*Araguás-Araguás et al.*, 2000]. Continental moisture recycling (evapo-transpiration) also affects the spatial distribution of $\delta^{18}O_p$ over land. A comparison of observed and modeled JJAS weighted mean $\delta^{18}O_p$ is depicted in Fig 5.3. The corresponding Taylor diagram is presented in Fig 5.4b. Correlation coefficient between the spatial patterns of the observed $\delta^{18}O_p$ (for the area $50-110^oE$ & 10^oS-40^oN) and the simulated $\delta^{18}O_p$ varied from 0.32 to 0.71 (correlations above 0.37 are significant at $P < 0.05$ level). Though some of the models show pattern correlations close to 0.70, the spread in simulated $\delta^{18}O_p$ values (standard deviation) is either too high or too low, compared to observations (except in the case of the free run of GSM). A better evaluation of the simulated $\delta^{18}O_p$ values is hampered by the sparsity of $\delta^{18}O_p$ observations.

If the local amount effect is the driver of spatial pattern of $\delta^{18}O_p$ (considering only the JJAS period of intense rain), $\delta^{18}O_p$ minima can be expected in the two regions of maximum rain: south western peninsular India and Myanmar coast. But such minima in $\delta^{18}O_p$ are observed neither in most SWING2 models, nor in GNIP observations (Fig 5.3). In GNIP observations, $\delta^{18}O_p$ minima (for JJAS) are observed over the East Asian region and the Tibetan Plateau.Further, $\delta^{18}O_p$

maxima are observed over western peninsular India. This feature is predicted well by SWING2 models. All the models produce a ^{18}O depleting trend along the Low Level Jet stream (LLJ, Fig 5.1) with $\delta^{18}O_p$ maxima over the Somali coast. This is likely due to the continuous rainfall along the LLJ with preferential removal of $H_2^{18}O$ (continental effect). This feature is consistent with the GNIP data from peninsular India.

5.2.3 Seasonality of $\delta^{18}O_p$ over India

Though the Indian plains get about 80% of their annual precipitation during the ISM season, significant amounts of rainfall are also obtained during the North East Monsoon (NEM, October to December) in peninsular India and during the Western disturbance season (January to March) over northern India. During these seasons, the wind patterns distinctly differ from the southwesterly ISM winds. This change of moisture source may impact the seasonal variation of $\delta^{18}O_p$. Most of the models are able to reproduce the observed seasonality of rainfall over the three GNIP stations (Kozhikode, Kakinada and Mumbai) over peninsular India (Fig 5.7). GNIP observations show that ISM $\delta^{18}O_p$ is relatively higher (by ∼2-4‰) over peninsular India compared to the NEM $\delta^{18}O_p$. This seasonal cycle of $\delta^{18}O_p$ is also captured by most of the models. The $\delta^{18}O$ of paleomonsoon proxies from this region should be interpreted carefully to avoid erroneous attributions; e.g., a very negative $\delta^{18}O_p$ interpreted as solely due to increase in ISM rain, whereas in reality it could be also due to an increased ^{18}O depleted NEM contribution (i.e., associated with a change in rainfall seasonality).

The observed seasonality of $\delta^{18}O_p$ at GNIP stations Jammu, Uttarkashi and New Delhi is characterized by relatively higher values during the western disturbance season and lower values during the ISM season. This could be due to higher rainout en-route of air parcels during the ISM while rain from the western disturbance possibly forms from vapor of continental origin [mainly transpiration flux; *Jasechko et al.*, 2013]. While the seasonal pattern of $\delta^{18}O_p$ at New Delhi

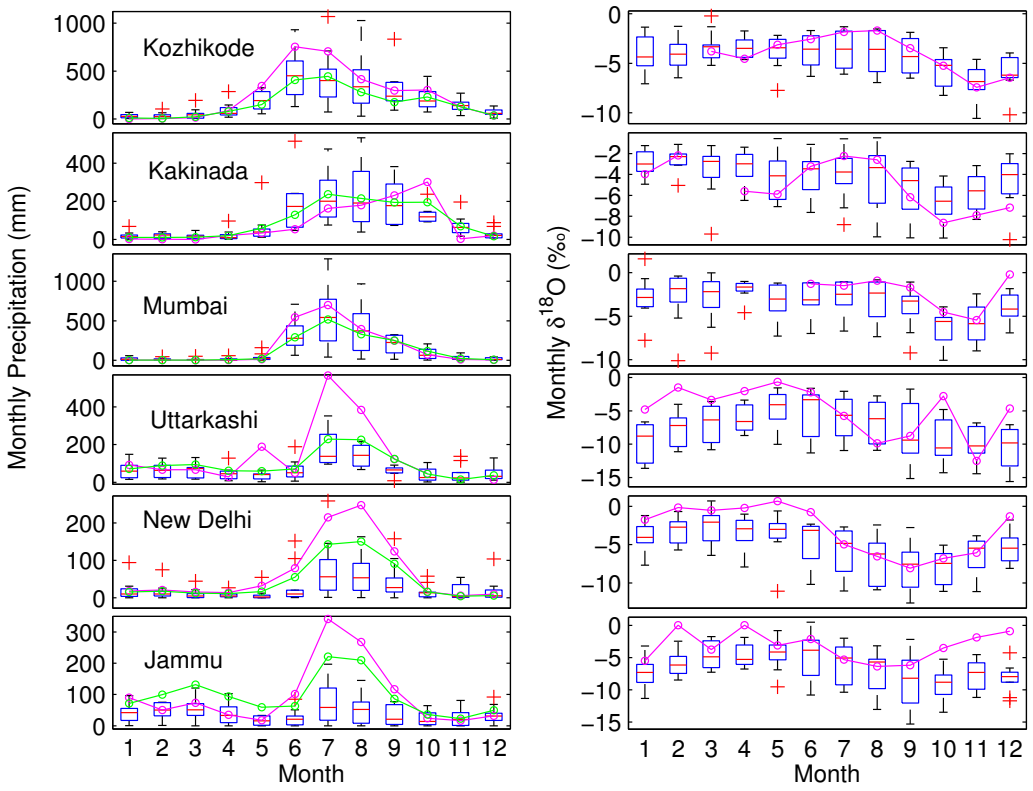

Figure 5.7: *Seasonal cycle of rainfall (left) and $\delta^{18}O_p$ (right). SWING2 simulations are represented by box and whisker diagram. A bias correction of +6 ‰ is applied to GENESIS simulated $\delta^{18}O_p$. Magenta lines represent GNIP (rainfall and $\delta^{18}O_p$) and green line represents GPCP (rainfall).*

is well captured in the model, those at Jammu and Uttarkashi differ from the observations: Simulations show stronger ^{18}O depletion during the winter months (December to February), which is not supported by observations. However an in-depth comparison of seasonality at these two stations is confounded by i) complex topography (Fig 5.1), which is not well represented in the coarse resolution GCMs and ii) possible errors in the observed seasonalities of $\delta^{18}O_p$ at Uttarkashi and Jammu due to limited data lengths. Nevertheless the seasonalities of $\delta^{18}O_p$ at stations with long term $\delta^{18}O_p$ observations (i.e., New Delhi, Mumbai and Kozhikode) are certainly well simulated by the models.

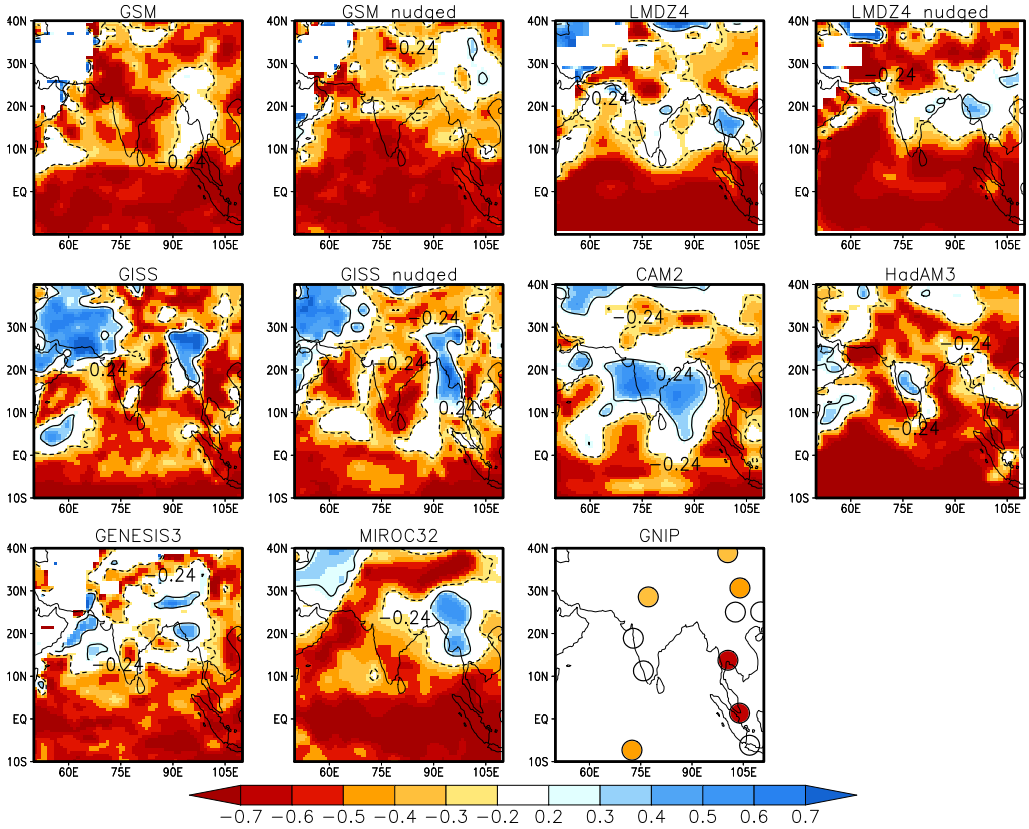

Figure 5.8: *Correlation coefficients between monthly (JJAS) rain rate and $\delta^{18}O_p$ at each grid point of model outputs for 19 years (1981-1999). Statistically significant correlation ($P< 0.05$) is represented by two contour lines; $+0.24$ and -0.24. The same analysis is done for GNIP stations where at least 30 months of JJAS $\delta^{18}O$ observations are available. For GNIP, sites represented by open circles show insignificant correlation at $P < 0.05$ level.*

5.2.4 Amount effect

We now examine rainfall- $\delta^{18}O_p$ correlations on two time scales; monthly for JJAS (Fig 5.8, 4 months per year for 19 years) and interannual for JJAS-average (Fig 5.9, 19 years). Though the amount effect defined by *Dansgaard* [1964] is for monthly rainfall and $\delta^{18}O_p$, we also used weighted average of JJAS period each year for studying the amount effect" on interannual scale. The latter is the signal more likely to be preserved in monsoon proxies that do not provide sub-annual resolution.

On the monthly scale, SWING2 models except CAM2 show a strong amount effect over the oceanic region, similar to GNIP observations at ocean islands [*Yurtsever and Gat*, 1981]. Models predict either no or an inverse amount effect over Myanmar and surrounding regions. Over the Indian subcontinent, simulated amount effects are compared with GNIP observations at Kozhikode, Mumbai and New Delhi. Over Kozhikode, GNIP data show lack of amount effect, whereas most of the models (except LMDZ free and CAM) simulate a strong amount effect (Fig 5.10). Recently *Lekshmy et al.* [2014] showed that ^{18}O depletion of rain during monsoon over the south west coast of India (including Kozhikode) is associated with large scale organized convective systems. The amount effect in observations here may be damped due to equal contributions of rainfall from both the large scale organized convective systems (with relatively depleted ^{18}O) and isolated rainfall events (with relatively enriched ^{18}O) to the JJAS total rain. Over Mumbai, no amount effect is observed in GNIP data as well as in some of the SWING2 models (LMDZ free, CAM and GENESIS); MIROC and GISS free simulation show a strong amount effect, for Mumbai while a few simulations (GSM free, GSM nudged, LMDZ nudged, GISS nudged and HadAM) depict a significant, but weaker amount effect (r ranges from -0.25 to -0.33) . Over New Delhi, the long-term GNIP observations show a significant amount effect and this is well reproduced by nine out of ten simulations (Fig 5.10).

On the interannual time scale, SWING2 models (except CAM2) exhibit a strong amount effect" over the equatorial Indian Ocean, while it is observed only over the island GNIP station Singapore (no amount effect" observed over GNIP stations Diego Garcia and Jakarta). Though most of the models produced significant negative correlation between rain amount and $\delta^{18}O_p$ over the Indian subcontinent, the correlation pattern appears quite noisy. In observations, only three stations show statistically significant negative correlations; Kozhikode, New Delhi and Bangkok. Over southern China, both model and observations show a weak or insignificant amount effect". A more detailed comparison of amount effect at Indian GNIP stations is shown in Figure 5.10

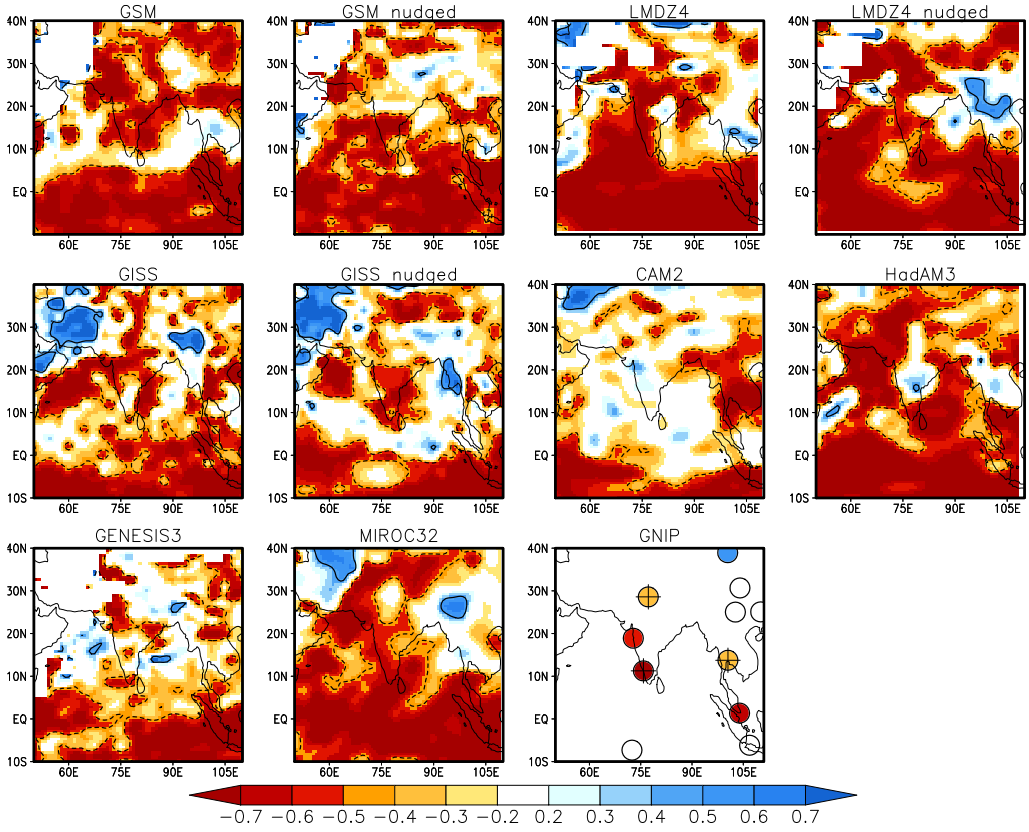

Figure 5.9: *Correlation coefficients between JJAS mean of rain rate and its $\delta^{18}O$ at each grid point of model outputs for 19 years (1981-1999). Statistically significant correlation ($p < 0.05$) is represented by two contour lines; +0.46 and -0.46. For GNIP data statistically significant correlations are represented by +" signs (bottom right panel).*

Most of the SWING2 models overestimate the rainfall- $\delta^{18}O_p$ relation at both seasonal and inter-annual time scales. The simulated amount effect is sensitive to the isotopic parameterization used for Post Condensation Exchange [PCE; *Field et al.*, 2010] this process enriches ^{18}O in low rainfall events via re-evaporation of rain into unsaturated sub-cloud layer, while it depletes ^{18}O in high rainfall events by the entrainment of re-evaporated vapor into the system [*Risi et al.*, 2008].*Risi et al.* [2010a] demonstrated that the effective relative humidity (relative humidity at raindrop-air interface) plays a critical role in simulating the strength of the amount effect. The effect of PCE on the simulated precipitation and vapor isotopic compositions ($\delta^{18}O_p$ & $\delta^{18}O_v$) depends on the fraction of the precipitation

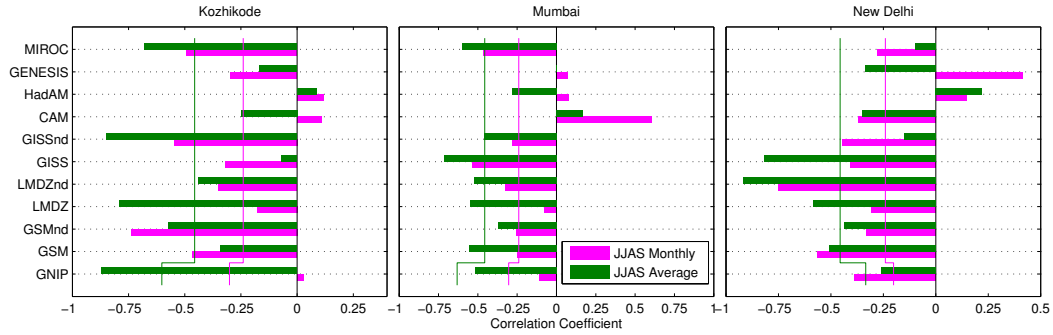

Figure 5.10: *Comparison of the amount effect (correlation coefficient between rainfall and $\delta^{18}O_p$)produced by SWING2 models with observations over three Indian stations on two time scales; monthly for JJAS period (magenta) and interannual for JJAS average (green). Vertical zigzag lines demarcate the significance at level $P = 0.05$.*

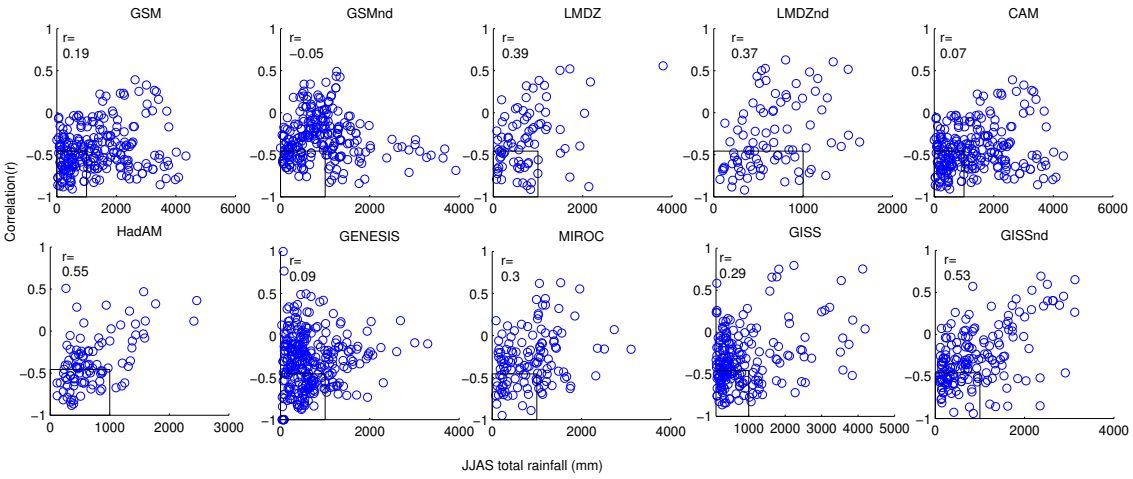

Figure 5.11: *Scatter plot between 19 year mean of JJAS total rainfall and correlation coefficients between rainfall and $\delta^{18}O_p$ (local amount effect in ISM on interannual timescale). Here, we omitted all the locations over the ocean. The grids over the land where the total JJAS rainfall is less than 100 mm are also omitted. Correlation coefficients below -0.46 represent significant amount effects. Many of the models do exhibit a significant correlation (r) between the total rainfall and amount effect correlation. Majority of the sites showing significant amount effects lie in moderate rainfall regions (highlighted as rectangle in the left bottom corner). In the areas of higher rainfall, most models generally show a lack of amount effect.*

that undergoes PCE, the degree of isotopic equilibration of raindrops with the vapor, the method by which the relative humidity near the raindrop surface is calculated, and all parameters controlling the fraction of the rain that evaporates.

Recent studies show the importance of isotopic composition of low level vapor ($\delta^{18}O_v$) on tropical $\delta^{18}O_p$ [*Kurita*, 2013; *Moore et al.*, 2014]. Tropical oceanic regions are characterized by high surface evaporation and produce vapor with relatively higher values of $\delta^{18}O_v$ than other regions of the ocean. During precipitation over the oceans, due to rain vapor interaction, $\delta^{18}O_v$ decreases [*Kurita*, 2013; *Lawrence*, 2004; *Midhun et al.*, 2013]. Low rainfall over the ocean mostly reflects the isotopic composition of evaporating vapor flux from the ocean, while during high rainfall $\delta^{18}O_p$ decreases due to the contribution of ^{18}O depleted vapor resulting from the rain-vapor interaction. These processes could lead to the simulation of a strong amount effect over oceans [*Lee et al.*, 2012]. Over land, vapor advected from the ocean is the major contributor during ISM. Hence the $\delta^{18}O_v$ of the surface continental vapor is mainly affected by the rainfall activity along the transport pathways. Thus the amount effect over the continents is modulated by the spatial precipitation pattern and it varies among the models (Fig 5.3). Over land, model simulates a significant amount effect in regions of low to moderate rainfall (Fig 5.11). In the low rainfall areas, the role of rain re-evaporation plays a major role in $\delta^{18}O_p$ variations and strengthens the amount effect [*Lee et al.*, 2012]. These processes could contribute to some noise in simulated amount effect over land.

5.2.5 Implications for interpretation of $\delta^{18}O$ of proxies

In the previous section we reported significant discrepancy among the modeled amount effects. Hence we checked role of upstream rainout on $\delta^{18}O_p$ at four cave locations (Fig 5.1): the four sites Akalagavi [Western Ghats, *Yadava and Ramesh*, 2005], Dandak [central eastern India, *Sinha et al.*, 2007], Mawmluh [north eastern India, *Berkelhammer et al.*, 2012] and Baratang [Andaman Islands, *Laskar et al.*, 2013] are influenced by strong moisture transport by the south westerly ISM winds. We restricted this analysis to nudged simulations, since they

simulate a rather reliable spatial pattern and interannual variation of monsoon rainfall (Fig 5.3 & 5.5). The local amount effect on interannual time scale at the each of the three sites is simulated by the three nudged simulations to varying degrees (Fig 5.9). But all the three simulations do show a significant negative correlation (Fig 5.12) of $\delta^{18}O_p$ at the respective cave sites with either interannual variations of regional amount of rainfall (as at Akalagavi) or upstream rainfall (as at Mawmluh, Dandak and Baratang). These correlation patterns in the three simulations are quite similar, suggesting the influence of upstream rainfall on $\delta^{18}O_p$ at cave sites. These results confirm earlier findings by *Lee et al.* [2012] and *Ishizaki et al.* [2012] over some Asian summer monsoon sites.

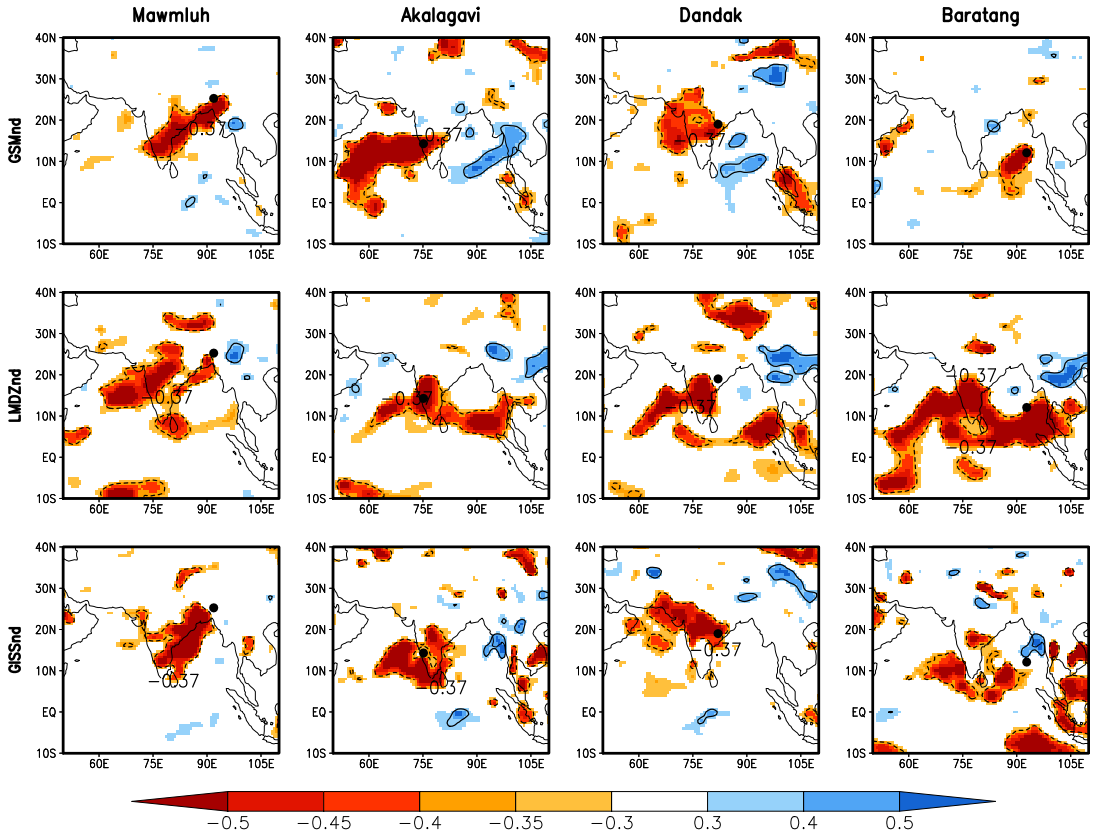

Figure 5.12: *Linear correlation coefficients between JJAS mean $\delta^{18}O_p$ at four cave sites (filled black circles) with the JJAS mean rain rates of surrounding grids, simulated by three nudged models. Model outputs for the period 1980-2007 are used in this analysis. Correlation coefficients less than -0.37 are significant at $P < 0.05$ level.*

5.3 ENSO and Indian Monsoon

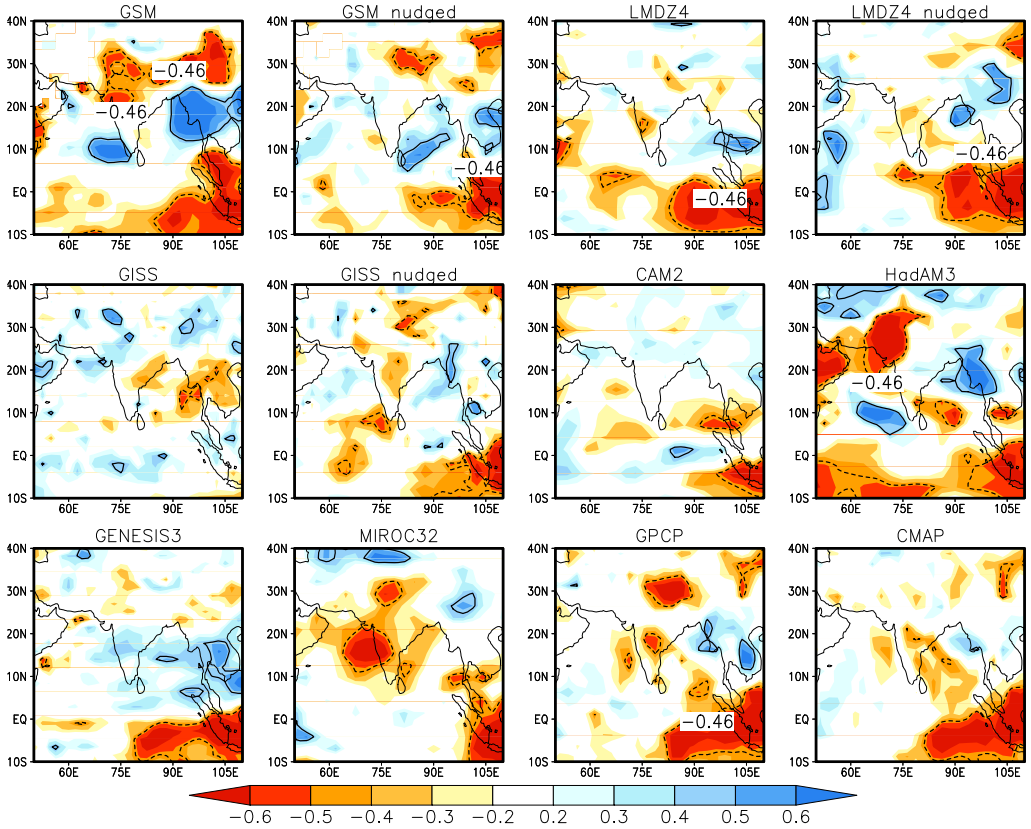

Figure 5.13: *Linear correlation coefficients between average JJAS-rainfall simulated by different models and JJAS-average Nino-3.4 SST anomaly for 19 years (1981-1999). Correlations above 0.46 and below −0.46 are statistically significant at $P < 0.05$ and are plotted as contours. Significant correlations of JJAS-average Nino-3.4 SST anomaly with GPCP and CMAP observations (bottom row last two panels) are also shown.*

Interannual variation of ISM is significantly influenced by ENSO [*Kumar*, 1999]. Most of the severe droughts over the Indian Subcontinent are often associated with El Niño . During El Niño , convection center shifts from the Western Pacific to Central or Eastern Pacific, resulting in anomalous subsidence over the Western Pacific. This area of subsidence extends up to the Indian subcontinent and suppresses convection, thus reducing ISM rainfall [*Kumar*, 1999; *Kumar et al.*, 2006]. However, this negative correlation between ENSO and Indian monsoon weakened after 1980s suggesting a possible inter-decadal modulation in the

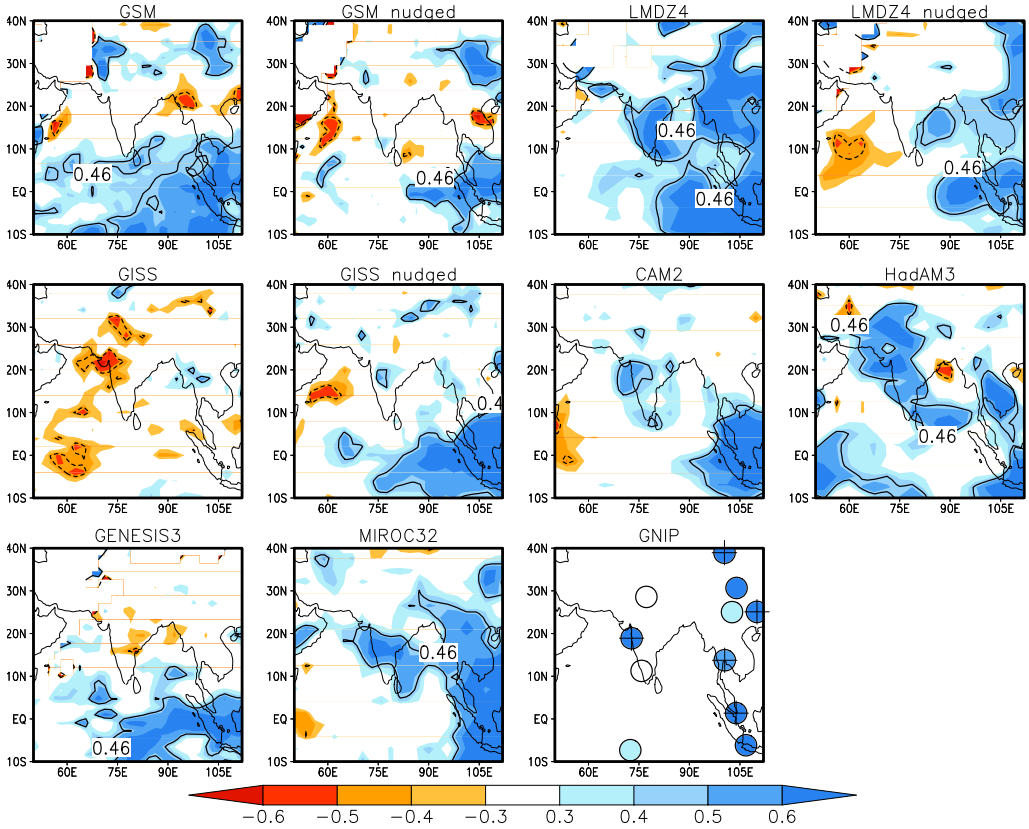

Figure 5.14: *Linear correlation coefficients between average $\delta^{18}O_p$ of JJAS-rainfall simulated by different models and JJAS-average Nino-3.4 SST anomaly for 19 years (1981-1999). Correlations above 0.46 and below −0.46 are statistically significant at $P < 0.05$ and are plotted as contours. Significant correlations of JJAS-average Nino-3.4 SST anomaly with GNIP $\delta^{18}O_p$ observations (bottom right panel), are denoted by a +" symbol.*

ENSO-ISM relation [*Kumar*, 1999]. Hence, isotope based climate proxies could be useful to understand ENSO-ISM relation on multi decadal timescales. Since our study is confined to 19 years of model simulations, we are unable to look at the ENSO-ISM relation on multi decadal timescale; instead, we investigate the role of ENSO on the interannual variability of ISM rainfall and $\delta^{18}O_p$.

The precipitation variability over tropical Pacific associated with ENSO is well simulated by SWING2 models [*Conroy et al.*, 2013]. Correlation between ENSO (i.e., JJAS-averaged Nino-3.4 SST anomaly) and JJAS-average rainfall is plotted in Fig 5.13. In CMAP and GPCP datasets, a strong negative correlation is

observed at the Indo-Pacific warm pool region (the region beyond longitude 110^oE is not shown in the figure) with a weak extension up to the peninsular India. This could be due to the weakening ENSO-ISM linkage after 1980s. Most of the models simulate a strong negative correlation at the Indo-pacific warm pool region, and a weak correlation over the Indian subcontinent, in agreement with GPCP and CMAP observations. The correlation pattern simulated by free model runs (except GISS) are similar to that of nudged simulations, implying that SST forcing is sufficient to create ENSO associated precipitation variability in the models.

The suppressed convection during El Niño causes relatively ^{18}O enriched precipitation in these regions. Thus a positive correlation between $\delta^{18}O$ of precipitation and ENSO is expected in the areas of associated subsidence. Fig 5.14 shows the correlation between $\delta^{18}O_p$ and ENSO for JJAS-average. Seven of ten the models and GNIP observations indeed show a positive correlation over the Indo-Pacific warm pool and the East-Asian region. A significant positive correlation is observed at Mumbai, but it is insignificant at New Delhi and Kozhikode. It should be noted that GNIP observations at Mumbai date prior to 1980. A few of the models simulated significant positive correlations over peninsular India. Long term observations are required in Eastern peninsular India and the Andaman islands to further characterize the ENSO signal in monsoon $\delta^{18}O_p$, and thus in $\delta^{18}O$ of monsoon proxies.

5.4 Conclusions

Most of the SWING2 models reproduce the characteristic high rainfall during JJAS over CMR, but a large spread among the models is observed. Simulated spatial patterns of monsoon rainfall and its $\delta^{18}O$ are in good agreement with GPCP, CMAP and GNIP observations.

Though *Conroy et al.* [2013] showed that nudged simulations are not superior to free simulations over the tropical Pacific, where SST is the major driver of rainfall,

we observe considerable improvements in the spatial patterns and interannual variability of ISM rainfall due to nudging. Nudged simulations of monthly $\delta^{18}O_p$ are also better correlated with GNIP observations. These improvements may be due to the role of large scale atmospheric circulation on the ISM rainfall (hence on $\delta^{18}O_p$), which are better represented in the nudged simulations. Hence the use of nudged simulations appears to be appropriate to establish the present day isotope-climate linkage over the ISM region.

On the interannual time scale, significant amount effect in ISM rainfall is observed at the two long-term GNIP sites over India. SWING2 simulated amount effect at these stations show large discrepancies among the models and also with observations. The spatial pattern of the simulated amount effect over India appears to be noisy. This may be due to the influence of spatial rainfall pattern on the modeled rainfall-$\delta^{18}O_p$ relation over land. Three nudged simulations show a consistent negative correlation between $\delta^{18}O_p$ and JJAS regional average rainfall on an interannual scale at Akalagavi; while at the other cave sites, Dandak, Mawmluh and Bratang, $\delta^{18}O_p$ is better correlated with upstream rainfall than local rainfall. These results suggest that integrated rainfall along the moisture transport pathways plays a major role in $\delta^{18}O_p$ variations at these cave sites.

ENSO and JJAS rainfall are negatively correlated on interannual timescales over the Eastern Equatorial Indian Ocean with a weak spatial extent up to peninsular India. The $\delta^{18}O_p$ values are positively correlated with ENSO both in models and observations over a larger spatial extent than rainfall. We could not find any consistent ENSO related variability either in rainfall or in $\delta^{18}O_p$ over the Indian subcontinent among the models; this may due to the weakened ENSO-ISM linkage after 1980s.

Assuming that $\delta^{18}O_p$ variability is the major factor that is recorded by the $\delta^{18}O$ of speleothems, this study has provided important results that can be used in interpreting annually or sub annually laminated speleothems (and tree rings) from the ISM region. Since our study presents only 19 years of model simulation,

simulations of paleoclimate using isotope enabled GCMs would be preferable to understand the ISM variability on centennial to millennial time scales. In this context the present study serves as a validation of such models for their performance to simulate the present day ISM.

Chapter 6

Summary and scope for future work

This thesis deals with the study on stable isotope variations in ISM rainfall and water vapor. Such studies are important due to their implications to paleoclimatic reconstructions, as yet limited over the ISM region. The present work has improved the understanding of stable isotope - climate linkages. The major results from this study are as follows:-

6.1 Results from the study on stable water vapor isotopes over Bay of Bengal

1. Direct measurements of $\delta^{18}O$ and δD surface water vapor were done over BoB during ISM and NEM seasons, providing a unique data set to validate the isotope enabled model simulations as well as the satellite based measurements of D/H ratios of atmospheric vapor.

2. $\delta^{18}O_v$ during NEM is more depleted (-13.4 ± 1.5) compared to that of ISM(-11.4 ± 0.9). Vapor d-excess show higher (22 ± 4) values during NEM compared that of ISM (13 ± 3).The observed seasonal difference in $\delta^{18}O_v$ and vapor d-excess is possibly due to i) change ocean surface conditions (humidity and SST), ii) $\delta^{18}O$ depletion in the surface sea water due to the

increased river runoff by the end of ISM season iii) shift in circulation pattern and iv) change in the weather systems (i.e., monsoon storm/depressions vs. tropical cyclones).

3. Estimation of $\delta^{18}O$ of near surface vapor over the Bay of Bengal using Craig-Gordon model with closure assumption is close to the observed $\delta^{18}O_v$ during non rainy days of ISM, but observed $\delta^{18}O_v$ is more negative during rainy days. This deviation arises from re-evaporation of falling rain drops along the parcel trajectory as well as the mixing of surface vapor with the more ^{18}O depleted vapor from higher altitudes by convective downdrafts.

4. During non-rainy days of the NEM, $\delta^{18}O_v$ is more depleted compared to Craig -Gordon model (with closure assumption) estimation. Like the observations made during the ISM season, $\delta^{18}O_v$ shows strong correlation with rainfall along the air parcel trajectory. This highlights the influence of rain-vapor interaction and mixing of vapor associated with convective downdraft on surface $\delta^{18}O_v$.

5. *d*-excess -humidity (humidity normalized with SST) relation appears to be weak during both ISM and NEM. Over BoB, humidity during ISM is higher compared to NEM and an inverse seasonal difference is observed in vapor *d*-excess , suggesting that *d*-excess -humidity relation over BoB could be stronger on seasonal time scale. This results will be helpful in interpreting ice core *d*-excess from Tibetan plateau.

6.2 Results from the study on $\delta^{18}O_p$ and δD_p using observation and IsoGSM simulations

1. As an outcome of this study a new data set for ISM $\delta^{18}O_p$ and δD_p with high spatial and temporal resolution has been generated.

2. On daily scale, local amount effect is observed at five out of six stations, but rainfall explains only 7-22 % of $\delta^{18}O_p$ variability.

3. IsoGSM simulates the large scale features of spatial rainfall pattern during 2013 ISM, except its north-western limit.

4. IsoGSM fails to simulate the temporal variation of daily rainfall nevertheless the simulated $\delta^{18}O_p$ is in good agreement with the observations.

5. Both back trajectory and correlation (between $\delta^{18}O_p$ and meridional moisture flux) analyses suggest that ISM $\delta^{18}O_p$ at Ahmedabad, Bhopal and Delhi are strongly influenced by the variations in moisture transport pathways. i.e., the contribution from AS enriches the $\delta^{18}O_p$ while it depletes during the rain which are fed by BoB component of moisture flux.

6. The observed correlation between $\delta^{18}O_p$ and meridional moisture flux is well simulated by IsoGSM at Ahmedabad and Bhopal, but not at at New Delhi.

7. The role of moisture transport pathways on $\delta^{18}O_p$ is observed on daily to interannual time scales over New Delhi.

6.3 Results from the inter-comparison of multi-GCM simulations of ISM $\delta^{18}O_p$

1. Most of the SWING2 models reproduce the characteristic high rainfall during JJAS over the core monsoon region, but a large spread among the models is observed. Simulated spatial patterns of monsoon rainfall and its $\delta^{18}O_p$ are in good agreement with GPCP, CMAP and GNIP observations.

2. Nudging technique considerably improves the spatial pattern and interannual variability of ISM rainfall. Nudged simulations of monthly $\delta^{18}O_p$ are also better correlated with GNIP observations. These improvements may be due to the role of large scale atmospheric circulation on the ISM rainfall and $\delta^{18}O_p$, which are better represented in the nudged simulations. Hence the use of nudged simulations would be more helpful to understand the present day isotope-climate linkage over the ISM region.

3. On the interannual time scale, significant local amount effect in ISM rainfall is observed at the two long-term GNIP sites over India. SWING2 simulated local amount effect at these stations show large discrepancies among the models and observations. The spatial pattern of simulated local amount effect over India appears to be noisy. This may be due to the influence of spatial rainfall pattern on the modeled rainfall-$\delta^{18}O_p$ relation over land.

4. Three nudged simulations show consistent negative correlations between $\delta^{18}O_p$ and JJAS regional average rainfall on interannual time scale at Akalagavi; while at the other cave sites, Dandak, Mawmluh and Bratang, $\delta^{18}O_p$ is better correlated with upstream rainfall than local rainfall. These results suggest that integrated rainfall along the moisture transport pathways seems to play a major role in $\delta^{18}O_p$ variations at these cave sites.

5. ENSO and JJAS rainfall are negatively correlated on interannual timescales over the Eastern Equatorial Indian Ocean with a weak spatial extent up to peninsular India. The $\delta^{18}O_p$ values are positively correlated with ENSO both in models and observations over a larger spatial extent than rainfall. No consistent ENSO related variability was found either in the rainfall or in $\delta^{18}O_p$ over the Indian subcontinent among the models; this may due to the weakened ENSO-ISM linkage after 1980s.

6.4 Scope for future studies

1. Vapor isotopic study over BoB shows a seasonal difference in SWI of water vapor. This needs to be checked with a year-long measurements at sites such as Andaman Islands.

2. Water vapor SWI over BoB cannot be fully explained using the Craig-Gordon model with closure assumption. This suggests that the vapor over BoB is not fully contributed by evaporation from BoB alone, the advected and recycled components also contribute significantly. Thus continuous monitoring of vapor isotope over ocean along with newly available satellite

based D/H ratios of atmospheric water vapor offer a good scope for the regional water vapor budget studies.

3. Since western equatorial Indian ocean and AS are the major sources of vapor during the ISM, direct measurement of $\delta^{18}O_v$ and δD_v needs to be done over this region. Along with the present study, this would also help understanding the $\delta^{18}O$ and d-excess variability in ice cores at southern Tibetan plateau [e.g., *Thompson*, 2000].

4. Laser spectroscopy for continuous vapor sampling [e.g., *Kurita et al.*, 2012] would be more useful to increase the sample throughput.

5. Potential of stable isotopes of rain and vapor to study the active active break cycles of ISM [*Rajeevan et al.*, 2010] needs to be explored.

6. The present study highlights a large intraseasonal variability in ISM $\delta^{18}O_p$ and the role of circulation on this variability. But the causes of such variations over the staions Dhanbad, Varanasi and Kanpur are not fully understood. This needs to be addressed by making long term high resolution (spatial and temporal) measurements of rainfall $\delta^{18}O_p$.

7. The simulations of $\delta^{18}O_p$ using IsoGSM is very much promising. But it needs to be improved to capture the spatio-temporal variations of rainfall. Sensitivity tests using such a model would help understand the cause of $\delta^{18}O_p$ variations on different time scales.

8. Isotope enabled GCM simulations can be improved over the ISM region by downscaling those simulations using high resolution regional atmospheric models [e.g., *Sturm et al.*, 2007; *Yoshimura et al.*, 2010].

9. Most of the isotope enabled GCMs (SWING2 models) are able to capture spatial and seasonal variation of ISM $\delta^{18}O_p$. Paleo climate simulations using such models would help improve paleoclimatic interpretations in the monsoon region.

Bibliography

Achyuthan, H., et al. (2013), Stable isotopes and salinity in the surface waters of the Bay of Bengal: Implications for water dynamics and palaeoclimate, *Marine Chemistry*, *149*, 51–62, doi:10.1016/j.marchem.2012.12.006.

Adler, R. F., et al. (2003), The Version-2 Global Precipitation Climatology Project (GPCP) Monthly Precipitation Analysis (1979-Present), *Journal of Hydrometeorology*, *4*(6), 1147–1167, doi:10.1175/1525-7541(2003)004⟨1147:TVGPCP⟩2.0.CO;2.

Araguás-Araguás, L., K. Froehlich, and K. Rozanski (2000), Deuterium and oxygen-18 isotope composition of precipitation and atmospheric moisture, *Hydrological Processes*, *14*(8), 1341–1355, doi:10.1002/1099-1085(20000615)14:8⟨1341::AID-HYP983⟩3.0.CO;2-Z.

Benetti, M., G. Reverdin, C. Pierre, L. Merlivat, C. Risi, H. C. Steen-Larsen, and F. Vimeux (2014), Deuterium excess in marine water vapor: Dependency on relative humidity and surface wind speed during evaporation, *Journal of Geophysical Research: Atmospheres*, *119*(2), 584–593, doi:10.1002/2013jd020535.

Berkelhammer, M., C. Risi, N. Kurita, and D. C. Noone (2012), The moisture source sequence for the Madden-Julian Oscillation as derived from satellite retrievals of HDO and H_2O, *Journal of Geophysical Research*, *117*(D3), 1–20, doi:10.1029/2011JD016803.

Bony, S., C. Risi, and F. Vimeux (2008), Influence of convective processes on the isotopic composition ($\delta^{18}O$ and δD) of precipitation and water vapor in the tropics: 1. Radiative-convective equilibrium and Tropical

Ocean-Global Atmosphere-Coupled Ocean-Atmosphere Response Experiment (TOGA-COARE) simulations, *Journal of Geophysical Research*, *113*(D19), 1–21, doi:10.1029/2008JD009942.

Breitenbach, S. F., J. F. Adkins, H. Meyer, N. Marwan, K. K. Kumar, and G. H. Haug (2010), Strong influence of water vapor source dynamics on stable isotopes in precipitation observed in Southern Meghalaya, NE India, *Earth and Planetary Science Letters*, *292*(1-2), 212–220, doi:10.1016/j.epsl.2010.01.038.

Chapman, S., and T. G. Cowling (1970), *The mathematical theory of non-uniform gases: an account of the kinetic theory of viscosity, thermal conduction and diffusion in gases*, Cambridge university press.

Clark, I. D., and P. Fritz (1997), *Environmental isotopes in hydrogeology*, CRC press.

Conroy, J. L., K. M. Cobb, and D. Noone (2013), Comparison of precipitation isotope variability across the tropical Pacific in observations and SWING2 model simulations, *Journal of Geophysical Research: Atmospheres*, *118*(April), 5867–5892, doi:10.1002/jgrd.50412.

Craig, H. (1957), Isotopic standards for carbon and oxygen and correction factors for mass-spectrometric analysis of carbon dioxide, *Geochimica et Cosmochimica Acta*, *12*(1-2), 133–149, doi:10.1016/0016-7037(57)90024-8.

Craig, H. (1961), Isotopic Variations in Meteoric Waters., *Science (New York, N.Y.)*, *133*(3465), 1702–1703, doi:10.1126/science.133.3465.1702.

Craig, H., and L. Gordon (1965), Deuterium and oxygen 18 variations in the ocean and the marine atmosphere, in *Stable Isotopes in Oceanographic Studies and Paleotemperatures*, pp. 9–130, Laboratorio di Geologia Nucleate, Pisa, Italy.

Dansgaard, W. (1964), Stable isotopes in precipitation, *Tellus*, *16*(4), 436–468, doi:10.1111/j.2153-3490.1964.tb00181.x.

Deshpande, R. D., a. S. Maurya, B. Kumar, A. Sarkar, and S. K. Gupta (2010), Rain-vapor interaction and vapor source identification using stable iso-

topes from semiarid western India, *Journal of Geophysical Research*, *115*(D23), D23,311, doi:10.1029/2010JD014458.

Draxler, R. R. (2003), Evaluation of an Ensemble Dispersion Calculation, *Journal of Applied Meteorology*, *42*(2), 308–317, doi:10.1175/1520-0450(2003)042⟨0308:EOAEDC⟩2.0.CO;2.

Draxler, R. R., and G. D. Rolph (2003), HYSPLIT (HYbrid Single-Particle Lagrangian Integrated Trajectory) model access via NOAA ARL READY website (http://www. arl. noaa. gov/ready/hysplit4. html). NOAA Air Resources Laboratory, Silver Spring.

Epstein, S., and T. Mayeda (1953), Variation of O-18 content of waters from natural sources, *Geochimica et cosmochimica acta*, *4*(5), 213–224.

Field, R. D., D. B. A. Jones, and D. P. Brown (2010), Effects of postcondensation exchange on the isotopic composition of water in the atmosphere, *Journal of Geophysical Research*, *115*(D24), D24,305, doi:10.1029/2010JD014334.

Field, R. D., D. Kim, A. N. LeGrande, J. Worden, M. Kelley, and G. A. Schmidt (2014), Evaluating climate model performance in the tropics with retrievals of water isotopic composition from Aura TES, *Geophysical Research Letters*, *41*(16), 6030–6036, doi:10.1002/2014GL060572.

Gadgil, S. (2003), The Indian monsoon and its variability, *Annual Review of Earth and Planetary Sciences*, *31*(1), 429–467, doi:10.1146/annurev.earth.31.100901.141251.

Gadgil, S., and S. Gadgil (2006), The Indian monsoon, GDP and agriculture, *Economic and Political Weekly*, pp. 4887–4895.

Gat, J. R., B. Klein, Y. Kushnir, W. Roether, H. Wernli, R. Yam, and A. Shemesh (2003), Isotope composition of air moisture over the Mediterranean Sea: An index of the air-sea interaction pattern, *Tellus, Series B: Chemical and Physical Meteorology*, *55*(5), 953–965, doi:10.1034/j.1600-0889.2003.00081.x.

Gonfiantini, R. (1978), Standards for stable isotope measurements in natural compounds, *Nature*, *271*(5645), 534–536.

Good, S. P., D. Noone, and G. Bowen (2015), Hydrologic connectivity constrains partitioning of global terrestrial water fluxes, *Science*, *349*(6244), 175–177, doi: 10.1126/science.aaa5931.

Gorski, G., C. Strong, S. P. Good, R. Bares, J. R. Ehleringer, and G. J. Bowen (2015), Vapor hydrogen and oxygen isotopes reflect water of combustion in the urban atmosphere, *Proceedings of the National Academy of Sciences*, p. 201424728, doi:10.1073/pnas.1424728112.

Goswami, B. N., V. Venugopal, D. Sengupta, M. S. Madhusoodanan, and P. K. Xavier (2006), Increasing trend of extreme rain events over India in a warming environment., *Science (New York, N.Y.)*, *314*(5804), 1442–5, doi: 10.1126/science.1132027.

Hoffmann, G., and M. Heimann (1997), Water isotope modeling in the Asian monsoon region, *Quaternary International*, *37*, 115–128, doi:10.1016/1040-6182(96) 00004-3.

Huffman, G. J., D. T. Bolvin, E. J. Nelkin, D. B. Wolff, R. F. Adler, G. Gu, Y. Hong, K. P. Bowman, and E. F. Stocker (2007), The TRMM Multisatellite Precipitation Analysis (TMPA): Quasi-Global, Multiyear, Combined-Sensor Precipitation Estimates at Fine Scales, doi:10.1175/JHM560.1.

Ishizaki, Y., K. Yoshimura, S. Kanae, M. Kimoto, N. Kurita, and T. Oki (2012), Interannual variability of $H_2^{18}O$ in precipitation over the Asian monsoon region, *Journal of Geophysical Research*, *117*(D16), 1–16, doi:10.1029/2011JD015890.

Jasechko, S., Z. D. Sharp, J. J. Gibson, S. J. Birks, Y. Yi, and P. J. Fawcett (2013), Terrestrial water fluxes dominated by transpiration, *Nature*, pp. 1–5, doi:10.1038/nature11983.

Joussaume, S., R. Sadourny, and J. Jouzel (1984), A general circulation model

of water isotope cycles in the atmosphere, *Nature*, *311*(5981), 24–29, doi:10.1038/311024a0.

Kalnay, E., et al. (1996), The NCEP/NCAR 40-Year Reanalysis Project, doi:http://dx.doi.org/10.1175/1520-0477(1996)077⟨0437:TNYRP⟩2.0.CO;2.

Kanamitsu, M., W. Ebisuzaki, J. Woollen, S.-K. Yang, J. J. Hnilo, M. Fiorino, and G. L. Potter (2002), NCEP-DOE AMIP-II Reanalysis (R-2), *Bulletin of the American Meteorological Society*, *83*(11), 1631–1644.

Kinzer, G. D., and R. Gunn (1951), The Evaporation, Temperature And Thermal Relaxation-Time Of Freely Falling Waterdrops, doi:10.1175/1520-0469(1951)008⟨0071:TETATR⟩2.0.CO;2.

Knupp, K. R., and W. R. Cotton (1985), Convective cloud downdraft structure: An interpretive survey, *Reviews of Geophysics*, *23*(2), 183–215, doi:10.1029/RG023i002p00183.

Krishnamurthy, R. V., and S. K. Bhattacharya (1991), Stable oxygen and hydrogen isotope ratios in shallow ground waters from India and a study of the role of evapotranspiration in the Indian monsoon, *Stable Isotope Geochemistry: A tribute to Samuel Epstein, Spec. Publ*, *3*, 187–203.

Kumar, B., et al. (2010), Isotopic characteristics of Indian precipitation, *Water Resources Research*, *46*(12), doi:10.1029/2009WR008532.

Kumar, K. K. (1999), On the Weakening Relationship Between the Indian Monsoon and ENSO, *Science*, *284*(5423), 2156–2159, doi:10.1126/science.284.5423.2156.

Kumar, K. K., B. Rajagopalan, M. Hoerling, G. Bates, and M. Cane (2006), Unraveling the mystery of Indian monsoon failure during El Niño ., *Science (New York, N.Y.)*, *314*(5796), 115–9, doi:10.1126/science.1131152.

Kurita, N. (2013), Water isotopic variability in response to mesoscale convective system over the tropical ocean, *Journal of Geophysical Research: Atmospheres*, *118*(18), 10,376–10,390, doi:10.1002/jgrd.50754.

Kurita, N., D. Noone, C. Risi, G. a. Schmidt, H. Yamada, and K. Yoneyama (2011), Intraseasonal isotopic variation associated with the Madden-Julian Oscillation, *Journal of Geophysical Research*, *116*(D24), D24,101, doi:10.1029/2010JD015209.

Kurita, N., B. D. Newman, L. J. Araguas-Araguas, and P. Aggarwal (2012), Evaluation of continuous water vapor δD and $\delta^{18}O$ measurements by off-axis integrated cavity output spectroscopy, *Atmospheric Measurement Techniques*, *5*(8), 2069–2080, doi:10.5194/amt-5-2069-2012.

Laskar, A. H., M. G. Yadava, R. Ramesh, V. J. Polyak, and Y. Asmerom (2013), A 4 kyr stalagmite oxygen isotopic record of the past Indian Summer Monsoon in the Andaman Islands, *Geochemistry, Geophysics, Geosystems*, *14*(9), 3555–3566, doi:10.1002/ggge.20203.

Lawrence, J. R. (2004), Stable isotopic composition of water vapor in the tropics, *Journal of Geophysical Research*, *109*(D6), D06,115, doi:10.1029/2003JD004046.

Lee, J.-E., and I. Fung (2008), Amount effect of water isotopes and quantitative analysis of post-condensation processes, *Hydrological Processes*, *22*(1), 1–8, doi:10.1002/hyp.6637.

Lee, J.-E., I. Fung, D. J. DePaolo, and C. C. Henning (2007), Analysis of the global distribution of water isotopes using the NCAR atmospheric general circulation model, *J. Geophys. Res.*, *112*(D16), doi:10.1029/2006jd007657.

Lee, J.-E., R. Pierrehumbert, A. Swann, and B. R. Lintner (2009), Sensitivity of stable water isotopic values to convective parameterization schemes, *Geophysical Research Letters*, *36*(23), L23,801, doi:10.1029/2009GL040880.

Lee, J.-E., C. Risi, I. Fung, J. Worden, R. a. Scheepmaker, B. Lintner, and C. Frankenberg (2012), Asian monsoon hydrometeorology from TES and SCIAMACHY water vapor isotope measurements and LMDZ simulations: Implications for speleothem climate record interpretation, *Journal of Geophysical Research*, *117*(D15), D15,112, doi:10.1029/2011JD017133.

Lekshmy, P. R., M. Midhun, R. Ramesh, and R. A. Jani (2014), ^{18}O depletion in monsoon rain relates to large scale organized convection rather than the amount of rainfall., *Scientific reports*, *4*, 5661, doi:10.1038/srep05661.

Majoube, M. (1971a), Oxygen-18 and deuterium fractionation between water and steam, *J. Chim. Phys. Phys. Chim. Biol*, *68*(10), 1423–1436.

Majoube, M. (1971b), Fractionation in O-18 between ice and water vapor, *J. Chim. Phys. Phys. Chim. Biol*, *68*(4), 625–636.

Masson-Delmotte, V., et al. (2008), A Review of Antarctic Surface Snow Isotopic Composition: Observations, Atmospheric Circulation, and Isotopic Modeling, *Journal of Climate*, *21*(13), 3359–3387, doi:10.1175/2007jcli2139.1.

Mathieu, R., D. Pollard, J. E. Cole, J. W. C. White, R. S. Webb, and S. L. Thompson (2002), Simulation of stable water isotope variations by the GENESIS GCM for modern conditions, *Journal of Geophysical Research*, *107*(D4), 4037, doi:10.1029/2001JD900255.

Merlivat, L. (1978), Molecular diffusivities of $H_2^{16}O$, $HD^{16}O$, and $H_2^{18}O$ in gases, *The Journal of Chemical Physics*, *69*(6), 2864, doi:10.1063/1.436884.

Merlivat, L., and J. Jouzel (1979), Global climatic interpretation of the deuterium-oxygen 18 relationship for precipitation, *Journal of Geophysical Research*, *84*(C8), 5029, doi:10.1029/JC084iC08p05029.

Midhun, M., P. R. Lekshmy, and R. Ramesh (2013), Hydrogen and oxygen isotopic compositions of water vapor over the Bay of Bengal during monsoon, *Geophysical Research Letters*, *40*(23), 6324–6328, doi:10.1002/2013GL058181.

Moore, M., Z. Kuang, and P. N. Blossey (2014), A moisture budget perspective of the amount effect, *Geophysical Research Letters*, *41*(4), 1329–1335, doi:10.1002/2013GL058302.

Nanjundiah, R. S., V. Vidyunmala, and J. Srinivasan (2005), On the difference in the seasonal cycle of rainfall over India in the Community Climate System

Model (CCSM2) and Community Atmospheric Model (CAM2), *Geophysical Research Letters*, *32*(20), 1–3, doi:10.1029/2005GL024278.

Noone, D. (2012), Pairing measurements of the water vapor isotope ratio with humidity to deduce atmospheric moistening and dehydration in the tropical midtroposphere, *Journal of Climate*, *25*(13), 4476–4494, doi:10.1175/JCLI-D-11-00582.1.

Noone, D. ., and C. Sturm (2010), Comprehensive dynamical models of global and regional water isotope distributions, in *Isoscapes: Understanding Movement, Pattern, and Process on Earth Through Isotope Mapping*, pp. 195—-219, Springer, doi:10.1007/978-90-481-3354-3.

Rajeevan, M., S. Gadgil, and J. Bhate (2010), Active and break spells of the indian summer monsoon, *Journal of Earth System Science*, *119*(3), 229–247, doi:10.1007/s12040-010-0019-4.

Rienecker, M. M., et al. (2011), MERRA: NASA's modern-era retrospective analysis for research and applications, *Journal of Climate*, *24*(14), 3624–3648, doi:10.1175/JCLI-D-11-00015.1.

Risi, C., S. Bony, and F. Vimeux (2008), Influence of convective processes on the isotopic composition ($\delta^{18}O$ and δD) of precipitation and water vapor in the tropics: 2. Physical interpretation of the amount effect, *Journal of Geophysical Research: Atmospheres*, *113*(19), D19,306, doi:10.1029/2008JD009943.

Risi, C., S. Bony, F. Vimeux, C. Frankenberg, D. Noone, and J. Worden (2010a), Understanding the Sahelian water budget through the isotopic composition of water vapor and precipitation, *Journal of Geophysical Research*, *115*(D24), 1–23, doi:10.1029/2010JD014690.

Risi, C., A. Landais, S. Bony, J. Jouzel, V. Masson-Delmotte, and F. Vimeux (2010b), Understanding the ^{17}O excess glacial-interglacial variations in Vostok precipitation, *Journal of Geophysical Research*, *115*(D10), 1–15, doi:10.1029/2008JD011535.

Risi, C., et al. (2012), Process-evaluation of tropospheric humidity simulated by general circulation models using water vapor isotopologues: 1. Comparison between models and observations, *Journal of Geophysical Research*, *117*(D5), 1–26, doi:10.1029/2011JD016621.

Sabin, T. P., et al. (2013), High resolution simulation of the South Asian monsoon using a variable resolution global climate model, *Climate Dynamics*, *41*(1), 173–194, doi:10.1007/s00382-012-1658-8.

Schmidt, G. A., A. N. LeGrande, and G. Hoffmann (2007), Water isotope expressions of intrinsic and forced variability in a coupled ocean-atmosphere model, *Journal of Geophysical Research*, *112*(D10), D10,103, doi:10.1029/2006JD007781.

Sengupta, S., and A. Sarkar (2006), Stable isotope evidence of dual (Arabian Sea and Bay of Bengal) vapour sources in monsoonal precipitation over north India, *Earth and Planetary Science Letters*, *250*(3-4), 511–521, doi:10.1016/j.epsl.2006.08.011.

Sengupta, S., A. Parekh, S. Chakraborty, K. Ravi Kumar, and T. Bose (2013), Vertical variation of oxygen isotope in bay of Bengal and its relationships with water masses, *Journal of Geophysical Research: Oceans*, *118*(12), 6411–6424, doi:10.1002/2013JC008973.

Sime, L. C., E. W. Wolff, K. I. C. Oliver, and J. C. Tindall (2009), Evidence for warmer interglacials in East Antarctic ice cores., *Nature*, *462*(7271), 342–345, doi:10.1038/nature08564.

Singh, A., R. Jani, and R. Ramesh (2010), Spatiotemporal variations of the $\delta^{18}O$-salinity relation in the northern Indian Ocean, *Deep Sea Research Part I: Oceanographic Research Papers*, *57*(11), 1422–1431, doi:10.1016/j.dsr.2010.08.002.

Singh, A., A. Mohiuddin, R. Ramesh, and S. Raghav (2014), Estimating the loss of Himalayan glaciers under global warming using the $\delta^{18}O-$salinity relation in

the Bay of Bengal, *Environmental Science & Technology Letters*, *1*(5), 249–253, doi:10.1021/ez500076z.

Sinha, A., K. G. Cannariato, L. D. Stott, H. Cheng, R. L. Edwards, M. G. Yadava, R. Ramesh, and I. B. Singh (2007), A 900-year (600 to 1500 A.D.) record of the Indian summer monsoon precipitation from the core monsoon zone of India, *Geophysical Research Letters*, *34*(16), doi:10.1029/2007GL030431.

Steen-Larsen, H. C., et al. (2014), Climatic controls on water vapor deuterium excess in the marine boundary layer of the North Atlantic based on 500 days of in situ, continuous measurements, *Atmospheric Chemistry and Physics*, *14*(15), 7741–7756, doi:10.5194/acp-14-7741-2014.

Stewart, M. K. (1975), Stable isotope fractionation due to evaporation and isotopic exchange of falling water drops, *Journal of Geophysical Research*, *80*(9), 1133–1146.

Sturm, C., G. Hoffmann, and B. Langmann (2007), Simulation of the Stable Water Isotopes in Precipitation over South America: Comparing Regional to Global Circulation Models, *Journal of Climate*, *20*(15), 3730–3750, doi:10.1175/JCLI4194.1.

Taylor, K. E. (2001), Summarizing multiple aspects of model performance in a single diagram, *Journal of Geophysical Research*, *106*(D7), 7183, doi:10.1029/2000JD900719.

Thompson, L. G. (2000), A high-resolution millennial record of the south Asian monsoon from Himalayan ice cores, doi:10.1126/science.289.5486.1916.

Uemura, R., Y. Matsui, K. Yoshimura, H. Motoyama, and N. Yoshida (2008), Evidence of deuterium excess in water vapor as an indicator of ocean surface conditions, *Journal of Geophysical Research*, *113*(D19), 1–10, doi:10.1029/2008JD010209.

Vuille, M., M. Werner, R. S. Bradley, and F. Keimig (2005), Stable isotopes in

precipitation in the Asian monsoon region, *Journal of Geophysical Research*, *110*(D23), 1–15, doi:10.1029/2005JD006022.

Wang, B. (2005), *The Asian monsoon*, Springer.

Warrier, C., M. Babu, and P. Manjula (2010), Isotopic characterization of dual monsoon precipitation-evidence from Kerala, India, *Current Science*, *98*(11), 1487–1495.

Washington, W. M., and C. L. Parkinson (2005), *An introduction to three-dimensional climate modeling*, University science books.

Worden, J., D. Noone, and K. Bowman (2007), Importance of rain evaporation and continental convection in the tropical water cycle., *Nature*, *445*(7127), 528–532, doi:10.1038/nature05508.

Xie, P., and P. A. Arkin (1997), Global precipitation: A 17-year monthly analysis based on gauge observations, satellite estimates, and numerical model outputs, *Bulletin of the American Meteorological Society*, *78*(11), 2539–2558, doi:http://dx.doi.org/10.1175/1520-0477(1997)078⟨2539:GPAYMA⟩2.0.CO;2.

Yadava, M., and R. Ramesh (2005), Monsoon reconstruction from radiocarbon dated tropical Indian speleothems, *The Holocene*, *15*(1), 48–59, doi:10.1191/0959683605h1783rp.

Yadava, M., R. Ramesh, and K. Pandarinath (2007), A positive 'amount effect' in the Sahayadri (Western Ghats) rainfall, *Current Science*, *93*(4).

Yoshimura, K., M. Kanamitsu, D. Noone, and T. Oki (2008), Historical isotope simulation using Reanalysis atmospheric data, *Journal of Geophysical Research*, *113*(D19), D19,108, doi:10.1029/2008JD010074.

Yoshimura, K., M. Kanamitsu, and M. Dettinger (2010), Regional downscaling for stable water isotopes: A case study of an atmospheric river event, *Journal of Geophysical Research*, *115*(D18), 1–13, doi:10.1029/2010JD014032.

Yurtsever, Y., and J. R. Gat (1981), Atmospheric waters, in *Stable isotope hydrology: deuterium and oxygen-18 in the water cycle*, vol. 210, edited by J. Gat and R. Gonfiantini, pp. 103–142, IAEA Technical Reports Series 210.

List of Publications

Publications in peer reviewed journals

1. Lekshmy P.R, **Midhun M** and R Ramesh 2015; Spatial variation of amount effect over peninsular India and Sri Lanka: role of seasonality, *Geophysical Research Letters, 42* (http://dx.doi.org/10.1002/2015GL064517)

2. **Midhun M** and R Ramesh 2015; Validation of $\delta^{18}O$ as a proxy for past monsoon rain by multi-GCM simulations, *Climate Dynamics* (http://dx.doi.org/10.1007/s00382-015-2652-8)

3. Lekshmy P.R , **Midhun M**, Ramesh R and R A Jani 2014;^{18}O depletion in monsoon rain relates to large scale organized convection rather than the amount of rainfall, *Scientific Reports, 1-5* (http://dx.doi.org/10.1038/srep05661)

4. **Midhun M**, Lekshmy P.R , and R Ramesh 2013; Hydrogen and oxygen isotopic compositions of water vapor over the Bay of Bengal during monsoon,*Geophysical Research Letters 40, 6324-6328* (http://dx.doi.org/10.1002/2013GL058181)

Papers in Conferences proceedings

1. **M.Midhun**, A.Kesarker, R.Ramesh; Simulation of Stable hydrogen and Oxygen Isotopes in Indian Monsoon Precipitation using IsoGSM. *National Space Science Symposium, 2012, Tirupati, India.*

2. **M.Midhun**, P.R.Lekshmy, R.Ramesh and R.A.Jani 2013; Stable Isotopic Composition of Atmospheric vapor over the Bay of Bengal and its Relation with Ocean Surface Conditions, *Proceedings of 12th ISMAS Triennial International Conference on Mass Spectrometry, 2013, Goa, India, pp 318-320.*

3. P.R.Lekshmy, **M.Midhun**, R.Ramesh and R.A.Jani; Is the Isotopic Composition of Rainfall of the South west coast of India Independent of Local Rainfall Amount? *Proceedings of 12th ISMAS Triennial International Conference on Mass Spectrometry-2013,Goa, India pp 306-308.*

4. **M.Midhun**, R.Ramesh; Stable Water Isotopologues in Indian Summer Monsoon Rainfall: A comparison between SWING2 model simulations and observations 13th *International Regional Spectral Model workshop 2014, Yokohama,Japan.*

5. **M.Midhun**, P.R.Lekshmy and R.Ramesh; Short-term Variability of Indian Summer Monsoon Rainfall δ^{18}O, *EGU General Assembly 2015, Vienna, Austria.*

6. P.R.Lekshmy, **M.Midhun** and R.Ramesh; Rain- vapour isotopic interaction over the south-west coast of India, *EGU General Assembly 2015, Vienna, Austria*

Publications attached with thesis

1. **Midhun M**, Lekshmy P.R , and R Ramesh 2013; Hydrogen and oxygen isotopic compositions of water vapor over the Bay of Bengal during monsoon,*Geophysical Research Letters 40, 6324-6328* (http://dx.doi.org/10.1002/2013GL058181)

2. **Midhun M** and R Ramesh 2015; Validation of $\delta^{18}O$ as a proxy for past monsoon rain by multi-GCM simulations, *Climate Dynamics* (http://dx.doi.org/10.1007/s00382-015-2652-8)

GEOPHYSICAL RESEARCH LETTERS, VOL. 40, 6324–6328, doi:10.1002/2013GL058181, 2013

Hydrogen and oxygen isotopic compositions of water vapor over the Bay of Bengal during monsoon

M. Midhun,[1] P. R. Lekshmy,[1] and R. Ramesh[1]

Received 3 October 2013; revised 30 October 2013; accepted 7 November 2013; published 12 December 2013.

[1] δD_v and $\delta^{18}O_v$ of ~70 water vapor samples collected at 6 and 25 m above sea level over the Bay of Bengal (BoB) during July–August 2012 are reported. This helps characterize the isotopic signature of monsoon vapor. No significant vertical variation is observed in δD_v, $\delta^{18}O_v$, or deuterium excess (defined as $\delta D - 8\delta^{18}O$); δD_v and $\delta^{18}O_v$ are significantly correlated ($r = 0.92$) at each height; the deuterium excess values do not, because the variation of δD_v and $\delta^{18}O_v$ relative to their uncertainties is much larger than that of the latter. The temporal variations of δD_v and $\delta^{18}O_v$ correlate well with air temperature rather than sea surface temperature. The control of normalized humidity on deuterium excess is less prominent. While the distribution of water vapor isotopologues over the BoB is primarily determined by the ocean surface conditions, they are significantly altered by laterally advected vapor from rain en route during the monsoon. **Citation:** Midhun, M., P. R. Lekshmy, and R. Ramesh (2013), Hydrogen and oxygen isotopic compositions of water vapor over the Bay of Bengal during monsoon, *Geophys. Res. Lett.*, *40*, 6324–6328, doi:10.1002/2013GL058181.

1. Introduction

[2] Stable water isotopologues, $H_2{}^{18}O$ and HDO, are widely used as tracers of the hydrological cycle [e.g., *Gat*, 1996] and paleomonsoon [e.g., *Ramesh et al*., 2010]. The relative mass difference of $H_2{}^{18}O$ and $H_2{}^{16}O$ (as well as HDO and $H_2{}^{16}O$) causes isotopic fractionation during phase change of water, including evaporation from open water bodies, condensation in clouds, and below-cloud reevaporation while rain falls through the undersaturated atmosphere. Isotopic fractionation during large-scale condensation is believed to be an equilibrium process, obeying Rayleigh isotopic fractionation [*Yurtsever and Gat*, 1981]. However, isotopic exchange processes in clouds formed due to intense convective activity are more complex [*Bony et al*., 2008; *Bolot et al*., 2012]. For treating isotopic fractionation during evaporation, a model proposed by Craig and Gordon [*Craig and Gordon*, 1965, hereinafter referred to as the C-G model] and later modified by Merlivat and Jouzel [*Merlivat and Jouzel*, 1979, hereinafter referred to as MJ79] is widely used. The relative abundance of the heavier isotope is usually represented as a delta value; $\delta = (R_{sample}/R_{VSMOW} - 1) \times 10^3$‰, where R_{sample} is the ratio of the abundances of the heavier to lighter isotope of interest (e.g., *D/H* or $^{18}O/^{16}O$) in the sample, and R_{VSMOW} is its value in the standard, here the Vienna Standard Mean Ocean Water [*Yurtsever and Gat*, 1981]. According to MJ79, the isotopic ratio of the evaporating flux is estimated by the equation

$$R_E = k\frac{\alpha R_L - hR_A}{1 - h} \quad (1)$$

where R_E, R_L, and R_A are, respectively, the isotopic ratios of the emanating vapor, ocean surface water, and preexisting atmospheric vapor. α, k, and h are, respectively, the equilibrium and kinetic fractionation factors between coexisting vapor and liquid water and the relative humidity at 10 m above sea level, normalized to saturation at the sea surface temperature (SST). Equation (1) is widely used in isotope-enabled general circulation models to parameterize the isotopic composition of the evaporated vapor [e.g., *Joussaume et al*., 1984; *Yoshimura et al*., 2008]. MJ79 predicts a relationship between ocean surface relative humidity and deuterium excess ($d_v = \delta D_v - 8\delta^{18}O_v$) by applying a global closure assumption (i.e., $<R_E> = <R_A>$ for global average values) in the equation. Though this leads to a systematic bias in predicting the vapor isotopic values [*Jouzel et al*., 1996], the relationship between h and d-excess is indeed observed in the marine vapor over the Southern Ocean [*Uemura et al*., 2008]. This relation is yet to be verified in the tropical oceans, a major moisture source for the global hydrological cycle. Here we attempt to understand the influence of boundary layer processes and ocean surface conditions on the stable hydrogen and oxygen isotopic compositions ($\delta^{18}O_v$ and δD_v) of atmospheric vapor over the Bay of Bengal (BoB). These are the first measurements being reported from the Bay of Bengal, one of the important sources for South Asian monsoon rain.

2. Sampling and Isotopic Measurements

[3] Water vapor samples were collected cryogenically using a glass trap maintained below –80°C with an ethanol liquid nitrogen bath (IAEA protocol, http://www-naweb.iaea.org/napc/ih/documents/miba/water_vapor_protocol.pdf), at locations shown in Figure 1. To ensure efficient trapping, the flow speed of air through the trap was maintained at 500 mL/min, sampling duration ~3 h to trap water vapor >2 mL in liquid form. The efficiency of the trap was checked by connecting an extra cold trap to the outlet of original trap, and no significant condensate was found in it. Forty-two samples of vapor were collected from the top mast (25 m above sea level) of R/V *Sagar Kanya* (cruise #SK-296). We carried out another simultaneous collection at 6 m height, but the number of samples at this height is less ($n = 28$) due to limited availability of liquid nitrogen for trapping. Rain water samples ($n = 15$, this number is limited by the occurrence of rain) and sea surface water samples ($n = 42$) were also collected, and all samples

Additional supporting information may be found in the online version of this article.

[1]Geosciences Division, Physical Research Laboratory, Ahmedabad, Gujarat, India.

Corresponding author: M. Midhun, Geosciences Division, Physical Research Laboratory, Ahmedabad, Gujarat 380009, India. (midhun@prl.res.in)

0094-8276/13/10.1002/2013GL058181

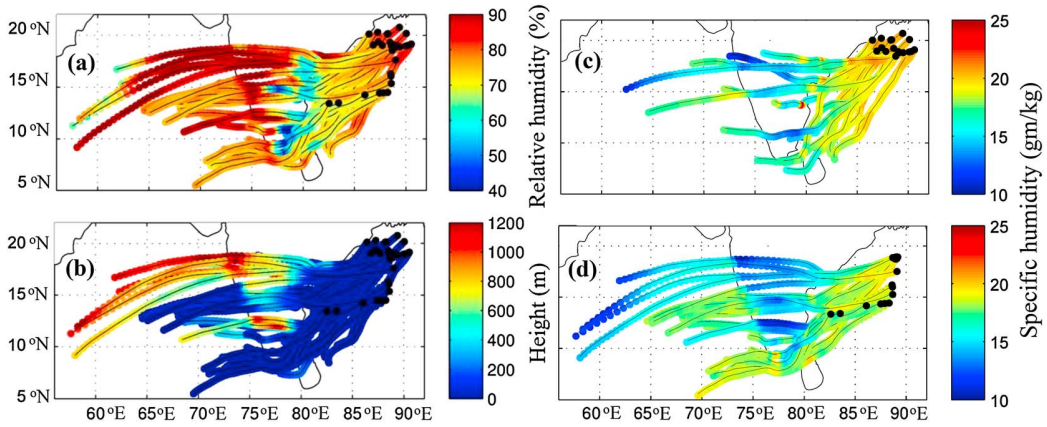

Figure 1. Seventy-two hour air mass back trajectories from the sampling locations with (a) relative humidity, (b) air parcel height along the trajectory, and (c) specific humidity (in grams/kilograms) along the trajectories for the 14 samples collected prior to 19 July. (d) Same as Figure 1c but for the rest of the 28 samples. Black dots in the diagrams represent sampling locations.

were analyzed for δD and δ^{18}O using a Thermo Delta-V-Plus isotope ratio mass spectrometer. The H_2O-CO_2 equilibrium method was adopted for δ^{18}O measurements [*Epstein and Mayeda*, 1953], while the H_2O-H_2 equilibration in the presence of a platinum catalyst was used for δD measurements (for more details, see *Srivastava et al.* [2010]). The precision values of the measurements are 1‰ for δD and 0.1‰ for δ^{18}O, and the propagated uncertainty in the estimation of d is 1.3‰.

3. Results and Discussion

3.1. Air Parcel Trajectory Analysis

[4] For all days of water vapor collection, 72 h air mass back trajectory analysis was done using the NOAA Hybrid Single-Particle Lagrangian Integrated Trajectory (HYSPLIT) model [*Draxler and Rolph*, 2003]. The GDAS (Global Data Assimilation System) data [*Kanamitsu*, 1989] is used as input to this model, which generates three-dimensional back trajectories of air parcels and meteorological variables such as rainfall, pressure, potential temperature, temperature, and relative humidity along the trajectory.

[5] Due to the strong westerly monsoon winds, air parcels traveled from the Arabian Sea to the BoB during the sampling period. While crossing the southern peninsular India, air parcels dehydrated due to condensation over the Western Ghats. Model-derived heights of air parcels show a descending motion of air to the east of the Western Ghats and mixing with hotter, drier air in the lower troposphere (the so-called "rain shadow effect"). This caused the low relative humidity over peninsular India, and the parcel gained moisture after entering the BoB (see Figures 1a and 1b). A major amount of the moisture collected by us thus seems to have originated from the BoB alone. There is no reported descending motion of air over the BoB during this active monsoon season, implying that there is little chance of mixing of air above the atmospheric boundary layer with the advected air parcel coming from over peninsular India.

3.2. Variations of δD and δ^{18}O of Vapor and Meteorological Parameters

[6] Figure 2 shows the time series of stable isotopic composition of water vapor and the associated meteorological parameters. $\delta^{18}O_v$ values at 25 m varied from −9.8‰ to −14.1‰ (mean ± standard deviation, −11.4 ±0.9‰), while δD_v varied from −69.1‰ to −97.2‰ (−78.2 ±5.7‰); the d_v varied from 6.9 to 19.4‰ (12.6 ±3.0‰); at 6 m, $\delta^{18}O_v$ varied from −10.0 to −13.6‰ (−10.9 ± 0.8‰), δD_v varied from −68.3‰ to −94.0‰ (−74.6 ±5.4‰), and d_v varied from 5.7‰ to 16.4‰ (12.7 ± 2.4‰). Stable isotopic compositions of sea surface water varied from −2.5‰ to 0‰ for $\delta^{18}O_s$ (−0.4 ±0.4‰) and from −8.9‰ to 5.2‰ for δD_s (−3.1 ±2.1‰), and d_s varied from 3.7‰ to 11.1‰ (6.3 ±1.2‰). The isotopic compositions of vapor and d_v at 6 and 25 m did not show any statistically significant difference. However, the linear correlation coefficients (r) between δD_v at 6 and 25 m ($r = 0.78$) and that between $\delta^{18}O_v$ values ($r = 0.63$) are significant. However, the d_v values between these heights are uncorrelated ($r = -0.13$). The reason is that the isotopic ratios show much larger range of variation relative to their respective experimental errors (a factor of 36–43 for $\delta^{18}O_v$ and 26–28 in δD_v while only 8–10 in d_v) than d_v.

[7] The 3 hourly averaged wind (i.e., averaged over the sample collection time) was less than 10 m/s up to 21 July, and it increased up to 20 m/s later (22 July to 6 August 2012). The measured latent heat flux also shows a similar trend with a linear correlation coefficient r of 0.78 ($P < 0.01$) with the wind speed. However, such a trend is observed in neither δD_v nor $\delta^{18}O_v$; rather, they show a correlation [$r = -0.66$ ($P < 0.01$) for $\delta^{18}O_v$ and $r = 0.68$ ($P < 0.01$) for d_v] with the latent heat flux and with the wind speed [$r = -0.53$ ($P < 0.01$) for $\delta^{18}O_v$ and $r = 0.47$ ($P < 0.05$) for d_v] during the latter sampling period. Two marked dips are observed in δD_v and $\delta^{18}O_v$, associated with the presence of monsoon depressions at the collection site, marked by a fall in atmospheric pressure and an increased rainfall (on 20 July and 4 August 2012).

3.3. Influence of Local Ocean Surface Conditions

[8] Figure 2 is useful to infer the relations between isotopic compositions of atmospheric vapor and sea surface meteorological conditions. The expected relation between relative humidity and d (due to diffusive transport) was not observed as SST variations were smaller than those in air temperature; thus, it appears that relative humidity may not be a good indicator here of kinetic fractionation during evaporation. As predicted by MJ79, d_v, however, is inversely correlated with normalized humidity h.

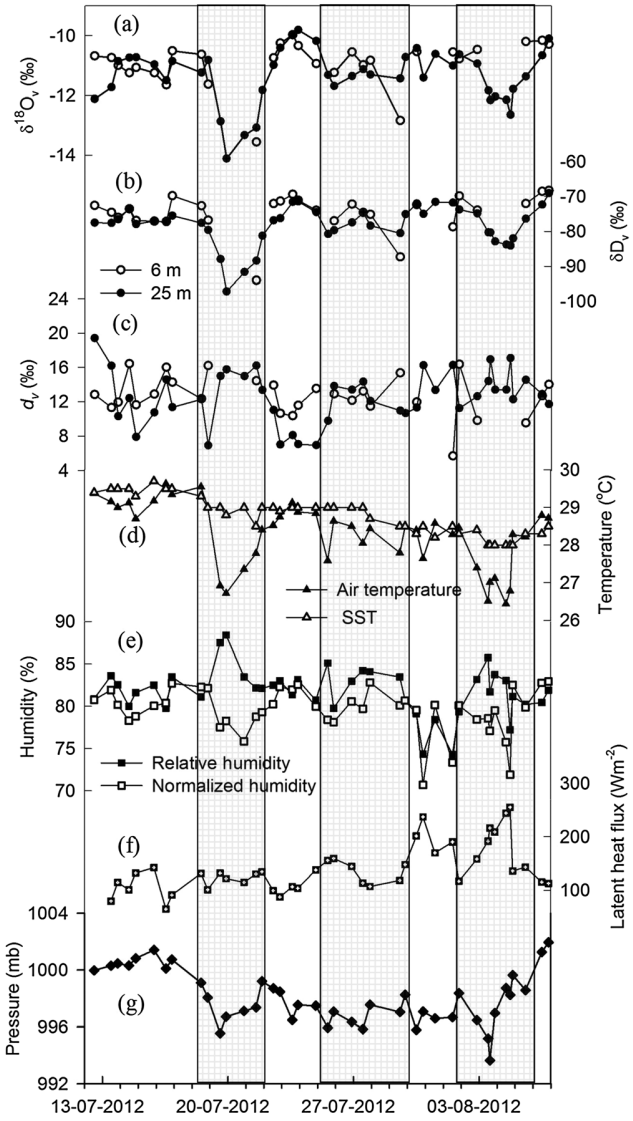

Figure 2. Time series of (a) $\delta^{18}O_v$, (b) δD_v, and (c) d_v values of marine vapor at 6 m (open symbols) and 25 m height (filled symbols) above sea level. (d) Air temperature and sea surface temperature. (e) Relative humidity and normalized humidity h. (f) Latent heat flux. (g) Atmospheric pressure at 25 m above sea level.

Twenty-five percent of the variance in d_v is explained by the normalized relative humidity [$d = (-0.55 \pm 0.14)^* h + (56 \pm 12)$, $r = 0.5$, $P < 0.01$]. Interestingly, the regression slope of −0.55‰/% and intercept 56‰ agree within the cited uncertainties, respectively, with the slope of −0.61‰/% and intercept 55‰ obtained by *Uemura et al.* [2008] for marine vapor over the Indian sector of the Southern Ocean (35–65°S and 20–115°E) during the Austral summer of 2006 (however, h correlated with relative humidity, i.e., $r = 0.9$ in their study). These results perhaps point toward the possible existence of a global relation between h and d_v as predicted by equation (1), although the coefficient of determination here is less than that in the Southern Ocean ($r \sim 0.8$) [*Uemura et al.*, 2008]. This may be a result of less temporal variability of h over the BoB during the sampling monsoon period or may be due to the weakening of the h-d_v relation above $h = 80\%$, as seen in isotope-enabled global models [*Uemura et al.*, 2008]. Atmospheric air temperature also shows a significant positive linear correlation δD_v and $\delta^{18}O_v$ [$r = 0.61$ ($P < 0.01$) for δD_v and $r = 0.62$ ($P < 0.01$) for $\delta^{18}O_v$], while they are uncorrelated with SST observations. This is likely due to the cooling of surface air during rainfall and associated isotopic equilibration of vapor with falling raindrops. Rain-vapor interactions are again discussed in section 3.4. Laser spectroscopy for continuous vapor sampling [e.g., *Kurita et al.*, 2012] would be more useful to increase the sample throughput to put such observations on a firmer footing.

[9] The factors determining the variations in $\delta^{18}O_v$ and d_v sampled up to 21 July 2012 and later appear to be quite different. The later samples exhibit better correlations with meteorological parameters such as air temperature, normalized humidity, latent heat flux, and wind speed than the earlier ones. Figures 1c and 1d show that less moisture is advected to the sampling location in the later than the earlier period. As local evaporation contributed more vapor than advection during the later period, this resulted in better correlation coefficients as observed (Table 1). Another reason could be that the spatial variability in the position of the vessel was more restricted for about 10 days in this period.

Table 1. Linear Correlation Coefficients (r) Between Different Parameters for All the Collected Samples (Second Column) and Only Samples Collected After 21 July 2012 (Third Column)[a]

Parameters	All Samples ($n=42$)	Post 21 July 2012 ($n=27$)
Normalized humidity with d-excess	−0.50**	−0.66**
d with latent heat flux	0.19	0.68**
$\delta^{18}O_v$ with air temperature	0.63**	0.80**
$\delta^{18}O_v$ with latent heat flux	−0.17	−0.66**
d with wind speed	0.24	0.47*
$\delta^{18}O_v$ with wind speed	−0.07	−0.53**

[a]Double star indicates significant r values with $P < 0.01$, single star indicates $P < 0.05$, and no star indicates insignificance. As $\delta^{18}O_v$ and δD_v are significantly correlated, only correlation with $\delta^{18}O_v$ is presented.

3.4. Comparison With the Craig and Gordon Model and Influence of Advected Moisture

[10] Figure 3 shows the comparison of data with predicted values from the C-G model, although the global closure assumption [$<R_E>=<R_A>$ in equation (1)] is not applicable on a regional scale. The equilibrium fractionation factor (α) is taken from *Majoube* [1971a, 1971b], and the kinetic fractionation factor k is calculated using wind-dependent parameterization proposed by MJ79. The model estimates that $\delta^{18}O_v$ is closer to observation during nonrainy days and not on rainy days. This is due to exchange and reevaporation from the falling raindrops, not taken into account by the C-G model. In addition, downdrafts during convective rain events can bring vapor with depleted δ values and higher d_v values from the boundary layer above to the surface [*Knupp and Cotton*, 1985; *Kurita*, 2013]. We infer that it is imperative to account for (a) isotopic exchange between vapor and raindrops [*Stewart*, 1975], (b) the mixing with the boundary layer vapor laterally advected to the collection site, and (c) vertical mixing during convective downdraft to significantly improve the model prediction.

[11] The strong southwesterly winds provide a continuous supply of the moisture to the sampling location, so the isotopic exchange occurring along its trajectory needs to be considered to explain the observed variations in $\delta^{18}O_v$. Evaporation of and isotopic exchange with falling raindrops along the air parcel trajectory may cause advection of depleted vapor to the collection site. The observed negative correlation of $r = -0.62$ between the observed deviations in $\delta^{18}O_v$ (−0.65 for δD_v) from the C-G model prediction and the average rain rate along the trajectory for the previous 24 h (HYSPLIT-derived rain rate) prior to sampling (see Figure 3) is consistent with the above hypothesis. Recently, *Kurita* [2013] have also

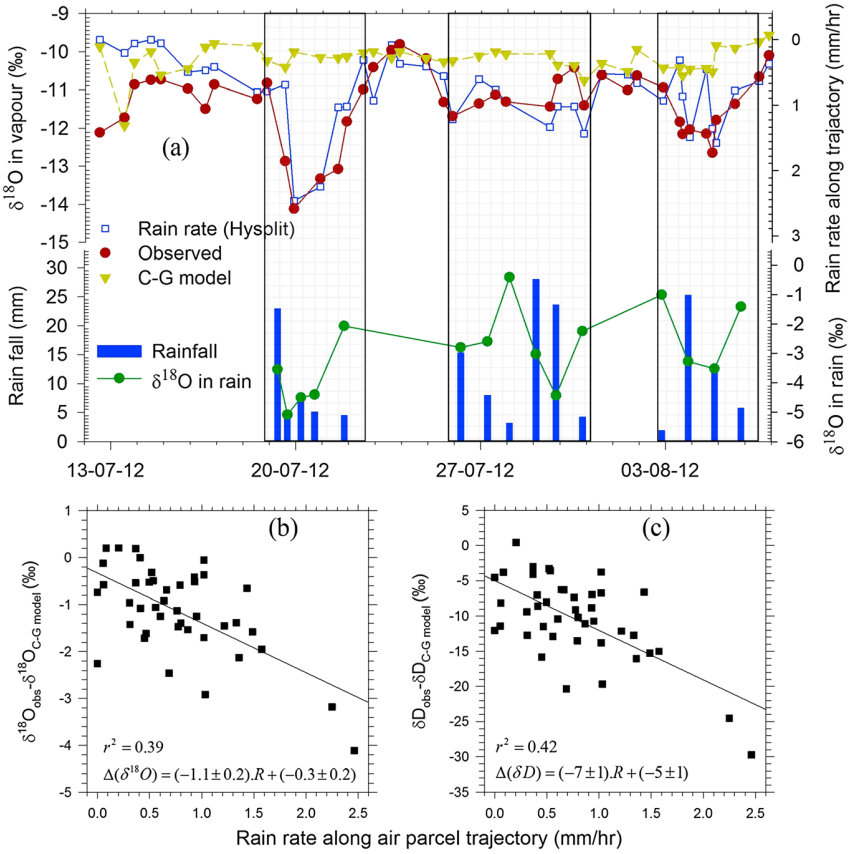

Figure 3. (a) Comparison of observed variations in $\delta^{18}O_v$ (filled circles) with C-G model results (inverted triangles). The shaded area shows three rain spells that occurred during sampling. The rain rate (open square) plotted in the upper panel is the average rain rate along the 24 h air parcel trajectory. The accumulated rain amount collected during the cruise (vertical bars) and its $\delta^{18}O_r$ (filled circle) are also shown in bottom panel. (b) The relation between the deviation between the observed $\delta^{18}O_v$ (represented as $\delta^{18}O_{obs}$) from the C-G model result [represented as $\Delta(\delta^{18}O)$ in the regression line] and the average rain rate along the 24 h back. The R in the regression equation represents the rain rate. (c) Same as Figure 3b but for δD_v.

shown that the rain activity along the air parcel back trajectory significantly depletes the isotopic composition of surface vapor over the tropical oceans. When raindrops evaporate into unsaturated air, vapor relatively depleted in ^{18}O (and D), with higher d_v values results, as observed by us during the three spells of rain (shaded area in Figure 2).

4. Conclusion

[12] The δD_v and $\delta^{18}O_v$ over the BoB are controlled mainly by the ocean surface conditions, while a lateral advection of vapor could alter their values significantly. The relation between deuterium excess and normalized humidity appears to be valid for the tropics, though it is less prominent than over the Southern Ocean, due to smaller variations in humidity during the monsoon. δD_v and $\delta^{18}O_v$ values correlate well with atmospheric temperature rather than SST. While the mean values of δD_v, $\delta^{18}O_v$, and *d*-excess at 6 and 25 m do not differ significantly, the *d*-excess values between these heights do not correlate as the isotope ratios do, as the variation in the former is relatively low. During the dry days, the Craig and Gordon model results are closer to the observed $\delta^{18}O$, while during rainy days, $\delta^{18}O$ is more depleted as a result of lateral advection of vapor derived from reevaporation from falling raindrops.

[13] **Acknowledgments.** We thank the MoES/CTCZ program and the captain crew, and participants of ORV *Sagar Kanya* cruise (#SK-296) for their assistance. We thank G. S. Bhat, CAOS, IISc, for providing latent heat flux data and Vijayakumar, NIO, Goa, for providing AWS data. We thank ISRO-GBP for the funding.

[14] The Editor thanks two anonymous reviewers for their assistance in evaluating this paper.

References

Bolot, M., B. Legras, and E. J. Moyer (2012), Modelling and intepreting the isotopic composition of water vapour in convective updrafts, *Atmos. Chem. Phys. Discuss.*, *12*(8), 22,451–22,533, doi:10.5194/acpd-12-22451-2012.

Bony, S., C. Risi, and F. Vimeux (2008), Influence of convective processes on the isotopic composition ($\delta^{18}O$ and δD) of precipitation and water vapor in the tropics: 2. Physical interpretation of the amount effect, *J. Geophys. Res.*, *113*, D19306, doi:10.1029/2008JD009942.

Craig, H., and L. Gordon (1965), Deuterium and oxygen 18 variations in the ocean and the marine atmosphere, in *Stable Isotopes in Oceanographic Studies and Paleotemperatures*, pp. 9–130, Lab. di Geol. Nucleate, Pisa, Italy.

Draxler, R. R., and G. D. Rolph (2003), HYSPLIT (HYbrid Single-Particle Lagrangian Integrated Trajectory) model access via NOAA ARL READY website (http://www.arl.noaa.gov/ready/hysplit4.html), NOAA Air Res. Lab., Silver Spring, Md.

Epstein, S., and T. Mayeda (1953), Variation of O18 content of waters from natural sources, *Geochim. Cosmochim. Acta*, *4*(5), 213–224.

Gat, J. R. (1996), Oxygen and hydrogen isotopes in the hydrologic cycle, *Annu. Rev. Earth Planet. Sci.*, *24*(1), 225–262, doi:10.1146/annurev.earth.24.1.225.

Joussaume, S., R. Sadourny, and J. Jouzel (1984), A general circulation model of water isotope cycles in the atmosphere, *Nature*, *311*(5981), 24–29, doi:10.1038/311024a0.

Jouzel, J., R. R. D. Koster, and D. Koster (1996), A reconsideration of the initial conditions used for stable water isotope models, *J. Geophys. Res.*, *101*(96), 22,933–22,938, doi:10.1029/96JD02362.

Kanamitsu, M. (1989), Description of the NMC global data assimilation and forecast system, *Weather Forecast.*, *4*(3), 335–342, doi:10.1175/1520-0434(1989)004<0335:DOTNGD>2.0.CO;2.

Knupp, K. R., and W. R. Cotton (1985), Convective cloud downdraft structure: An interpretive survey, *Rev. Geophys.*, *23*(2), 183–215, doi:10.1029/RG023i002p00183.

Kurita, N. (2013), Water isotopic variability in response to mesoscale convective system over the tropical ocean, *J. Geophys. Res. Atmos.*, *118*, 10,376–10,390, doi:10.1002/jgrd.50754.

Kurita, N., B. D. Newman, L. J. Araguas-Araguas, and P. Aggarwal (2012), Evaluation of continuous water vapor δD and $\delta^{18}O$ measurements by off-axis integrated cavity output spectroscopy, *Atmos. Meas. Tech.*, *5*(8), 2069–2080, doi:10.5194/amt-5-2069-2012.

Majoube, M. (1971a), Fractionation in O-18 between ice and water vapor, *J. Chim. Phys. Phys. Chim. Biol.*, *68*(4), 625–636.

Majoube, M. (1971b), Oxygen-18 and deuterium fractionation between water and steam, *J. Chim. Phys. Phys. Chim. Biol.*, *68*(10), 1423–1436.

Merlivat, L., and J. Jouzel (1979), Global climatic interpretation of the deuterium-oxygen 18 relationship for precipitation, *J. Geophys. Res.*, *84*(C8), 5029–5033, doi:10.1029/JC084iC08p05029.

Ramesh, R., M. Tiwari, S. Chakraborty, S. R. Managave, M. G. Yadava, and D. K. Sinha (2010), Retrieval of south Asian monsoon variation during the Holocene from natural climate archives, *Curr. Sci.*, *99*(12), 1770–1786.

Srivastava, R., R. Ramesh, R. A. Jani, N. Anilkumar, and M. Sudhakar (2010), Stable oxygen, hydrogen isotope ratios and salinity variations of the surface Southern Indian Ocean waters, *Curr. Sci.*, *99*(10), 1395–1399.

Stewart, M. K. (1975), Stable isotope fractionation due to evaporation and isotopic exchange of falling water drops, *J. Geophys. Res.*, *80*(9), 1133–1146.

Uemura, R., Y. Matsui, K. Yoshimura, H. Motoyama, and N. Yoshida (2008), Evidence of deuterium excess in water vapor as an indicator of ocean surface conditions, *J. Geophys. Res.*, *113*, D19114, doi:10.1029/2008JD010209.

Yoshimura, K., M. Kanamitsu, D. Noone, and T. Oki (2008), Historical isotope simulation using reanalysis atmospheric data, *J. Geophys. Res.*, *113*, D19108, doi:10.1029/2008JD010074.

Yurtsever, Y., and J. R. Gat (1981), Atmospheric waters, *Stable Isot. Hydrol. Deuterium Oxyg. Water Cycle*, *210*, 103–142.

Clim Dyn
DOI 10.1007/s00382-015-2652-8

Validation of $\delta^{18}O$ as a proxy for past monsoon rain by multi-GCM simulations

M. Midhun[1,2] · **R. Ramesh**[1,3]

Received: 13 March 2015 / Accepted: 9 May 2015

Abstract Stable oxygen isotope ratios ($\delta^{18}O$) of tree cellulose and speleothem carbonate are useful proxies for past monsoon rain in many tropical regions, as a decrease in rain $\delta^{18}O$ is observed with increase in rainfall on a monthly time scale. This amount effect varies spatially; therefore a local calibration, with actual measurements of rain amount and its $\delta^{18}O$ is required. Such observations, however, are quite limited in space and time. To circumvent this difficulty, many isotope enabled general circulation models (GCMs) are used to aid the interpretation of ^{18}O proxies; nevertheless, *all such simulations taken together* are yet to be evaluated against observations over the Indian summer monsoon (ISM) region. Here we examine ten such GCM simulations archived by the stable water isotope INtercomparison Group, phase 2. The spatial patterns of simulated ISM rainfall and its $\delta^{18}O$ are in good agreement with the limited observations available. Simulations nudged with observed wind fields show better skill in reproducing the observed spatio-temporal pattern of rainfall and its $\delta^{18}O$. A large discrepancy is observed in the magnitude of the simulated amount effect over the Indian subcontinent between the models and observation, probably because models simulate the spatial distribution of monsoon precipitation differently. Nudged simulations show that interannual variability of rainfall $\delta^{18}O$ at proxy sites are controlled by either regional (rather than local) rainfall or upstream rain out. Interannual variability of rainfall $\delta^{18}O$ over the East Asian region is well correlated with ENSO, while it is only weakly correlated over the Indian sub-continent.

Keywords Indian summer monsoon · Stable isotopes · Speleothem · Amount effect · Isotope enabled GCMs · Model intercomparison · Paleoclimatology

1 Introduction

Stable water isotopologues ($H_2^{18}O$, HDO) undergo fractionation in the hydrological cycle due to their relative mass difference and attendant vapor pressure differences (Dansgaard 1964; Gat and Gonfiantini 1981). This fractionation is a function of temperature, and the relative abundances of isotopologues in precipitation are correlated with climatic parameters such as temperature or precipitation amount (Dansgaard 1964; Gat 1996). Such relations are useful in reconstructing past climate from natural archives such as cave calcites (speleothems), tree rings and ice cores (e.g., Augustin et al. 2004; Yadava and Ramesh 2005; Ramesh et al. 2010). Simple theoretical models (e.g., Rayleigh model) are used to explain the physical mechanisms that are responsible for this isotope-climate linkage, but these models inadequately represent all the complex processes (e.g., convection, atmospheric circulation etc.) occurring in the atmosphere. During the last three decades, stable isotope physics has been incorporated into GCMs, and relevant equations of atmospheric processes are solved numerically (Joussaume et al. 1984). These studies have helped improve our knowledge regarding factors controlling the stable water isotopologues of precipitation.

Electronic supplementary material The online version of this article (doi:10.1007/s00382-015-2652-8) contains supplementary material, which is available to authorized users.

✉ M. Midhun
midhun.ndr@gmail.com; midhun@prl.res.in

[1] Geosciences Division, Physical Research Laboratory, Ahmedabad 380009, India

[2] Indian Institute of Technology Gandhinagar, VGEC Campus, Ahmedabad 382424, India

[3] Sardar Patel University, Vallabh Vidyanagar 388120, India

Published online: 19 May 2015

Rainfall $\delta^{18}O$ ($\delta^{18}O_p$) is defined as ($R_{sample}/R_{VSMOW} - 1$) * 1000, where R_{sample} is the ratio of abundances of $H_2^{18}O$ and H_2O in the sample, and R_{VSMOW} is that of Vienna Standard Mean Ocean Water. Unlike in the higher latitudes, $\delta^{18}O_p$ in the tropics, especially where the mean annual surface air temperature is >15 °C, does not correlate with surface air temperature; but has a negative correlation with the amount of precipitation (the amount effect, Dansgaard 1964). Studies carried out using numerical models (ranging from a simple 1-D model to isotope enabled GCMs) to understand the physical mechanism that leads to the amount effect (Dansgaard 1964; Lee and Fung 2008; Risi et al. 2008, 2010a) show the major reasons to be: (1) Heavier isotopologues preferentially condense during precipitation; higher the rainfall, larger is the depletion in ^{18}O of the remaining vapor, leading to a stronger ^{18}O depletion of rain, (2) ^{18}O enrichment in rain due to re-evaporation of rain at sub-cloud level, which is likely to be higher when rain amounts are low, and (3) more intense the convection, the stronger is the convective downdraft, bringing more of ^{18}O depleted vapor from the higher altitudes to the sub-cloud layer and subsequently feeding the system through convective updraft. Recent studies suggest that the monthly mean $\delta^{18}O_p$ variability in the tropics is also related to the extent of organized convection, the $\delta^{18}O$ of vapor that converges at low levels or the altitude of moisture convergence (Lawrence 2004; Kurita 2013; Lekshmy et al. 2014; Moore et al. 2014), in addition to the monthly rain amount.

Limited observational data on $\delta^{18}O_p$ [Global Network of Isotope in Precipitation (GNIP), http://www-naweb.iaea.org/napc/ih/IHS_resources_isohis.html] over the Indian summer monsoon (ISM) region indicate large spatial variations in the amount effect. South western coastal India and north-east India show no, or even an inverse (i.e., a positive correlation between $\delta^{18}O_p$ and rainfall) amount effect (Yadava et al. 2007; Breitenbach et al. 2010; Lekshmy et al. 2013), whereas inland stations do show a significant amount effect (Yadava and Ramesh 2005). Hence a more quantitative understanding of isotope climate linkage in the ISM region may help improve the calibration of paleomonsoon proxies. Limited spatial and temporal coverage of $\delta^{18}O_p$ data complemented with data from an isotope enabled GCM could be useful in this endeavor.

Over the Asian monsoon region, pioneering work using GCM was done by Hoffmann and Heimann (1997) using ECHAM3, demonstrating the control of amount of precipitation on the seasonal and spatial distribution of $\delta^{18}O_p$ over the monsoon region. Later (Vuille et al. 2005) ECHAM4 produced a strong temperature effect in the tropics, but unsupported by observations: The simulated amount effect too was stronger than in observations. A negative relation between the interannual variation of monsoon $\delta^{18}O_p$ and the JJAS wind shear index, which is a good indicator of large scale monsoon circulation intensity was also found. More recently, Ishizaki et al. (2012) showed that condensation along the trajectory before an air mass reaches a site drives interannual variation of $\delta^{18}O_p$ at the site, using an isotope enabled model (CCSR/NIES/FRCGC AGCM5.7b).

Although the parameterization of isotopic fractionation relies on simple equations, $\delta^{18}O_p$ simulated by GCMs is highly sensitive to other physical parameterizations, such as the ones for convection and boundary layer. (Lee et al. 2009; Noone and Sturm 2010; Field et al. 2014). As the parameterization of convection in the tropics differs significantly among models, inference based on a single model output could perhaps be biased. Consequently, a multi-model simulation inter-comparison could be quite useful to improve the calibration of $\delta^{18}O_p$ with rainfall.

Here we analyze the outputs from SWING2 and assess the ability of isotope enabled GCMs to simulate the present day $\delta^{18}O_p$ of ISM. First, we check their ability to reproduce the annual cycle of rainfall over India, and spatial distribution of rainfall over the ISM region (10°S–40°N and 50°E–110°E, Fig. 1). This region, besides India, includes the Equatorial Indian Ocean in addition to some stations from southern China and South East Asia, which are all under the influence of ISM. Next, we assess the skill of SWING2 models in reproducing the spatio-temporal variations of $\delta^{18}O_p$ over the ISM region. Finally, the possible role of local precipitation, regional precipitation and ENSO on the interannual variability of summer monsoon $\delta^{18}O_p$ is discussed.

2 Models, data and methods

We use ten model simulations from SWING2, archived at ftp://swi.geo.su.se/swing2. Details of SWING2 model simulations are presented in Table 1. All the models are forced with observed monthly sea surface temperatures (SST) (Risi et al. 2012; Conroy et al. 2013). Three of the ten simulations were nudged with the reanalysis wind field (NCEP or ECMWF). We restrict our analysis to the years 1981–1999, which are common for the different simulations. For some specific analysis (section 3.2.5) we also used data from three nudged simulations for an extended period (1980–2007). For validating the models, we used GPCP (Global Precipitation Climatology Project, Adler et al. 2003) and CMAP (CPC Merged Analysis of Precipitation, Xie and Arkin 1997) rainfall datasets, while the source for the observed $\delta^{18}O_p$ data is the GNIP network. We use data from GNIP stations where at least 3 years of monthly $\delta^{18}O_p$ are available. For the analysis of amount effect, we selected stations that had more than 30 monthly observations of $\delta^{18}O_p$ during the ISM season. For plotting Taylor diagrams (Taylor 2001), we interpolated the model outputs

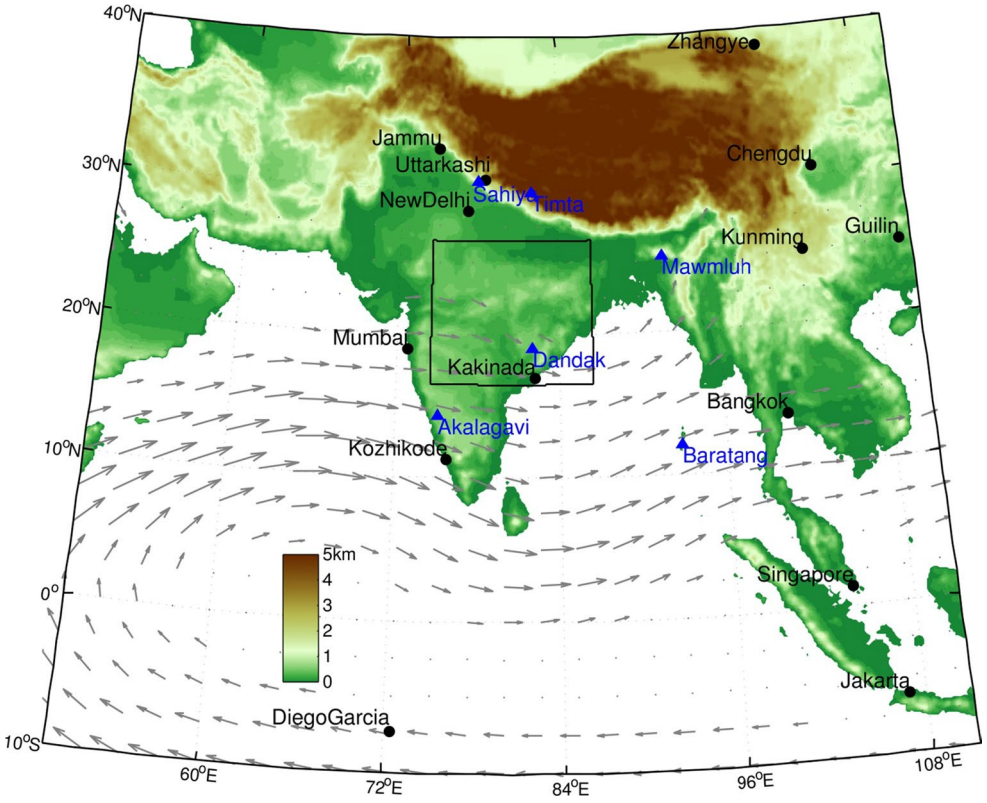

Fig. 1 Geographical map of South Asia showing topography (*shaded*, altitude above mean sea level), location of GNIP stations (*black circles*, data used in section 3.2.3 & 3.2.4) and locations of major cave sites (*blue triangles*) over India. The area highlighted by the *black rectangle* indicates the core monsoon region (CMR). Winds at 850 hPa during ISM (called the Low Level Jet) shown using *gray arrows*

Table 1 Details of SWING2 models used for the present study

Model	Resolution (°) (latitude × longitude)	Simulation type	References
GSM	1.914 × 1.875	Free and nudged with NCEP R2	Yoshimura et al. (2008)
LMDZ4	2.5 × 3.75	Free and nudged with ECMWF	Risi et al. (2010b)
GISS ModelE	2 × 2.5	Free and nudged with NCEP	Schmidt et al. (2007)
CAM2	2.812 × 2.812	Free	Lee et al. (2007)
HadAM3	2.43 × 3.75	Free	Sime et al. (2009)
GENESIS3	1.875 × 1.875	Free	Mathieu et al. (2002)
MIROC32	2.812 × 2.812	Free	Kurita et al. (2011)

Further details can be found at http://www.giss.nasa.gov/projects/swing2

and observed gridded rainfall datasets to a T63 Gaussian grid using the bilinear interpolation technique (Climate Data Operator, https://code.zmaw.de/projects/cdo).

3 Results and discussion

3.1 Indian monsoon rainfall

3.1.1 Annual cycle of precipitation over the core monsoon region (CMR)

The annual cycle of rainfall over India is characterized by ISM rainfall peaking during June–September (JJAS). To check the skill of SWING2 models in simulating this cycle, we analyze rainfall simulations over the CMR (74.5–86.5°E, 16.5–26.5°N), where the mean and standard deviation of JJAS rainfall are homogeneous (Goswami et al. 2006). Figure 2a depicts the annual cycle of rainfall over CMR. Though most of the models produce high rainfall during JJAS, the amounts of rainfall simulated by different models show a large spread. Model simulations exhibit good correlations with observation (GPCP), ranging from ~0.85 to ~0.99 (significant at $P < 0.01$ level) (Fig. 2b). Rainfall simulated (Fig. 2b) by MIROC32, nudged GSM and free GISS are the closest to observations, whereas LMDZ (free and nudged) and nudged GISS exhibit significant dry bias while CAM2 and HadAM3 show wet bias.

CAM2 simulates intense rainfall during pre-monsoon months as well, in contrast to observations (Nanjundiah et al. 2005). Nudged simulations of rainfall from GSM and LMDZ improved compared to their free runs, whereas no significant improvement was observed in nudged GISS relative to its free run.

3.1.2 Spatial pattern of JJAS precipitation

The observed ISM rainfall shows a large spatial variability over the Indian subcontinent, with two rainfall maxima over the mountain ranges of Western Ghats (western coast of peninsular India) and Myanmar (extending up to northern Bay of Bengal). Its northwestern limit lies in the arid regions of Rajasthan, Punjab and parts of Pakistan. Model simulations of climatological mean JJAS precipitation over the ISM region are plotted in Fig. 3 and their coherence with observations are illustrated using a Taylor diagram in Fig. 4a. Though all the models simulate the annual cycle of rainfall with higher amounts during JJAS over CMR, the spatial patterns of rainfall vary significantly. Major features, e.g., rainfall peaks along the south western coast of India and the northern Bay of Bengal, are captured by most models. They fail to simulate the observed north western limit of JJAS rainfall (except for CAM2 and HadAM3). Recently, a very high resolution simulation of ISM using LMDZ (zoomed LMDZ with ~35 km resolution over the ISM region) drastically improved the spatial pattern of ISM rain over India (Sabin et al. 2013). Hence the model resolution appears to significantly influence its output. Pattern correlation of gridded rainfall (for the area 50–110°E and 10°S–40°N) between GPCP data and SWING2 models varied from ~0.45 to ~0.82 (significant at $P < 0.01$ level). The GPCP dataset is used as a reference in the Taylor diagram (CMAP shows a standard deviation similar to GPCP, but with a correlation of 0.90 with GPCP). Spatial patterns of rainfall are considerably improved by the nudging technique in GSM, LMDZ and GISS (Figs. 3, 4a); these are the best SWING2 models in this respect. The problem of over-prediction of rainfall peaks in the free runs of GSM and GISS vanished in their respective nudged simulations, whereas rainfall was underestimated in both (nudged and free runs) simulations for LMDZ.

Fig. 3 Comparison of spatial patterns of precipitation simulated by SWING2 models with observed (GPCP) rainfall (*left two columns*) and their $\delta^{18}O_p$ with GNIP $\delta^{18}O_p$ (*right two columns*) for the months June–September. A bias correction of +6 ‰ was applied to GENESIS simulated $\delta^{18}O_p$ (Mathieu et al. 2002)

3.1.3 Interannual variability of ISM in CMR

A comparison of the interannual variability of JJAS rainfall simulated by SWING2 models with observations over CMR is presented in Fig. 5. Nudged simulations of GSM, LMDZ and GISS display significant positive correlations ($P < 0.05$) with the observations, while all the other models (forced by SST only) fail. Though the nudged simulation of LMDZ underestimates the JJAS rainfall, its interannual variability is the closest to observations among all the

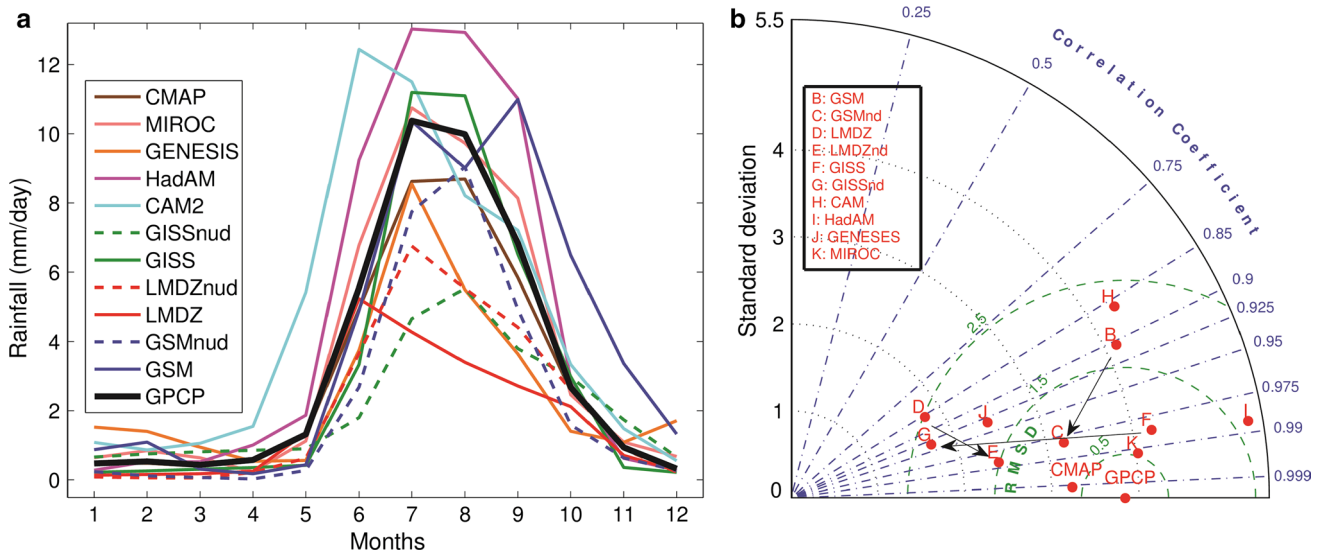

Fig. 2 **a** Observed (GPCP and CMAP) annual cycle of monthly mean (1981–1999) rainfall over CMR, and those simulated by SWING2 models. **b** Taylor diagram of annual cycle of rainfall over CMR simulated by different models and observations (GPCP, CMAP). GPCP rainfall is used as reference. *Black arrows* indicate the change from "free" model simulation to model nudged with reanalysis winds

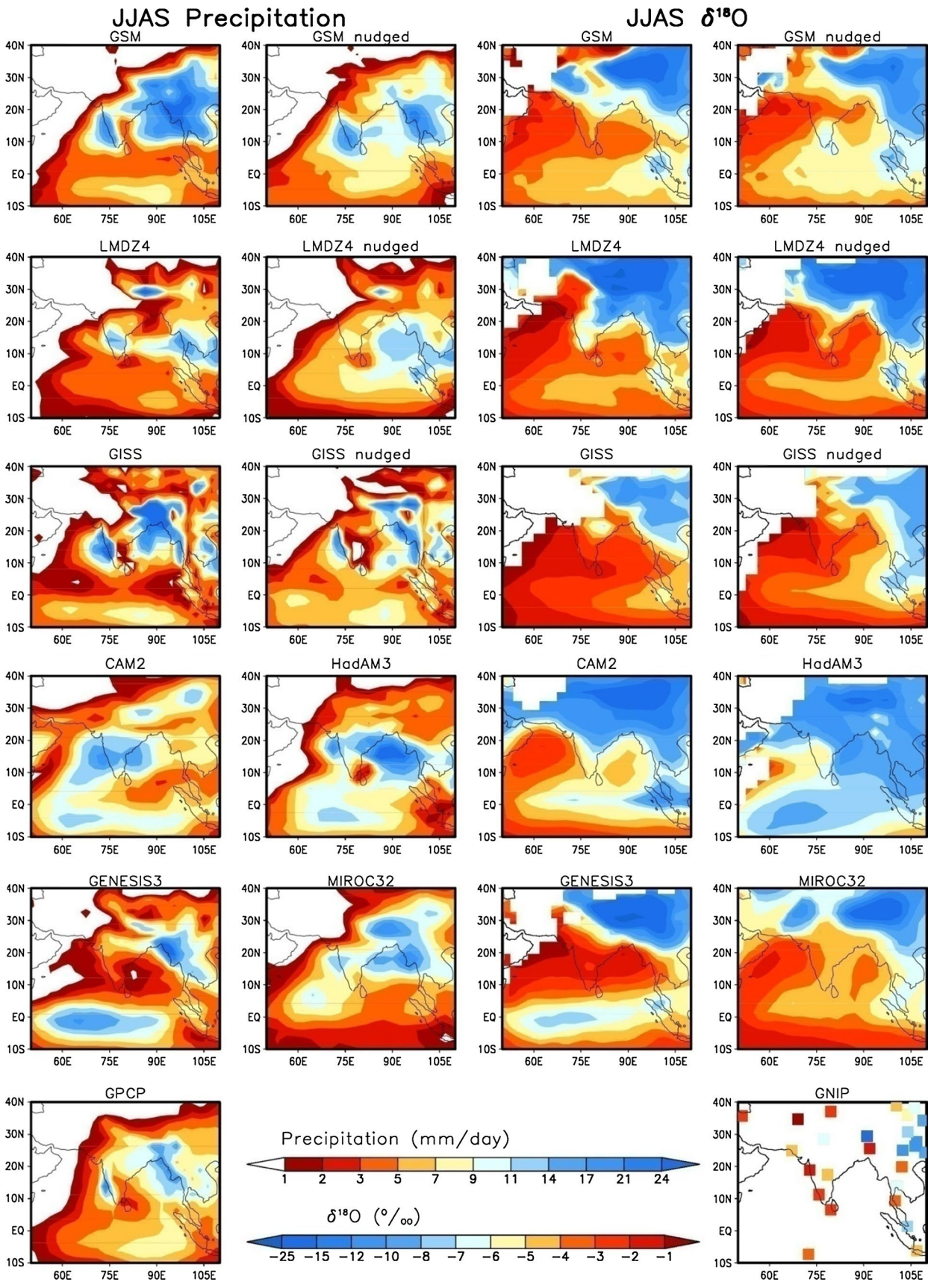

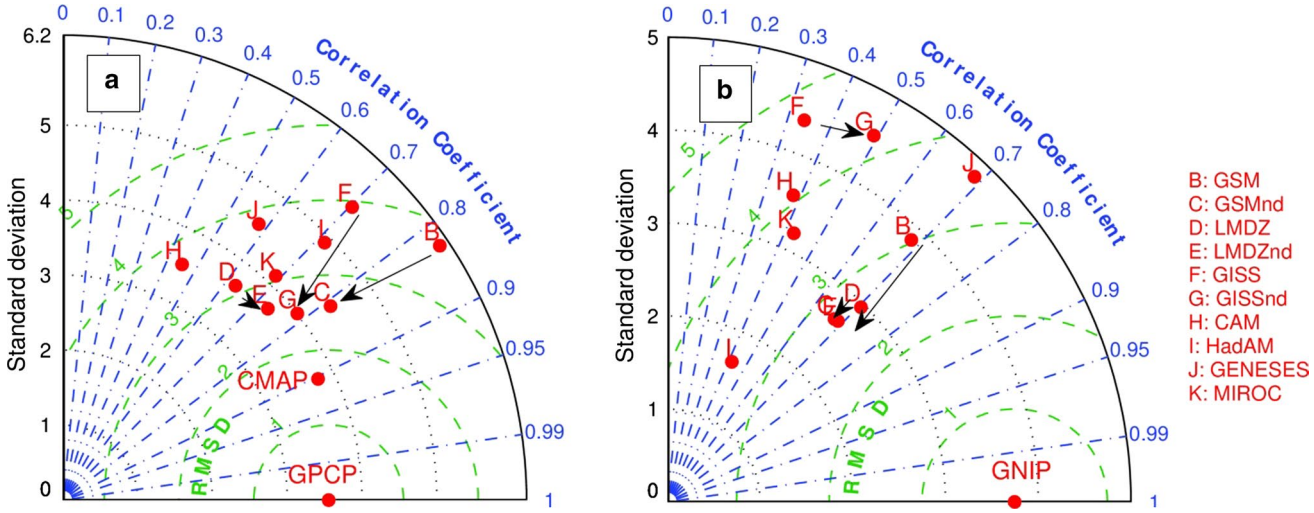

Fig. 4 **a** Taylor diagram showing multi model comparison of spatial pattern of precipitation and **b** its $\delta^{18}O_p$. GPCP rainfall data and GNIP $\delta^{18}O_p$ data are taken as references. *Black arrows* indicate the change from "free" model simulation to model nudged with reanalysis winds

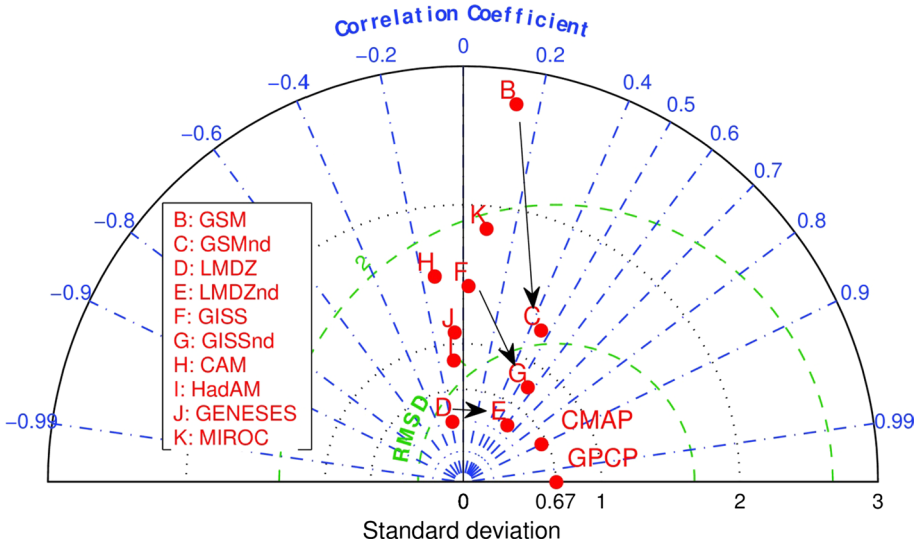

Fig. 5 Taylor diagram showing the performance of SWING2 models in reproducing interannual variations of ISM rainfall (JJAS-average rainfall) over CMR. GPCP data are used as reference. *Black arrows* indicate the change from "free" model simulation to model nudged with reanalysis winds

SWING2 models. Though SST fluctuations do lead to rainfall variability and circulation changes in the tropics, modeling ISM using SST forcing alone is inadequate; a realistic representation of the atmospheric circulation plays a major role in the correct simulation of interannual variability of ISM.

3.2 δ^{18}O of precipitation

3.2.1 Comparison of observed $\delta^{18}O_p$ time series with that simulated by SWING2 models

To validate the SWING2 models, we compared the time series of monthly $\delta^{18}O_p$ simulations and observations (Fig. 6). For this, we selected 11 GNIP stations which have at least 60 monthly $\delta^{18}O_p$ observations in common with the SWING2 simulation period (i.e., 1981–1999). Linear correlation coefficients (r) between each of the ten SWING2 simulated $\delta^{18}O_p$ and the observed GNIP $\delta^{18}O_p$ at these stations were calculated. The median correlation coefficients of the 10 simulations ranged from ~0.2 to ~0.7. For 3 GNIP stations over the East Asian region (Zhangye, Guilin and Kunming), all SWING2 models show significantly (at $P < 0.05$) strong positive correlations. Generally, the nudged simulations from GSM, LMDZ and GISS are closer to observations compared to (1) their respective free runs; and (2) the rest of the SWING2 models as well. Improvements in correlation coefficients, relative to their free runs are statistically significant ($P < 0.05$) for 7 stations for GSM and LMDZ and 8 stations for GISS (Table

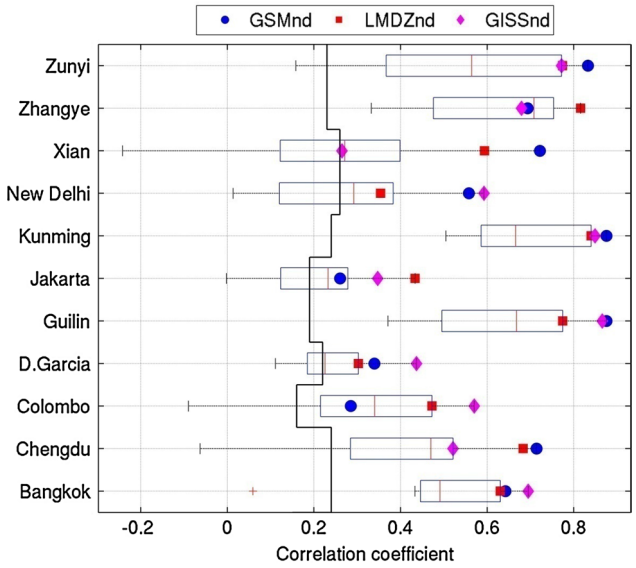

Fig. 6 The linear correlation coefficients between observations (GNIP) and simulations (SWING2) of monthly $\delta^{18}O_p$. All available monthly observations during 1981–1999 are used for this calculation. On *each box*, the *central mark* is the median, the *edges of the box* are the 25th and 75th percentiles, the *whiskers* extend to the most extreme data points not considered outliers, and outliers are plotted individually using "+" symbol. At each station, correlation coefficients for each of the ten simulations are represented by *box* and *whisker plots*. Nudged simulations by GSM, LMDZ and GISS are also plotted using *filled symbols* (suffix "nd" refers to nudged). Values significant at $P = 0.05$ lie to the right of the *zig-zag vertical black line*

S1 in supplementary material). This highlights the influence of the circulation pattern, better represented in the three nudged simulations, on rainfall $\delta^{18}O_p$.

3.2.2 *Spatial pattern of JJAS $\delta^{18}O_p$*

Spatial variations of $\delta^{18}O_p$ are mainly governed by isotopic effects such as latitudinal effect, continental effect, altitude effect, amount effect etc. (Araguás-Araguás et al. 2000). Continental moisture recycling (evapo-transpiration) also affects the spatial distribution of $\delta^{18}O_p$ over land. A comparison of observed and modeled JJAS weighted mean $\delta^{18}O_p$ is depicted in Fig. 3. The corresponding Taylor diagram is presented in Fig. 4b. Pattern correlation between the observed $\delta^{18}O_p$ (for the area 50–110°E and 10°S–40°N) and the simulated $\delta^{18}O_p$ varied from 0.32 to 0.71 (correlations above 0.37 are significant at $P < 0.05$ level). Though some of the models show pattern correlations close to 0.70, the spread in simulated $\delta^{18}O_p$ values (standard deviation) is either too high or too low, compared to observations (except in the case of the free run of GSM). A better evaluation of the simulated $\delta^{18}O_p$ values is hampered by the sparsity of $\delta^{18}O_p$ observations.

If the amount effect is the driver of spatial pattern of $\delta^{18}O_p$ (considering only the JJAS period of intense rain), $\delta^{18}O_p$ minima can be expected in the two regions of maximum rain: south western peninsular India and Myanmar coast. But such minima in $\delta^{18}O_p$ are observed neither in most SWING2 models, nor in GNIP observations (Fig. 3). In GNIP observations, $\delta^{18}O_p$ minima (for JJAS) are observed over the East Asian region and the Tibetan Plateau.Further, $\delta^{18}O_p$ maxima are observed over western peninsular India. This feature is predicted well by SWING2 models. All the models produce a ^{18}O depleting trend along the Low Level Jet stream (LLJ, Fig. 1) with $\delta^{18}O_p$ maxima over the Somali coast. This is likely due to the continuous rainfall along the LLJ with preferential removal of $H_2^{18}O$ (continental effect). This feature is consistent with the GNIP data from peninsular India.

3.2.3 *Seasonality of $\delta^{18}O_p$ over India*

Though India gets about 80 % of its annual precipitation during the ISM season, significant amounts of rainfall are also obtained during the north east monsoon (NEM, October–December) in peninsular India and during the Western disturbance season (Jan to March) over northern India. During these seasons, the wind patterns distinctly differ from the southwesterly ISM winds. This switch of moisture source may impact the seasonal variation of $\delta^{18}O_p$. Most of the models are able to reproduce the observed seasonality of rainfall over the three GNIP stations (Kozhikode, Kakinada and Mumbai) over peninsular India (Fig. 7). GNIP observations show that ISM $\delta^{18}O_p$ is relatively higher (by ~2–4 ‰) over peninsular India compared to the NEM $\delta^{18}O_p$. This seasonal cycle of $\delta^{18}O_p$ is also captured by most of the models. The $\delta^{18}O$ of paleomonsoon proxies from this region should be interpreted carefully to avoid erroneous attributions; e.g., a very negative $\delta^{18}O_p$ interpreted as solely due to increase in ISM rain, whereas in reality it could be also due to an increased ^{18}O depleted NEM contribution (i.e., associated with a change in rainfall seasonality).

The observed seasonality of $\delta^{18}O_p$ at GNIP stations Jammu, Uttarkashi and New Delhi is characterized by relatively higher values during the western disturbance season and lower values during the ISM season. This could be due to higher rainout en-route of air parcels during the ISM while rain from the western disturbance possibly forms from vapor of continental origin (mainly transpiration flux; Jasechko et al. 2013). While the seasonal pattern of $\delta^{18}O_p$ at New Delhi is well captured in the model, those at Jammu and Uttarkashi differ from the observations: Simulations show stronger ^{18}O depletion during the winter months (December to February), which is not supported by observations. However an in-depth comparison of seasonality at these two stations is confounded by (1)

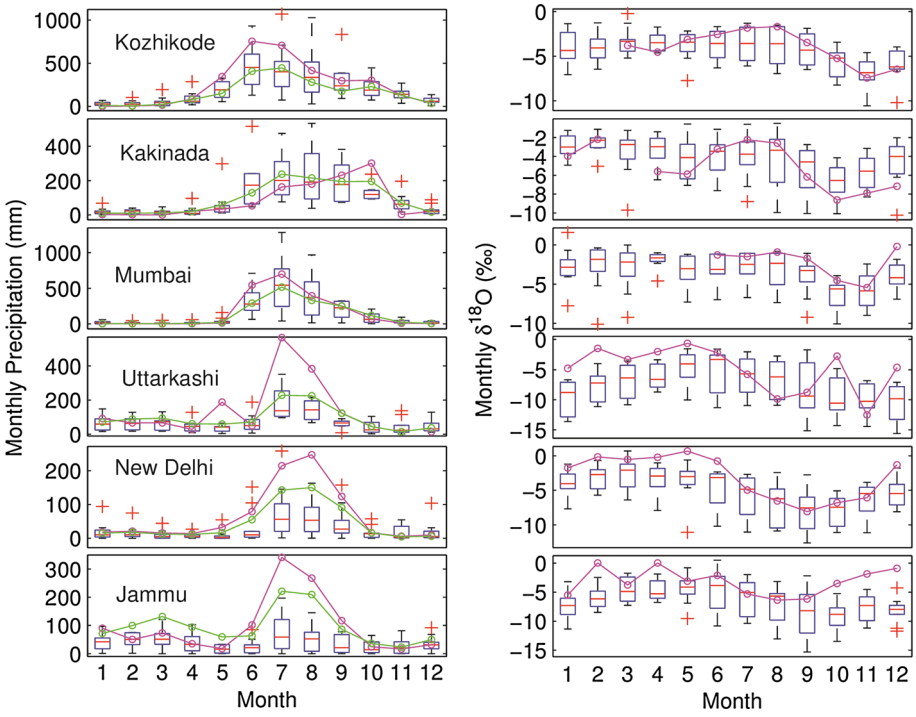

Fig. 7 Seasonal cycle of rainfall (*left*) and $\delta^{18}O_p$ (*right*). SWING2 simulations are represented by *box* and *whisker diagram* (see Fig. 6 for the details of *box* and *whisker diagram*). A bias correction of '+6 ‰' is applied to GENESIS simulated $\delta^{18}O_p$. *Magenta lines* represent GNIP (rainfall and $\delta^{18}O_p$) and *green lines* represent GPCP (rainfall)

complex topography (Fig. 1), which is not well represented in the coarse resolution GCMs and (2) possible errors in the observed seasonalities of $\delta^{18}O_p$ at Uttarkashi and Jammu due to limited data lengths. Nevertheless the seasonalities of $\delta^{18}O_p$ at stations with long term $\delta^{18}O_p$ observations (i.e., New Delhi, Mumbai and Kozhikode) are certainly well simulated by the models.

3.2.4 Amount effect

We now examine rainfall-$\delta^{18}O_p$ correlations on two time scales; monthly for JJAS (Fig. 8, 4 months per year for 19 years) and interannual for JJAS-average (Fig. 9, 19 years). Though the amount effect defined by Dansgaard (1964) is for monthly rainfall and $\delta^{18}O_p$, we also used weighted average of JJAS period each year for studying the "amount effect" on interannual scale. The latter is the signal more likely to be preserved in monsoon proxies that do not provide sub-annual resolution.

On the monthly scale, SWING2 models except CAM2 show a strong amount effect over the oceanic region, similar to GNIP observations at ocean islands (Yurtsever and Gat 1981). Models predict either no or an inverse amount effect over Myanmar and surrounding regions. Over the Indian subcontinent, simulated amount effects are compared with GNIP observations at Kozhikode, Mumbai and New Delhi. Over Kozhikode, GNIP data show lack of amount effect, whereas most of the models (except LMDZ free and CAM) simulate a strong amount effect (supplementary Fig S1). Recently Lekshmy et al. (2014) showed that ^{18}O depletion of rain during monsoon over the south west coast of India (including Kozhikode) is associated with large scale organized convective systems. The amount effect in observations here may be damped due to equal contributions of rainfall from both the large scale organized convective systems (with relatively depleted ^{18}O) and isolated rainfall events (with relatively enriched ^{18}O) to the JJAS total rain. Over Mumbai, no amount effect is observed in GNIP data as well as in some of the SWING2 models (LMDZ free, CAM and GENESIS); MIROC and GISS free simulation show a strong amount effect for Mumbai while a few simulations (GSM free, GSM nudged, LMDZ nudged, GISS nudged and HadAM) depict a significant, but weaker amount effect (r ranges from -0.25 to -0.33). Over New Delhi, the long-term GNIP observations show a significant amount effect and this is well reproduced by nine out of ten simulations (supplementary Fig S1).

On the interannual time scale, SWING2 models (except CAM2) exhibit a strong "amount effect" over the equatorial Indian Ocean, while it is observed only over the island GNIP station Singapore (no "amount effect" observed over GNIP stations Diego Garcia and Jakarta). Though most of the models produced significant negative correlation between rain amount and $\delta^{18}O_p$ over the Indian subcontinent, the correlation pattern appears quite noisy. In observations, only three stations show statistically significant negative correlations; Kozhikode, New Delhi and Bangkok. Over southern China, both model and observations show a weak or insignificant "amount effect". A more detailed comparison of amount effect at Indian GNIP stations is shown in supplementary Fig. S1.

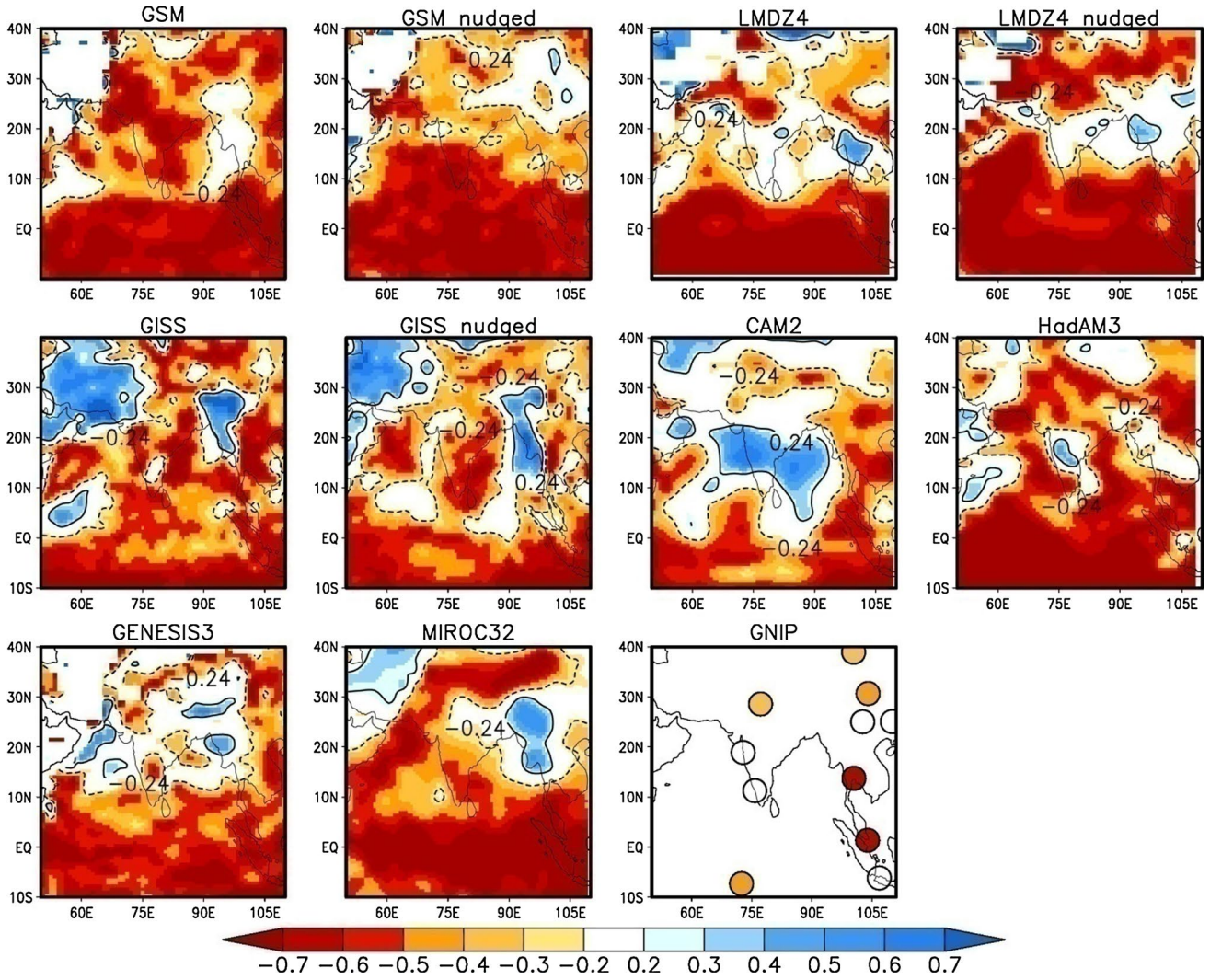

Fig. 8 Correlation coefficients between monthly (JJAS) rain rate and $\delta^{18}O_p$ at each grid point of model outputs for 19 years (1981–1999). Statistically significant correlation ($P < 0.05$) is represented by two *contour lines*; +0.24 and −0.24. The same analysis is done for GNIP stations where at least 30 months of JJAS $\delta^{18}O$ observations are available. For GNIP, sites represented by *open circles* show insignificant correlation at $P < 0.05$ level

Most of the SWING2 models overestimate the rainfall-$\delta^{18}O_p$ relation at both seasonal and inter-annual time scales. The simulated amount effect is sensitive to the isotopic parameterization used for post condensation exchange (PCE) (Field et al. 2010); this process enriches ^{18}O in low rainfall events via re-evaporation of rain into unsaturated sub-cloud layer, while it depletes ^{18}O in high rainfall events by the entrainment of re-evaporated vapor into the system (Risi et al. 2008). Risi et al. (2010b) demonstrated that the effective relative humidity (relative humidity at raindrop-air interface) plays a critical role in simulating the strength of the amount effect. The effect of PCE on the simulated precipitation and vapor isotopic compositions ($\delta^{18}O_p$ and $\delta^{18}O_v$) depends on the fraction of the precipitation that undergoes PCE, the degree of isotopic equilibration of raindrops with the vapor, the method by which the relative humidity near the raindrop surface is calculated, and all parameters controlling the fraction of the rain that evaporates.

Recent studies show the importance of isotopic composition of low level vapor ($\delta^{18}O_v$) on tropical $\delta^{18}O_p$ (Kurita 2013; Moore et al. 2014). Tropical oceanic regions are characterized by high surface evaporation and produce vapor with relatively higher values of $\delta^{18}O_v$ than other regions of the ocean. During precipitation over oceans, due to rain vapor interaction, $\delta^{18}O_v$ decreases (Lawrence 2004; Kurita 2013; Midhun et al. 2013). Low rainfall over the ocean mostly reflects the isotopic composition of evaporating vapor flux from the ocean, while during high rainfall $\delta^{18}O_p$ decreases due to the contribution of ^{18}O depleted

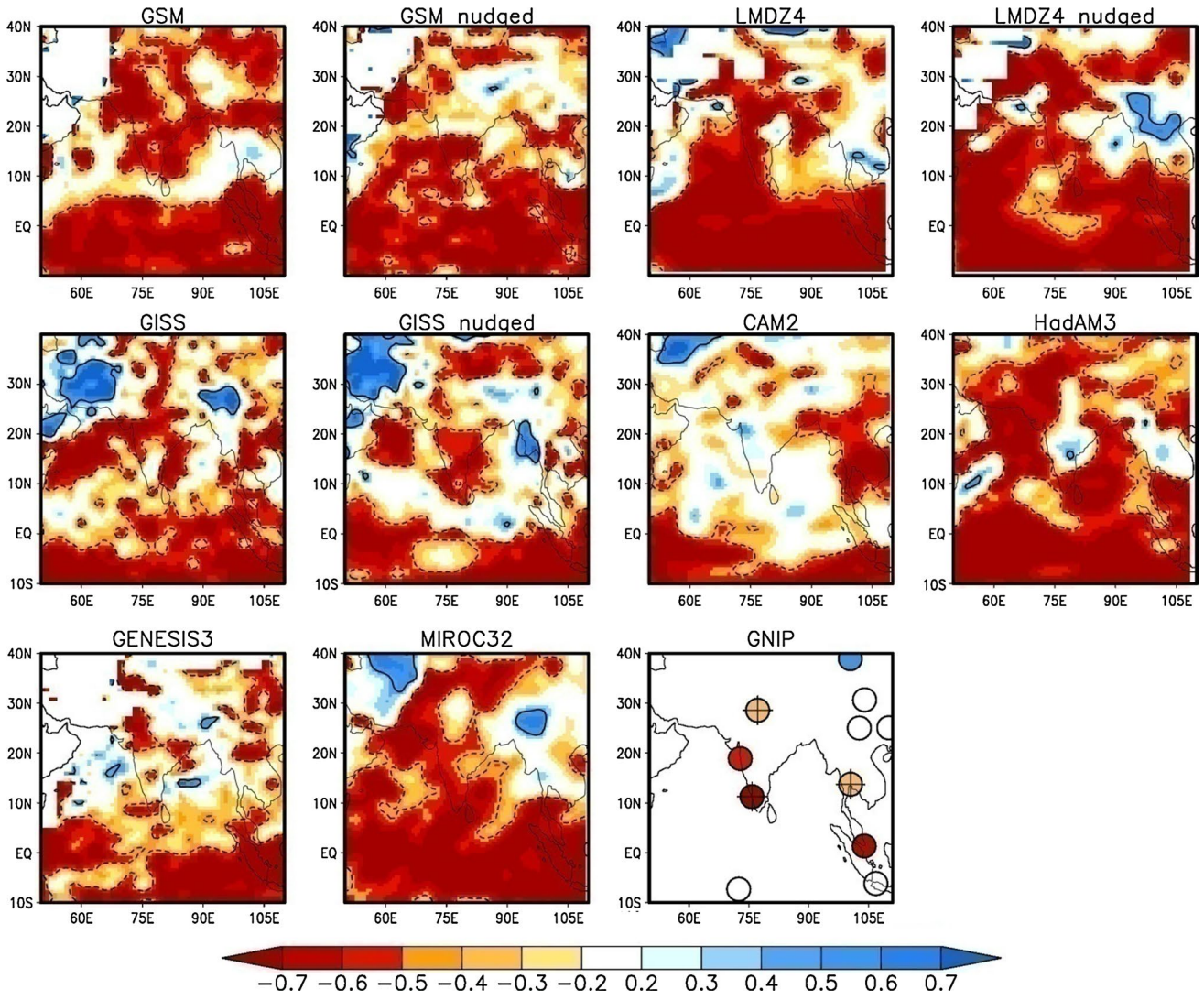

Fig. 9 Correlation coefficients between JJAS mean of rain rate and its $\delta^{18}O$ at each grid point of model outputs for 19 years (1981–1999). Statistically significant correlation ($P < 0.05$) is represented by two *contour lines*; +0.46 and −0.46. For GNIP data statistically significant correlations are represented by "+" signs (*bottom right panel*)

vapor resulting from the rain-vapor interaction. These processes could lead to the simulation of a strong amount effect over oceans (Lee et al. 2012). Over land, vapor advected from the ocean is the major contributor during ISM. Hence the $\delta^{18}O_v$ of the surface continental vapor is mainly affected by the rainfall activity along the transport pathways. Thus the amount effect over the continents is modulated by the spatial precipitation pattern and it varies among the models (Fig. 3). Over land, model simulates a significant amount effect in the region of low to moderate rainfall (supplementary Fig S2). In the low rainfall areas, the role of rain re-evaporation plays a major role in $\delta^{18}O_p$ variations and strengthens the amount effect (Lee et al. 2012). These processes could contribute to some noise in simulated amount effect over land.

3.2.5 *Implications for interpretation of $\delta^{18}O$ of proxies*

In the previous section we reported significant discrepancy among the modeled amount effects. Hence we checked role of upstream rainout on $\delta^{18}O_p$ at four cave locations (Fig. 1): the four sites Akalagavi (Western Ghats, Yadava and Ramesh 2005), Dandak (central eastern India, Sinha et al. 2007), Mawmluh (north eastern India Berkelhammer et al. 2012) and Baratang (Andaman Islands, Laskar et al. 2013) are influenced by strong moisture transport by the south westerly ISM winds. We restricted this analysis to nudged simulations, since they simulate a rather reliable spatial pattern and interannual variation of monsoon rainfall (Figs. 3, 5). The local amount effect on interannual time scale at the each of the three sites is simulated by the

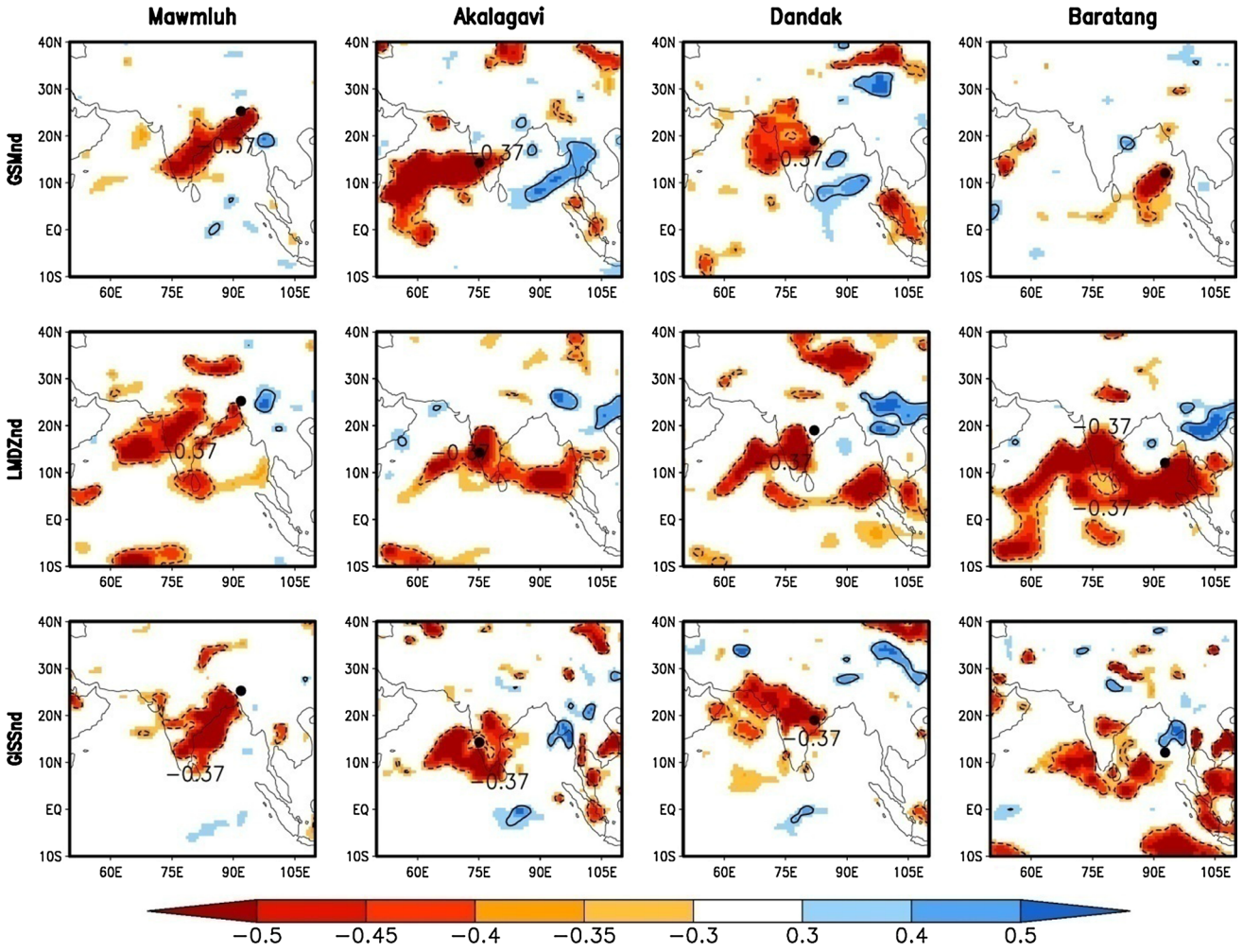

Fig. 10 Linear correlation coefficients between JJAS mean $\delta^{18}O_p$ at four cave sites (*filled black circles*) with the JJAS mean rain rates of surrounding grids, simulated by three nudged models. Model outputs for the period 1980–2007 are used in this analysis. Correlation coefficients less than −0.37 are significant at $P < 0.05$ level

three nudged simulations to varying degrees (Fig. 10). But all the three simulations do show a significant negative correlation of $\delta^{18}O_p$ at the respective cave sites with either interannual variations of regional amount of rainfall (as at Akalagavi) or upstream rainfall (as at Mawmluh, Dandak and Baratang). These correlation patterns in the three simulations are quite similar, suggesting the influence of upstream rainfall on $\delta^{18}O_p$ at cave sites. These results confirm earlier findings by Lee et al. (2012) and Ishizaki et al. (2012) over some Asian summer monsoon sites.

3.3 ENSO and Indian monsoon

Interannual variation of ISM is significantly influenced by ENSO (Kumar 1999). Most of the severe droughts over the Indian Subcontinent are often associated with El-Niño. During El-Niño, convection center shifts from the Western Pacific to Central or Eastern Pacific, resulting in anomalous subsidence over the Western Pacific. This area of subsidence extends up to the Indian subcontinent and suppresses convection, thus reducing ISM rainfall (Kumar 1999; Kumar et al. 2006). However, this negative correlation between ENSO and Indian monsoon weakened after 1980s suggesting a possible inter-decadal modulation in the ENSO–ISM relation (Kumar 1999). Hence, isotope based climate proxies could be useful to understand ENSO–ISM relation on multi decadal timescales. Since our study is confined to 19 years of model simulations, we are unable to look at the ENSO–ISM relation on a multi decadal timescale; instead, we investigate the role of ENSO on the interannual variability of ISM rainfall and $\delta^{18}O_p$. The precipitation variability over tropical Pacific associated with ENSO is well simulated by SWING2 models (Conroy et al. 2013). Correlation between ENSO (i.e., JJAS-averaged Nino-3.4 SST anomaly) and JJAS-average rainfall is plotted in Fig. 11. In CMAP and GPCP datasets, a strong negative

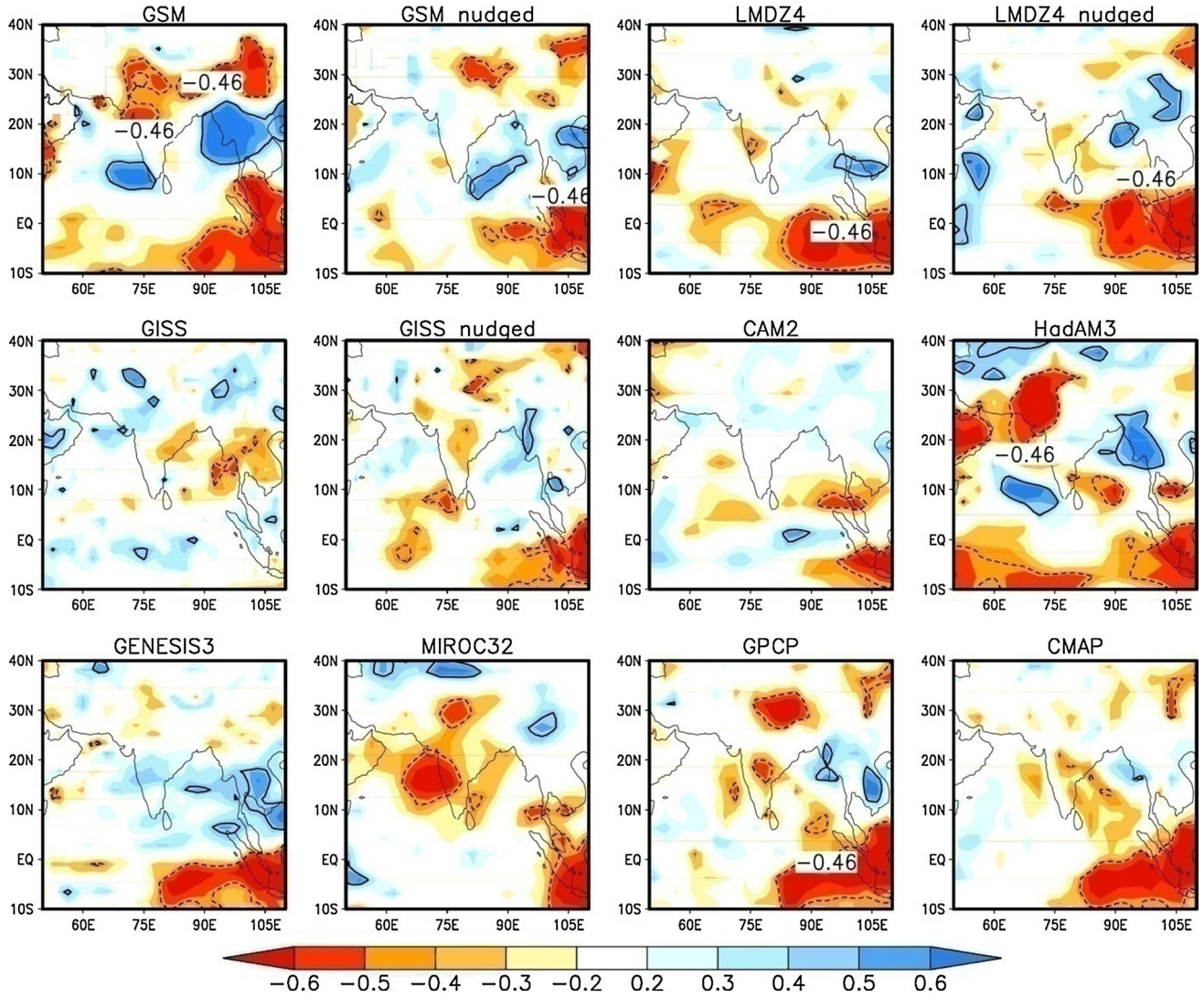

Fig. 11 Linear correlation coefficients between average JJAS-rainfall simulated by different models and JJAS-average Nino-3.4 SST anomaly for 19 years (1981–1999). Correlations above 0.46 and below −0.46 are statistically significant at $P < 0.05$ and are plotted as *contours*. Significant correlations of JJAS-average Nino-3.4 SST anomaly with GPCP and CMAP observations (*bottom row last two panels*) are also shown

correlation is observed at the Indo-Pacific warm pool region (the region beyond longitude 110°E is not shown in the figure) with a weak extension up to the peninsular India. This could be due to the weakening ENSO–ISM linkage after 1980s. Most of the models simulate a strong negative correlation at the Indo-pacific warm pool region, and a weak correlation over the Indian subcontinent, in agreement with GPCP and CMAP observations. The correlation pattern simulated by free model runs (except GISS) are similar to that of nudged simulations, implying that SST forcing is sufficient to create ENSO associated precipitation variability in the models.

The suppressed convection during El-Niño causes relatively ^{18}O enriched precipitation in these regions. Thus a positive correlation between $\delta^{18}O$ of precipitation and ENSO is expected in the areas of associated subsidence. Figure 12 shows the correlation between $\delta^{18}O_p$ and ENSO for JJAS-average. Seven of ten the models and GNIP observations indeed show a positive correlation over the Indo-Pacific warm pool and the East-Asian region. A significant positive correlation is observed at Mumbai, but it is insignificant at New Delhi and Kozhikode. It should be noted that GNIP observations at Mumbai date prior to 1980. A few of the models simulated significant positive correlations over peninsular India. Long term observations are required in Eastern peninsular India and the Andaman islands to further characterize the ENSO signal in monsoon $\delta^{18}O_p$, and thus in $\delta^{18}O$ of monsoon proxies.

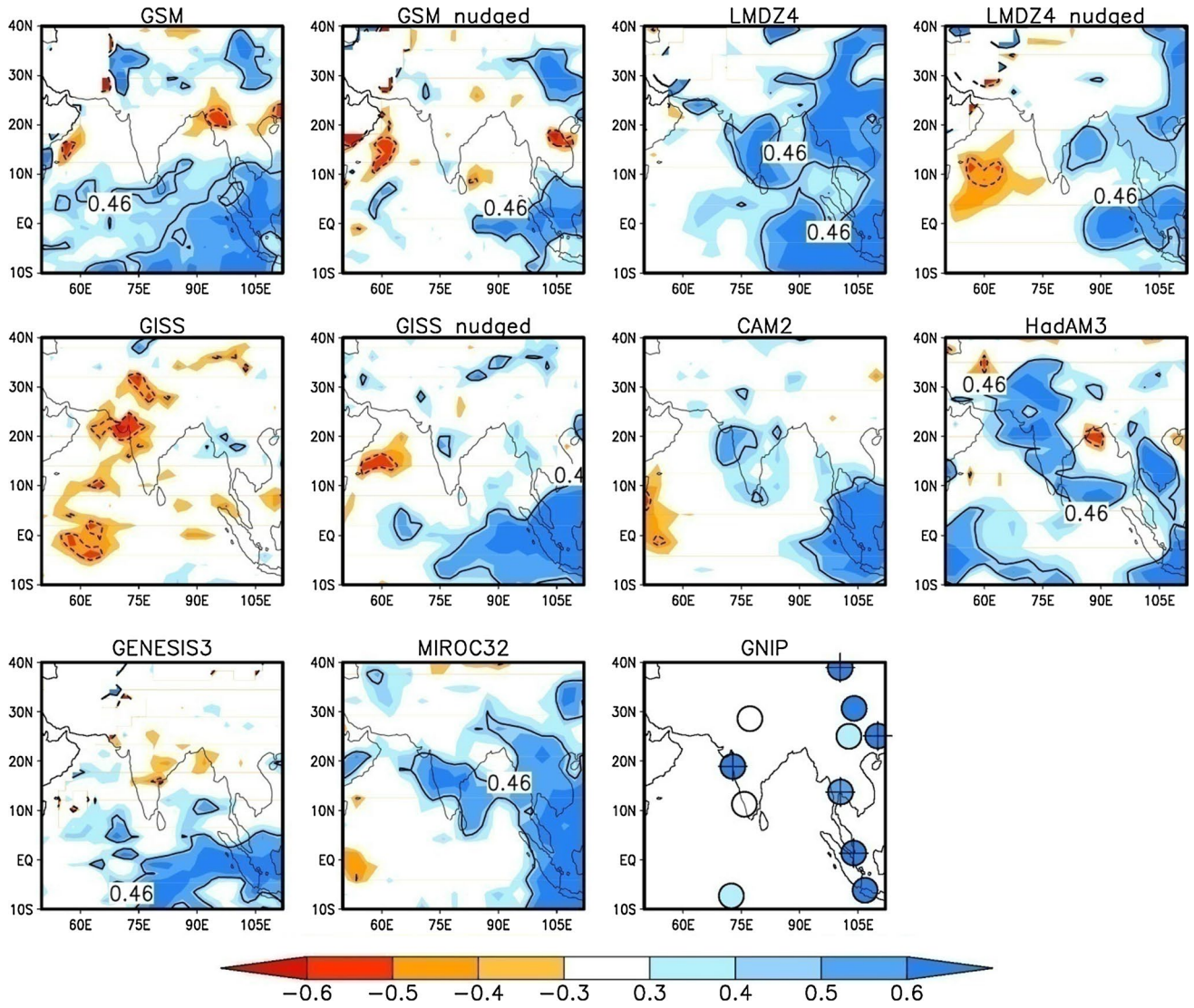

Fig. 12 Linear correlation coefficients between average $\delta^{18}O_p$ of JJAS-rainfall simulated by different models and JJAS-average Nino-3.4 SST anomaly for 19 years (1981–1999). Correlations above 0.46 and below −0.46 are statistically significant at $P < 0.05$ and are plotted as *contours*. Significant correlations of JJAS-average Nino-3.4 SST anomaly with GNIP $\delta^{18}O_p$ observations (*bottom right panel*), are denoted by a "+" symbol

4 Conclusions

Most of the SWING2 models reproduce the characteristic high rainfall during JJAS over CMR, but a large spread among the models is observed. Simulated spatial patterns of monsoon rainfall and its $\delta^{18}O$ are in good agreement with GPCP, CMAP and GNIP observations.

Though Conroy et al. (2013) showed that nudged simulations are not superior to free simulations over the tropical Pacific, where SST is the major driver of rainfall, we observe considerable improvements in the spatial patterns and interannual variability of ISM rainfall due to nudging. Nudged simulations of monthly $\delta^{18}O_p$ are also better correlated with GNIP observations. These improvements may be due to the role of large scale atmospheric circulation on the ISM rainfall (hence on $\delta^{18}O_p$), which are better represented in the nudged simulations. Hence the use of nudged simulations appears to be appropriate to establish the present day isotope-climate linkage over the ISM region.

On the interannual time scale, significant amount effect in ISM rainfall is observed at the two long-term GNIP sites over India. SWING2 simulated amount effect at these stations show large discrepancies among the models and observations. The spatial pattern of simulated amount effect over India appears to be noisy. This may be due to the influence of spatial rainfall pattern on modeled rainfall-$\delta^{18}O_p$ relation over land areas. Three nudged simulations show a consistent negative correlation between $\delta^{18}O_p$ and JJAS

regional average rainfall on interannual scale at Akalagavi; while at the other cave sites, Dandak, Mawmluh and Bratang $\delta^{18}O_p$ is better correlated with upstream rainfall than local rainfall. These results suggest that integrated rainfall along the moisture transport pathways plays a major role in $\delta^{18}O_p$ variations at these cave sites.

ENSO and JJAS rainfall are negatively correlated on interannual timescales over the Eastern Equatorial Indian Ocean with a weak spatial extent up to peninsular India. The $\delta^{18}O_p$ values are positively correlated with ENSO both in models and observations over a larger spatial extent than rainfall. We could not find any consistent ENSO related variability either in rainfall or in $\delta^{18}O_p$ over the Indian subcontinent among the models; this may due to the weakened ENSO–ISM linkage after 1980s.

Assuming that $\delta^{18}O_p$ variability is the major factor controlling $\delta^{18}O$ of speleothems, this study has provided important results that can be used in interpreting annually or sub annually laminated speleothems (and tree rings) from the ISM region. Since our study presents only 19 years of model simulation, simulations of paleoclimate using isotope enabled GCMs would be preferable to understand the ISM variability on centennial to millennial time scales. In this context the present study serves as a validation of such models for their performance to simulate the present day ISM.

Acknowledgments We acknowledge the contributors to SWING2 project. We thank two anonymous reviewers, whose comments considerably improved the manuscript. We thank ISRO-GBP for funding.

References

Adler RF, Huffman GJ, Chang A, Ferraro R, Xie P-P, Janowiak J, Rudolf B, Schneider U, Curtis S, Bolvin D, Gruber A, Susskind J, Arkin P, Nelkin E (2003) The version-2 global precipitation climatology project (GPCP) monthly precipitation analysis (1979–present). J Hydrometeorol 4:1147–1167. doi:10.1175/1525-7541(2003)004<1147:TVGPCP>2.0.CO;2

Araguás-Araguás L, Froehlich K, Rozanski K (2000) Deuterium and oxygen-18 isotope composition of precipitation and atmospheric moisture. Hydrol Process 14:1341–1355. doi:10.1002/1099-1085(20000615)14:8<1341:AID-HYP983>3.0.CO;2-Z

Augustin L, Barbante C, Barnes PRF, Barnola JM, Bigler M, Castellano E, Cattani O, Chappellaz J, Dahl-Jensen D, Delmonte B, Dreyfus G, Durand G, Falourd S, Fischer H, Flückiger J, Hansson ME, Huybrechts P, Jugie G, Johnsen SJ, Jouzel J, Kaufmann P, Kipfstuhl J, Lambert F, Lipenkov VY, Littot GC, Longinelli A, Lorrain R, Maggi V, Masson-Delmotte V, Miller H, Mulvaney R, Oerlemans J, Oerter H, Orombelli G, Parrenin F, Peel DA, Petit J-R, Raynaud D, Ritz C, Ruth U, Schwander J, Siegenthaler U, Souchez R, Stauffer B, Steffensen JP, Stenni B, Stocker TF, Tabacco IE, Udisti R, Van De Wal RSW, Van Den Broeke M, Weiss J, Wilhelms F, Winther J-G, Wolff EW, Zucchelli M (2004) Eight glacial cycles from an Antarctic ice core. Nature 429:623–628. doi:10.1038/nature02599

Berkelhammer M, Sinha A, Stott L, Cheng H, Pausata FSR, Yoshimura K (2012) An Abrupt Shift in the Indian Monsoon 4000 Years Ago. In: Giosan L, Fuller DQ, Nicoll K, Flad RK, Clift PD (eds) Climates, landscapes, and civilizations. American Geophysical Union, Washington, DC

Breitenbach SFM, Adkins JF, Meyer H, Marwan N, Kumar KK, Haug GH (2010) Strong influence of water vapor source dynamics on stable isotopes in precipitation observed in Southern Meghalaya, NE India. Earth Planet Sci Lett 292:212–220. doi:10.1016/j.epsl.2010.01.038

Conroy JL, Cobb KM, Noone D (2013) Comparison of precipitation isotope variability across the tropical Pacific in observations and SWING2 model simulations. J Geophys Res Atmos 118:5867–5892. doi:10.1002/jgrd.50412

Dansgaard W (1964) Stable isotopes in precipitation. Tellus 16:436–468. doi:10.1111/j.2153-3490.1964.tb00181.x

Field RD, Jones DBA, Brown DP (2010) Effects of postcondensation exchange on the isotopic composition of water in the atmosphere. J Geophys Res 115:D24305. doi:10.1029/2010JD014334

Field RD, Kim D, LeGrande AN, Worden J, Kelley M, Schmidt GA (2014) Evaluating climate model performance in the tropics with retrievals of water isotopic composition from Aura TES. Geophys Res Lett 41:6030–6036. doi:10.1002/2014GL060572

Gat JR (1996) Oxygen and hydrogen isotopes in the hydrologic cycle. Annu Rev Earth Planet Sci 24:225–262. doi:10.1146/annurev.earth.24.1.225

Gat J, Gonfiantini R (1981) Stable isotope hydrology. Deuterium and oxygen-18 in the water cycle. In: IAEA technical reports series 210, Vienna

Goswami BN, Venugopal V, Sengupta D, Madhusoodanan MS, Xavier PK (2006) Increasing trend of extreme rain events over India in a warming environment. Science 314:1442–1445. doi:10.1126/science.1132027

Hoffmann G, Heimann M (1997) Water isotope modeling in the Asian monsoon region. Quat Int 37:115–128. doi:10.1016/1040-6182(96)00004-3

Ishizaki Y, Yoshimura K, Kanae S, Kimoto M, Kurita N, Oki T (2012) Interannual variability of H 2 18 O in precipitation over the Asian monsoon region. J Geophys Res 117:1–16. doi:10.1029/2011JD015890

Jasechko S, Sharp ZD, Gibson JJ, Birks SJ, Yi Y, Fawcett PJ (2013) Terrestrial water fluxes dominated by transpiration. Nature 1–5 496:347–350. doi:10.1038/nature11983

Joussaume S, Sadourny R, Jouzel J (1984) A general circulation model of water isotope cycles in the atmosphere. Nature 311:24–29. doi:10.1038/311024a0

Kumar KK (1999) On the weakening relationship between the indian monsoon and ENSO. Science 284:2156–2159. doi:10.1126/science.284.5423.2156

Kumar KK, Rajagopalan B, Hoerling M, Bates G, Cane M (2006) Unraveling the mystery of Indian monsoon failure during El Niño. Science 314:115–119. doi:10.1126/science.1131152

Kurita N (2013) Water isotopic variability in response to mesoscale convective system over the tropical ocean. J Geophys Res Atmos 118:10,376–10390. doi:10.1002/jgrd.50754

Kurita N, Noone D, Risi C, Schmidt GA, Yamada H, Yoneyama K (2011) Intraseasonal isotopic variation associated with the Madden-Julian Oscillation. J Geophys Res 116:D24101. doi:10.1029/2010JD015209

Laskar AH, Yadava MG, Ramesh R, Polyak VJ, Asmerom Y (2013) A 4 kyr stalagmite oxygen isotopic record of the past Indian Summer Monsoon in the Andaman Islands. Geochem Geophys Geosyst 14:3555–3566. doi:10.1002/ggge.20203

Lawrence JR (2004) Stable isotopic composition of water vapor in the tropics. J Geophys Res 109:D06115. doi:10.1029/2003JD004046

Lee J-E, Fung I (2008) "Amount effect" of water isotopes and quantitative analysis of post-condensation processes. Hydrol Process 22:1–8. doi:10.1002/hyp.6637

Lee J-E, Fung I, DePaolo DJ, Henning CC (2007) Analysis of the global distribution of water isotopes using the NCAR atmospheric general circulation model. J Geophys Res 112:D16306. doi:10.1029/2006JD007657

Lee J-E, Pierrehumbert R, Swann A, Lintner BR (2009) Sensitivity of stable water isotopic values to convective parameterization schemes. Geophys Res Lett 36:L23801. doi:10.1029/2009GL040880

Lee J-E, Risi C, Fung I, Worden J, Scheepmaker RA, Lintner B, Frankenberg C (2012) Asian monsoon hydrometeorology from TES and SCIAMACHY water vapor isotope measurements and LMDZ simulations: implications for speleothem climate record interpretation. J Geophys Res 117:D15112. doi:10.1029/2011JD017133

Lekshmy PR, Midhun M, Ramesh R, Jani RA (2013) Is the Isotopic Composition of Rainfall of the South west coast of India Independent of Local Rainfall Amount? In: 12th ISMAS Triennial international conference on mass spectrometry, pp 306–308

Lekshmy PR, Midhun M, Ramesh R, Jani RA (2014) ^{18}O depletion in monsoon rain relates to large scale organized convection rather than the amount of rainfall. Sci Rep 4:5661. doi:10.1038/srep05661

Mathieu R, Pollard D, Cole JE, White JWC, Webb RS, Thompson SL (2002) Simulation of stable water isotope variations by the GENESIS GCM for modern conditions. J Geophys Res 107:4037. doi:10.1029/2001JD900255

Midhun M, Lekshmy PR, Ramesh R (2013) Hydrogen and oxygen isotopic compositions of water vapor over the Bay of Bengal during monsoon. Geophys Res Lett 40:6324–6328. doi:10.1002/2013GL058181

Moore M, Kuang Z, Blossey PN (2014) A moisture budget perspective of the amount effect. Geophys Res Lett 41:1329–1335. doi:10.1002/2013GL058302

Nanjundiah RS, Vidyunmala V, Srinivasan J (2005) On the difference in the seasonal cycle of rainfall over India in the Community Climate System Model (CCSM2) and Community Atmospheric Model (CAM2). Geophys Res Lett 32:1–3. doi:10.1029/2005GL024278

Noone D, Sturm C (2010) Comprehensive dynamical models of global and regional water isotope distributions. In: Isoscapes. Springer, pp 195–219

Ramesh R, Tiwari M, Chakraborty S, Managave SR, Yadava MG, Sinha DK (2010) Retrieval of south Asian monsoon variation during the Holocene from natural climate archives. Curr Sci 99:1770–1786

Risi C, Bony S, Vimeux F (2008) Influence of convective processes on the isotopic composition ($\delta^{18}O$ and δD) of precipitation and water vapor in the tropics: 2. Physical interpretation of the amount effect. J Geophys Res 113:D19306. doi:10.1029/2008JD009943

Risi C, Bony S, Vimeux F, Chong M, Descroix L (2010a) Evolution of the stable water isotopic composition of the rain sampled along Sahelian squall lines. Q J R Meteorol Soc 136:227–242. doi:10.1002/qj.485

Risi C, Bony S, Vimeux F, Jouzel J (2010b) Water-stable isotopes in the LMDZ4 general circulation model: model evaluation for present-day and past climates and applications to climatic interpretations of tropical isotopic records. J Geophys Res Atmos 115:1–27. doi:10.1029/2009JD013255

Risi C, Noone D, Worden J, Frankenberg C, Stiller G, Kiefer M, Funke B, Walker K, Bernath P, Schneider M, Wunch D, Sherlock V, Deutscher N, Griffith D, Wennberg PO, Strong K, Smale D, Mahieu E, Barthlott S, Hase F, García O, Notholt J, Warneke T, Toon G, Sayres D, Bony S, Lee J, Brown D, Uemura R, Sturm C (2012) Process-evaluation of tropospheric humidity simulated by general circulation models using water vapor isotopologues: 1. Comparison between models and observations. J Geophys Res 117:1–26. doi:10.1029/2011JD016621

Sabin TP, Krishnan R, Ghattas J, Denvil S, Dufresne J-L, Hourdin F, Pascal T (2013) High resolution simulation of the South Asian monsoon using a variable resolution global climate model. Clim Dyn 41:173–194. doi:10.1007/s00382-012-1658-8

Schmidt GA, LeGrande AN, Hoffmann G (2007) Water isotope expressions of intrinsic and forced variability in a coupled ocean-atmosphere model. J Geophys Res 112:D10103. doi:10.1029/2006JD007781

Sime LC, Wolff EW, Oliver KIC, Tindall JC (2009) Evidence for warmer interglacials in East Antarctic ice cores. Nature 462:342–345. doi:10.1038/nature08564

Sinha A, Cannariato KG, Stott LD, Cheng H, Edwards RL, Yadava MG, Ramesh R, Singh IB (2007) A 900-year (600 to 1500 A.D.) record of the Indian summer monsoon precipitation from the core monsoon zone of India. Geophys Res Lett. doi:10.1029/2007GL030431

Taylor KE (2001) Summarizing multiple aspects of model performance in a single diagram. J Geophys Res 106:7183. doi:10.1029/2000JD900719

Vuille M, Werner M, Bradley RS, Keimig F (2005) Stable isotopes in precipitation in the Asian monsoon region. J Geophys Res 110:1–15. doi:10.1029/2005JD006022

Xie P, Arkin PA (1997) Global precipitation: a 17-year monthly analysis based on gauge observations, satellite estimates, and numerical model outputs. Bull Am Meteorol Soc 78:2539–2558. doi:10.1175/1520-0477(1997)078<2539:GPAYMA>2.0.CO;2

Yadava MG, Ramesh R (2005) Monsoon reconstruction from radiocarbon dated tropical Indian speleothems. Holocene 15:48–59. doi:10.1191/0959683605h1783rp

Yadava M, Ramesh R, Pandarinath K (2007) A positive "amount effect" in the Sahayadri (Western Ghats) rainfall. Curr Sci 93:560–564

Yoshimura K, Kanamitsu M, Noone D, Oki T (2008) Historical isotope simulation using Reanalysis atmospheric data. J Geophys Res 113:D19108. doi:10.1029/2008JD010074

Yurtsever Y, Gat JR (1981) Atmospheric waters. In: Gat J, Gonfiantini R (eds) Stable isotope hydrology: deuterium and oxygen-18 in the water cycle. IAEA technical reports series 210, pp 103–142